

Algebraic Methods for Dynamical Systems and Optimisation

Nidhi Kaihnsa

Von der Fakultät für Mathematik und Informatik
der Universität Leipzig
angenommene

D I S S E R T A T I O N

zur Erlangung des akademischen Grades

DOCTOR RERUM NATURALIUM
(Dr.rer.nat.)

im Fachgebiet

Mathematik

vorgelegt

von Diplommathematikerin Nidhi Kaihnsa
geboren am 10.12.1992 in India

Die Annahme der Dissertation wurde empfohlen von: Gutachter

1. Professor Dr. Bernd Sturmfels (MPI, MIS, Leipzig)
2. Professor Dr. Timo de Wolff (TU Braunschweig)

Die Verleihung des akademischen Grades erfolgt mit Bestehen der Verteidigung am
03.07.2019 mit dem Gesamtprädikat magna cum laude.

Abstract

This thesis develops various aspects of Algebraic Geometry and its applications in different fields of science.

In Chapter 2 we characterise the feasible set of an optimisation problem relevant in chemical process engineering. We consider the polynomial dynamical system associated with mass-action kinetics of a chemical reaction network. Given an initial point, the attainable region of that point is the smallest convex and forward closed set that contains the trajectory. We show that this region is a spectrahedral shadow for a class of linear dynamical systems. As a step towards representing attainable regions we develop algorithms to compute the convex hulls of trajectories. We present an implementation of this algorithm which works in dimensions 2,3 and 4. These algorithms are based on a theory that approximates the boundary of the convex hull of curves by a family of polytopes. If the convex hull is represented as the output of our algorithms we can also check whether it is forward closed or not.

Chapter 3 has two parts. In this first part, we do a case study of planar curves of degree 6. It is known that there are 64 rigid isotopy types of these curves. We construct explicit polynomial representatives with integer coefficients for each of these types using different techniques in the literature. We present an algorithm, and its implementation in *Mathematica*, for determining the isotopy type of a given sextic. Using the representatives various sextics for each type were sampled. On those samples we explored the number of real bitangents, inflection points and eigenvectors. We also computed the tensor rank of the representatives by numerical methods. We show that the locus of all real lines that do not meet a given sextic is a union of up to 46 convex regions that is bounded by its dual curve.

In the second part of Chapter 3 we consider a problem arising in molecular biology. In a system where molecules bind to a target molecule with multiple binding sites, cooperativity measures how the already bound molecules affect the chances of other molecules binding. We address an optimisation problem that arises while quantifying cooperativity. We compute cooperativity for the real data of molecules binding to hemoglobin and its variants.

In Chapter 4, given a variety X in \mathbb{P}^n we look at its image $X^{\circ r}$ under the map that takes each point $[x_0 : \dots : x_n]$ in X to its coordinate-wise r -th power $[x_0^r : \dots : x_n^r]$. We compute the degree of the image. We also study their defining equations, particularly for hypersurfaces and linear spaces. We exhibit the set-theoretic equations of the coordinate-wise square of a linear space L of dimension k embedded in a high dimensional ambient space. We also establish a link between coordinate-wise squares of linear spaces and the study of real symmetric matrices with degenerate eigenspectrum.

Contents

List of Figures	vi
List of Tables	viii
1 Introduction	1
1.1 Algebraic Geometry and Chemical Reaction Networks	1
1.2 Optimisation and Polynomials	2
1.3 Understanding Powers of Varieties	4
2 Chemistry and Convexity	5
2.1 The Attainable Region	5
2.1.1 Chemical Reaction Networks	5
2.1.2 Spectrahedra	7
2.1.3 Linear Systems	8
2.1.4 Weakly Reversible Chemical Reaction Networks	11
2.1.5 Facial Structure	13
2.2 Representing Convex Hulls	16
2.2.1 Limiting Faces	17
2.2.2 Convex Hulls in Bensolve	21
2.2.3 Boundary of Convex Hulls	24
2.3 Forward Closed Convex Sets	30
2.3.1 Planar Case	30
2.3.2 General Case	32
2.4 Applications	34
3 Optimisation and Real Algebraic Geometry	37
3.1 Sixty Four Curves	37
3.1.1 Discriminantal Transitions	40
3.1.2 Construction of Representatives	43
3.1.3 Identifying the Type	47
3.1.4 Probability Distribution and Experiments	48
3.1.5 Avoidance Locus	55
3.1.6 List of Representatives	61
3.2 Biology and Optimisation	64
3.2.1 The Mathematical Framework	65
3.2.2 The Algebraic Optimisation Problem	67
3.2.3 Experimental Results	72
4 Coordinate-wise Powers	75
4.1 Degree Formula	75
4.1.1 Orthostochastic Matrices	77
4.1.2 Linear Spaces	79

4.2	Hypersurfaces	81
4.2.1	The Defining Equation	81
4.2.2	Duals and Reciprocals of Power Sum Hypersurfaces	84
4.2.3	From Hypersurfaces to Arbitrary Varieties?	87
4.3	Linear Spaces	89
4.3.1	Point Configurations	90
4.3.2	Degenerate Eigenvalues and Squaring	91
4.3.3	Squaring Lines and Planes	93
4.3.4	Squaring in High Ambient Dimensions	96
5	References	103

List of Figures

1	Three vertices are the chemical complexes. The labels κ_i are the rates of reactions.	6
2	Trajectory and its convex hull	12
3	Face(2) of a curve in 3-space.	14
4	Face(3) with initial point as one vertex of the 3-face for a curve in 4-space.	14
5	Face(3) of a 5-dimensional convex body	15
6	A Hausdorff convergent sequence of facets F_ϵ of A_ϵ need not converge to a face F of C . The face F in the left diagram contains a curve point $y \in \mathcal{C}$ which is not extremal in C . The endpoint F of the curve \mathcal{C} on the right is an exposed face of C but it is not uniquely exposed. There is no sequence of facets F_ϵ of A_ϵ that Hausdorff converges to exposed face F	19
7	A sample of points (left) from a space curve and its convex hull (right)	24
8	Patches on the convex hull.	26
9	Two 2-patches (left) and three 1-patches (right) in the boundary of a 4-dimensional convex body, obtained as the convex hull of a trigonometric curve of degree six. The picture shows the graph G , with five connected components G_i , that is computed by Algorithm 2.2.18.	27
10	The convex hull of a trigonometric curve of degree 14 in 3-space. The boundary of this convex body consists of triangles and of 1-patches in a ruled surface of degree 286.	29
11	The Hamiltonian vector field defined by the Trott curve and two of its trajectories.	31
12	A pair of ellipses encloses the Trott curve and bounds the attainable region.	32
13	Convex hull of a trajectory of the Van de Vusse reaction and the partition of its boundary	35
14	Convex hull of a trajectory of a weakly reversible system that is not forward closed	36
15	The 56 types of smooth plane sextics form a partially ordered set. The colour code indicates whether the real curve divides its Riemann surface. The red curves are dividing, the blue curves are non-dividing, and the purple curves can be either dividing or non-dividing.	39
16	Type (21)2d transitions into Type (21)2nd by turning an oval inside out.	42
17	A sextic of Type (11)7 is constructed by perturbing the union of three quadrics.	45
18	The discriminant divides the Robinson net (42) into 15 components that realise four topological types. The green region represents smooth sextics with 10 non-nested ovals.	45
19	Using local perturbations to create sextics that are dividing or non-dividing	46
20	The Edge quartic C and its dual C^V ; the avoidance locus \mathcal{A}_C is coloured.	56
21	A sextic curve C with 8 non-nested ovals; its 68 relevant bitangents represent \mathcal{A}_C	59
22	A smooth sextic with 10 non-nested ovals whose avoidance locus is empty	60
23	The effect of cooperativity on a binding curve	64

24	A molecule with 4 binding sites.	66
25	Minimal molecules for binding polynomial P_1, P_2, P_3	68
26	Computing cooperativity for a molecule with 3 sites using SCIP	71
27	Minimal molecules for binding polynomials P_1, P_5, P_6	73
28	The coordinate-wise square of the plane $V(x_0 + x_1 + x_2 + x_3) \subset \mathbb{P}^3$	83
29	Circles and their coordinate-wise squares	84
30	The iterated dual-reciprocal $\mathcal{DRDR}V(f) \subset \mathbb{P}^3$	87
31	Distinction between $V(f_1^{\circ 2}, f_2^{\circ 2})$ and $V(f_1, f_2)^{\circ 2}$	88
32	Dependence of $L^{\circ 2}$ on the planar point configuration Z	94

List of Tables

1	Census of random trigonometric curves in 3-space	29
2	Rokhlin–Nikulin classification of smooth sextics in the real projective plane .	38
3	Counts of topological types sampled from the $U(3)$ -invariant distribution . .	49
4	Sextics with coefficients in $\{-10^{12}, \dots, 10^{12}\}$ uniformly distributed	50
5	Symmetric sextics with coefficients in $\{-10^{12}, \dots, 10^{12}\}$ uniformly distributed	50
6	Sextics that are determinants of random symmetric matrices with linear entries	50
7	Sextics that are signed sums of n sixth powers of linear forms	50
8	Computational results for the number of real solutions for inflection points, eigenvectors, bitangents and real rank among the 64 rigid isotopy classes of smooth sextics in $\mathbb{P}_{\mathbb{R}}^2$	52
9	Binding polynomials 1 to 8 and the relation of their degree of cooperativity according to the maximal slope of the Hill plot n_{max} (\succ = bigger n_{max} , DPG = 2,3-diphosphoglycerate)	73
10	Binding polynomials 9 to 13	73
11	Bounds on the minimal absolute interaction	74
12	The degrees of $\mathbb{S}\mathbb{O}(m)$ and $\mathbb{S}\mathbb{O}(m)^{\circ 2}$ in comparison.	79

Acknowledgements

First and foremost, I express my gratitude towards my advisor Bernd Sturmfels for accepting me as his student and guiding me through my PhD. I am grateful to him for sharing his insights on various academic aspects, for his constant support and for the invaluable advice on all things small and large. I greatly enjoyed working with him. I am grateful to be a part of the Non-Linear Algebra group. It has been wonderful interacting with various mathematicians with different backgrounds over the span of my PhD here. Those interactions and discussions made mathematics more exciting. I would also like to thank Jürgen Jost for giving me the amazing opportunity to join the Max Planck Institute.

Many thanks to my collaborators: Daniel Ciripoi, Papri Dey, Paul Görlach, Mario Kummer, Andreas Löhne, Johannes Martini, Daniel Plaumann, Yue Ren, Mohab Safey El Din, Mahsa Sayyary, for various interesting discussions and sharing their mathematical insights.

My thanks to fellow graduate students Paul Görlach, Orlando Marigliano, Mahsa Sayyary, and Tim Seynnaeve for various outings and game nights. I would also like to thank Eliana Duarte, Christiane Görgen, and Saskia Gutzschebauch for amazing conversations paired with mojito Mondays or wine nights and keeping me sane. I also thank Eliana, Christiane, Avinash Kulkarni, Yue Ren, Emre Sertöz, and Maddie Weinstein for various useful comments on the thesis. Special thanks to Saskia for the smooth sailing on the administration front.

I acknowledge the Max Planck Institute for Mathematics in the Sciences and International Max Planck Research School (IMPRS) for their financial support.

I am grateful to my family for their unconditional love and support. Thanks to my friends Arul Ganesh, Akanksha Katoch, Debanjana Kundu, Mahendra Singh for keeping me grounded and lending their listening ears when I needed one. Finally, I thank Jim Portegies for his moral support and for his endearing presence in my life.

1 Introduction

Understanding dynamical systems has been the focus of research for a very long time. It was being deliberated upon when Aristotle wanted to understand “change”. Leibniz and Newton founded calculus to formalise the mathematics of dynamics. Poincaré and Lyapunov used the methods of topology and geometry towards understanding chaos and the stabilities of equilibria. This field has a very complex history. Until recently, the main motivation for dynamics and dynamical systems came from the want of understanding the physical systems. Results originated from various research areas in engineering, physics, mathematics, and their interfaces. The past century has seen a surge of activities at the interface of dynamics and biology. Among the systems studied, polynomial dynamical systems are now widely explored in systems biology and chemical reaction networks.

In applications, dynamical systems and optimisation problems come together in numerous ways. The field of optimisation by itself is a very vast and an active research area. Optimisation problems appears in various fields ranging from algebra, combinatorics, computer science, computational biology, chemical engineering, financial mathematics, operation research, control theory and many others. These problems can be extremely challenging. Polynomial optimisation forms a major class of these problems. These have been of purely mathematical interest since Hilbert’s 17th problem. The discussion of sum of squares and non-negativity that Hilbert started in 1900 has led us today to the methods in sum-of-squares optimisation. In recent years, dynamical systems and polynomial optimisation have come together in interesting ways and at their interface new research problems and exciting results are being developed.

I work at the Max-Planck Institute dedicated to *Mathematics in the Sciences*. Being a member of the Non-Linear Algebra group at the institute, I was motivated to connect algebra in a truly meaningful way with the new challenges and opportunities of the data science era. This thesis, as a result, presents work at the interface of polynomial dynamical systems and optimisation problems. The focus lies on algebraic and numerical methods with a view towards applications in biology and chemistry. The thesis provides an insight into how the problems in biology and chemistry can benefit from the tools developed in algebraic geometry and polynomial optimisation. It is divided into three parts, led by my interest in the problems of different flavours. The subsequent sections give the layout of the thesis.

1.1 Algebraic Geometry and Chemical Reaction Networks

Chemical reaction networks have now gathered a lot of attention in the mathematics community [16, 35, 38, 70], and is a fast growing field. In Chapter 2 we focus on the optimisation problem that has been of interest in chemical process engineering for over half a century now. This part of the thesis is based on two works [30, 71]. Given a set of chemical reactions, a chemical reactor is a system where a set of reactions and their mixing takes place. Our aim is to find the most cost-efficient reactor for any given reactions. Fritz Horn in 1964 was the first to attempt to describe the feasible set of this optimisation problem [65]. He termed this feasible set the *attainable region*. This optimisation problem has been foremostly worked

upon by Martin Feinberg, Roy Jackson, David Glasser, and Diane Hildebrandt [46, 47, 66]. For detailed exposition of the problem from a chemical point of view, the reader is referred to the book [95].

Driving motivation for Chapter 2 has been to describe the attainable region. This region is a convex set. The chapter is titled *Chemistry and Convexity* and we aim to find a representation of the convex object that appears in an application in chemistry. The layout of the chapter is as follows: We first explain the basic set up of chemical reaction networks as graphs and describe the dynamics associated with mass action kinetics. We present a rigorous mathematical treatment of attainable regions and formalise the definition for these in Subsection 2.1.1. As a first case, in Subsection 2.1.3 we characterise them for linear systems. We show that, for certain subclasses of linear systems, the attainable regions are spectrahedral shadows. These objects are feasible sets of semidefinite programming in convex optimisation and are widely studied in *polynomial optimisation* and *real algebraic geometry*.

As a next step, we look at the problem of computing the convex hull of the trajectory of a dynamical system. This problem is of general interest in *convex algebraic geometry* [10]. Our results also apply to the convex hulls of algebraic curves and parts of algebraic curves since every curve can be locally expressed as a trajectory of a polynomial dynamical system. In Section 2.2, we develop a theory of approximating the convex hull of curves by polytopes. The main idea is to use inner approximations by convex polytopes to the actual convex body. The boundary of the convex body in n -dimensional space is stratified into $(n - k - 1)$ -dimensional families of k -dimensional faces. These strata are called *patches* and are defined using the notion of *normal cycles* [53]. We present a general numerical algorithm and its implementation in dimension 3 and 4 for finding these patches. Our implementation is based on the software **Bensolve Tools** [31]. In [102] the authors give a description of the boundary of the convex hull of space curves. In particular, they give the number of complex tritangent planes and degree of the edge surface (1-dimensional family of 1-dimensional faces) forming the boundary of the convex hull of degree d and genus g generic space curve. Using our implementation, we experimented on trigonometric curves and report in Subsection 2.2.3 on the number of real tritangents and the number of patches of the edge surface observed.

The vector field at every boundary point of the attainable regions points inwards for every supporting hyperplane. Such regions are called *forward closed*. In Section 2.3 we give an algorithm to decide whether a convex hull is forward closed. The algorithm finds the points that partition the facets into the areas where the vectorfield is pointing inwards or outwards. If there is no such region where the vector field points outwards then we say that the convex hull is forward closed. We implemented this and used it to resolve a conjecture which was stated in the author's earlier works in [71].

1.2 Optimisation and Polynomials

Classical optimisation problems include computing eigenvectors and finding tensor rank decomposition of a given polynomial. These problems appear in numerous emerging applications. These applications, notably in the analysis of data from the life sciences, now rely

on computational tools from topology and algebraic geometry. The most basic objects in algebraic geometry are plane curves. Section 3.1 of Chapter 3 is a case study of homogeneous polynomials of degree 6 in three variables using such tools. This section is based on the article [72] which is published online in *Experimental Mathematics*.

Hilbert’s 16th problem is a classical problem in *real algebraic geometry* regarding the topological types of planar curves of degree d . For $d = 6$, the classification of these curves is known due to Rokhlin and Nikulin (Theorem 3.1.1). There are 56 topological types that are distinguished by the number of ovals ranging from 0 to 11 and their placement in the plane. We explore the 27-dimensional space of plane sextic curves. In Subsection 3.1.1 we present a method for computing the discriminant in that space. The complement of the discriminant has 64 connected components. These correspond to 64 rigid isotopy types. A real curve may or may not divide the corresponding complex Riemann surface into two components. There are 6 of the 56 types which always divide the Riemann surface. Eight of those can be of either kind and the rest are always non-dividing. The numbers of types add up to 64.

We then use various constructions in the literature to give explicit polynomials with integer coefficients for each type. Their constructions have been worked on by various mathematicians [54, 59, 119]. The constructed polynomials are listed in Subsection 3.1.6. In Subsection 3.1.3 we present an implementation called `SexticClassifier` written in `Mathematica` that classifies a ternary sextic. It takes a homogeneous degree 6 polynomial in 3 variables as an input and if it is nonsingular, returns its topological type. This program is based on *Cylindrical Algebraic Decomposition* which is an important tool in real algebraic geometry. It partitions \mathbb{R}^n into semialgebraic sets depending on the signs of polynomials on each set.

In Subsection 3.1.4 we report on experimental results concerning the real geometric properties of the curves. We sample the curves from probability distributions on the coefficients of the sextic and use the `SexticClassifier` to find the empirical distribution of the curves. Once we have these representatives, we explore in their neighbourhood to obtain more samples around them of the same type. For each of the types, the observed number of bitangents, inflection points and eigenvectors are recorded in Table 8. We use numerical methods to compute the real tensor rank for each of the representatives listed in Subsection 3.1.6.

In Section 3.2 we shift gears and focus on an optimisation problem coming from the want of a better measure to quantify a phenomenon in molecular biology. This part of Chapter 3 is based on the article [73]. In chemistry and biology, a ligand is a substance that binds to a target molecule inside a bigger system. When a target molecule has multiple binding sites, *cooperativity* measures how the already bound ligands affect the chance of other ligands binding to the still open sites. If the chances increase then cooperativity is said to be positive, else negative.

In Subsection 3.2.1 we setup the notations and give the mathematical framework of the problem. We explain the background and the optimisation problem that we consider in Subsection 3.2.2. We mainly focus on the case where the target molecule has 4 sites. The original optimisation problem poses various challenges. We elaborate on the steps taken to simplify the problem. In Subsection 3.2.3 we experiment on various molecules listed in the literature. We compute the upper bounds and the lower bounds on the measure of

cooperativity using the software SCIP [56].

1.3 Understanding Powers of Varieties

Chapter 4 is based on the article [41] and delves into the product of varieties. Hadamard products of varieties arise from multiplying coordinate-by-coordinate any two points $x \in X$, $y \in Y$ in given subvarieties X, Y of \mathbb{P}^n . In applications, they first appeared in [36], where the variety associated to the restricted Boltzmann machine was described as a repeated Hadamard product of the secant variety of $\mathbb{P}^1 \times \dots \times \mathbb{P}^1 \subset \mathbb{P}^{2^n-1}$ with itself.

The original motivation for this work was to understand the variety of orthostochastic matrices. An orthostochastic matrix is a matrix arising by squaring each entry of an orthogonal matrix. In other words, they are points in the coordinate-wise square of the variety of orthogonal matrices. Orthostochastic matrices play a central role in the theory of majorization [88] and are closely linked to finding real symmetric matrices with prescribed eigenvalues and diagonal entries, see [64] and [96]. Recently, it has also been shown that studying the variety of orthostochastic matrices is central to the existence of determinantal representations of bivariate polynomials and their computation, see [39].

We, therefore, consider a projective variety $X \subset \mathbb{P}^n$ and we study its r -th *coordinate-wise power* X^{or} . This is the image of X under the rational map $\varphi_r : \mathbb{P}^n \rightarrow \mathbb{P}^n$ given by $[x_0 : \dots : x_n] \mapsto [x_0^r : \dots : x_n^r]$. In Section 4.1 we derive a formula for computing the degree of X^{or} given the degree of X . In combinatorics, a *matroid* abstracts the notion of bases in vector spaces. For a linear space $L \subset \mathbb{P}^n$ we relate the degree of L^{or} and the combinatorial information given by the associated *linear matroid*.

For hypersurfaces we give an explicit way to find the defining equation of the image in Section 4.2. We define the notion of r -th power basis. We prove the existence of such a power basis for all r and pose the question whether there exists a power basis for a given ideal which is same for all r and how to compute it if it does.

For a general variety it is hard to find the ideal that describes its coordinate-wise power. In Section 4.3 we worked on the case of coordinate-wise square of a linear space. We consider a linear space L of dimension k embedded in \mathbb{P}^n for $n \gg k$. The linear equations that describe the embedding are considered as points in the dual of the linear space. When these points lie on a unique quadric of rank s , we exhibit the set-theoretic equations for the coordinate-wise square L^{o2} . We also remark that the problem of finding the ideal of L^{o2} for arbitrary L can be reduced to a certain problem of matrix completion.

2 Chemistry and Convexity

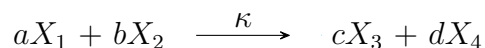
This chapter is based on two articles [30, 71]. Article [30] is a joint work with Daniel Ciripoi, Andreas Löhne, and Bernd Sturmfels. This has been submitted to *Revista de la Unión Matemática Argentina* for publication. Article [71] is a single author paper and has been accepted for presentation at *MEGA: Effective Methods in Algebraic Geometry, 2019*.

2.1 The Attainable Region

The term *attainable region* finds its origin in the paper [65] by Fritz Horn. He coined this term to denote the feasible set of an optimisation problem in chemical process engineering. For a given chemical reaction network, a chemical reactor is where the chemical reactions take place. The problem is to find an optimum reactor under the conditions that chemical species are allowed to react amongst themselves as well as can be mixed. For detailed exposition of this problem from chemical point of view, the reader is referred to [95]. Subsection 2.1.1 gives the basic setup of chemical reaction network and the dynamics that we considered. We follow the notations for chemical reaction networks set up in Anne Shiu’s PhD dissertation [112]. Subsection 2.1.2 recalls some basic notions in semidefinite programming. In Subsection 2.1.3 we describe the attainable region for the linear systems.

2.1.1 Chemical Reaction Networks

Let X_1, \dots, X_n be chemical species. A chemical reaction takes place when these species combine together in certain ratio to form another set of species. For instance, consider a units of species X_1 and b units of species X_2 that combines as follows



to give c and d units of X_3 and X_4 respectively. The coefficients a , b , c and d are positive integers. We call the linear combinations $aX_1 + bX_2$ and $cX_3 + dX_4$ *chemical complexes*. The transformation of these complexes from one to the other represented by weighted arrow is called a *chemical reaction*. The weight κ measures how fast the reaction takes place and is called the *rate of reaction*. One or more such reactions together form a *chemical reaction network*.

Definition 2.1.1 (Chemical Reaction Networks). *A chemical reaction network (CRN) is a graph whose vertices are chemical complexes and edges are the chemical reactions weighted by their reaction rates.*

Example 2.1.2. We now illustrate a network of chemical reactions amongst 5 chemical species in Figure 1. We denote the concentration of each species X_i by x_i . Throughout, we consider that the concentration of the species evolve according to the laws of *mass action kinetics*. In each reaction the species react proportional to their concentration in the system and the rates of reaction are the proportionality constants. In the figure note that one unit of X_1 is consumed in reactions $X_1 + X_3 \xrightarrow{\kappa_1} X_4$ and $X_1 + X_3 \xrightarrow{\kappa_5} X_2 + 2X_5$.

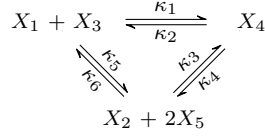


Figure 1: Three vertices are the chemical complexes. The labels κ_i are the rates of reactions.

One unit of X_1 is produced by $X_4 \xrightarrow{\kappa_2} X_1 + X_3$ and $X_2 + 2X_5 \xrightarrow{\kappa_6} X_1 + X_3$. Therefore, the change in concentration of X_1 is given by

$$\dot{x}_1 = \frac{dx_1}{dt} = -1 \cdot \kappa_1 x_1 x_3 - 1 \cdot \kappa_5 x_1 x_3 + 1 \cdot \kappa_2 x_4 + 1 \cdot \kappa_6 x_2 x_5^2 \quad (1)$$

Similarly, computing for other species with respect to each reaction, we get

$$\begin{aligned}
\dot{x}_2 &= \frac{dx_2}{dt} = \kappa_5 x_1 x_3 + \kappa_4 x_4 + (-\kappa_3 - \kappa_6) x_2 x_5^2 \\
\dot{x}_3 &= \frac{dx_3}{dt} = (-\kappa_1 - \kappa_5) x_1 x_3 + \kappa_2 x_4 + \kappa_6 x_2 x_5^2 \\
\dot{x}_4 &= \frac{dx_4}{dt} = \kappa_1 x_1 x_3 + (-\kappa_2 - \kappa_4) x_4 + \kappa_3 x_2 x_5^2 \\
\dot{x}_5 &= \frac{dx_5}{dt} = 2(\kappa_5 x_1 x_3 + \kappa_4 x_4 + (-\kappa_3 - \kappa_6) x_2 x_5^2).
\end{aligned} \quad (2)$$

We now give the general notation for the dynamics associated with a given CRN. For a chemical reaction network with n species and s complexes consider a $s \times n$ matrix $Y = (y_{ij})$ where y_{ij} is the coefficient of the j th species in the i th complex. With each vertex associate the monomial $x^{y_i} = x_1^{y_{i1}} x_2^{y_{i2}} \cdots x_n^{y_{in}}$. Let $A_\kappa = (\kappa_{ij})$ be the $s \times s$ matrix with ij -th entry given by the rates of reactions from the i -th complex to the j -th complex for $i \neq j$. The diagonal entry $\{ii\}$ of A_κ is the negative of the sum of the rest of the entries in the row i and therefore, $\sum_j \kappa_{ij} = 0$ for all i . This matrix is the negative of the Laplacian of the weighted digraph that represents the CRN. The above dynamics can then also be written as the product of matrices in the following manner

$$\dot{x} = \frac{dx}{dt} = \Psi(x) \cdot A_\kappa \cdot Y \quad (3)$$

where $\Psi(x) = [x^{y_1} \quad x^{y_2} \quad \cdots \quad x^{y_s}]$.

The main focus in this thesis is on dynamical systems given by a system of ordinary differential equations (ODE's). We consider

$$\dot{x} = \frac{dx}{dt} = f(x) \quad (4)$$

where $x : \mathbb{R} \rightarrow \mathbb{R}^n$ is an unknown function of time and $f : \mathbb{R}^n \rightarrow \mathbb{R}^n$ is a known polynomial map. Given an initial starting point this system always have a unique solution.

We particularly focus on the dynamics of the chemical reaction networks (CRN). In that case $f(x) = \Psi(x) \cdot A_\kappa \cdot Y$. The image of the solution of the given ODE with an initial point $x(0) = (x_1(0), \dots, x_n(0))$ at time $t = 0$ in the state space is called the *trajectory*. We will denote the trajectory by \mathcal{C} and the initial point $x(0)$ by x_0 . In (3) the matrix Y is called the stoichiometric matrix. Let y_j be the vector given by the j -th row of the matrix Y . The linear subspace in \mathbb{R}^n spanned by the vectors $y_j - y_i$ for $i \neq j$ is called the *stoichiometry subspace* and we will henceforth denote it by P .

Definition 2.1.3 (Forward Closed). *A subset $S \subset \mathbb{R}^n$ is said to be forward closed for a given ODE if for all points $y \in S$ as the initial point $x_0 = y$, all the resulting trajectories lie in S , i.e. $x(t) \in S$ for all $t > 0$.*

In this work, we aim to characterise all the possible sets of the species concentrations attainable from the continuous reaction, according to the dynamics, and mixing of the concentrations of the species at all times. This approach to the reactor optimisation problem has been explored and discussed in [95]. We approach this problem by building on a new mathematical definition of this attainable region, and we study these regions for various kinds of dynamical systems.

Definition 2.1.4 (Attainable Region). *The attainable region, $\mathcal{A}(x_0)$ is the smallest convex forward closed subset of \mathbb{R}^n that contains the point x_0 .*

By definition, for CRNs the attainable region is a convex subset in the positive orthant of real space \mathbb{R}^n of the chemical species. Note that the attainable region contains the convex hull of the trajectory and is unique. In the Subsection 2.1.3 we first discuss the attainable regions of linear dynamical systems.

2.1.2 Spectrahedra

In the next subsection we give a condition on the Laplacian of linear systems for which the attainable region can be represented as the feasible set of a semidefinite programming. These sets are called *spectrahedral shadows*. In this subsection we review some definitions and results. For more information on these objects the reader is referred to [10]. A real symmetric $n \times n$ matrix A is said to be positive definite if all its eigenvalues are strictly positive. It is positive semidefinite if the eigenvalues are non-negative. We use the symbol $A \succcurlyeq 0$ to denote that the matrix A is positive semidefinite. The set of real positive semidefinite $n \times n$ matrices is a convex cone. We denote this cone by \mathcal{S}_n^+ .

Definition 2.1.5 (Spectrahedron). *Let A_0, \dots, A_m be real symmetric $n \times n$ matrices. The spectrahedron is a convex set $S \subset \mathbb{R}^m$ which can be expressed as*

$$S = \{(x_1, \dots, x_m) \in \mathbb{R}^m \mid A_0 + \sum_{i=1}^m x_i A_i \succcurlyeq 0\}.$$

In other words, a spectrahedron is the intersection of an affine linear subspace with the cone \mathcal{S}_n^+ . The condition $A_0 + \sum_{i=1}^m x_i A_i \succcurlyeq 0$ is also termed as *linear matrix inequality*.

Definition 2.1.6 (Spectrahedral Shadow). *A convex set is S a spectrahedral shadow if there exists a spectrahedron S' and a linear map $\phi : \mathbb{R}^n \rightarrow \mathbb{R}^m$ such that $\phi(S') = S$.*

A semi-algebraic set in \mathbb{R}^n is the solution set of finitely many polynomial inequalities as: $\mathcal{S} = \{x \in \mathbb{R}^n \mid f_1(x) \geq 0, \dots, f_m(x) \geq 0\}$ where $f_i \in \mathbb{R}[x_1, \dots, x_n]$ for all $i \in 1, \dots, m$. These sets are important objects in real algebraic geometry and can sometimes be represented as a spectrahedral shadow. The following theorem is due to Scheiderer in [110].

Theorem 2.1.7. *Let $C \subset \mathbb{R}^n$ be the closed convex hull of a semi-algebraic set of dimension ≤ 1 . Then C has a semidefinite representation.*

By the theorem above, the convex hull C of an algebraic curve \mathcal{C} can be represented as a spectrahedral shadow. Next, we discuss linear chemical reactions and use Theorem 2.1.7 to give results on their attainable region.

2.1.3 Linear Systems

A dynamical system is said to be a *linear dynamical system* if in (4) the polynomial map is linear. A chemical reaction network is linear when the chemical complexes at each vertex are single unit species. Equivalently, the matrix Y in (3) is an identity matrix. Note that for a linear dynamical system matrix A_κ does **not** necessarily have to be the negative of the Laplacian of a graph.

Let A_κ be an $n \times n$ matrix. The linear dynamical system is then written as

$$\begin{bmatrix} \dot{x}_1 & \dot{x}_2 & \dots & \dot{x}_n \end{bmatrix} = \begin{bmatrix} x_1 & x_2 & \dots & x_n \end{bmatrix} \cdot A_\kappa$$

If A_κ is diagonalisable, the solution to such a system is given by

$$x(t) = \sum_{k=1}^n (x_0 \cdot r_k) l_k \exp(\lambda_k t) \quad (5)$$

where l_k and r_k are the left and the right eigenvectors of A_κ corresponding to the eigenvalues λ_k , respectively, and $y = x(0)$ is the initial starting point. In the theorem below we show that the convex hull of the trajectory for such a system is forward closed.

Theorem 2.1.8. *The convex hull of the trajectory of a linear dynamical system is forward closed.*

Proof. Any point c in the convex hull, $\text{conv}(\mathcal{C}) = C \subset \mathbb{R}^n$, of the trajectory \mathcal{C} can be expressed as $c = \sum_i \mu_i c_i$, where c_i are points on the trajectory, $\mu_i \geq 0$, and $\sum_{i=1}^{n+1} \mu_i = 1$ for $i \in \{1, 2, \dots, n+1\}$. First let us consider the case where the Laplacian is diagonalisable. With c as the starting point, the new trajectory, as in (5), is given by

$$x(t) = \sum_k \left(\left(\sum_i \mu_i c_i \right) \cdot r_k \right) l_k \exp(\lambda_k t) = \sum_i \mu_i \left(\sum_k (c_i \cdot r_k) l_k \exp(\lambda_k t) \right) \quad (6)$$

and right hand side is the convex sum of trajectories in S . Thus, S is forward closed.

For the dynamical system $\dot{x} = x \cdot A_\kappa$ where A_κ is not diagonalisable we perform a coordinate change by the matrix U such that the matrix UAU^{-1} is in its Jordan canonical form. It is enough to consider a single Jordan block J of the matrix UAU^{-1} . The solution of a single Jordan block form is given by $x(t) = x U^{-1} \exp(tJ) U$. Proceeding same as above with c as the starting point, we have

$$\begin{aligned} x(t) &= \left(\sum_i \mu_i c_i \right) U^{-1} \exp(tJ) U \\ &= \left(\sum_i \mu_i (x U^{-1} \exp(t_i J) U) \right) U^{-1} \exp(tJ) U \\ &= \sum_i \mu_i (x U^{-1} \exp((t_i + t)J) U) \end{aligned} \tag{7}$$

Hence, the convex hull of the trajectory of a linear dynamical system is forward closed. \square

Any convex set that contains the trajectory with a given starting point also contains the convex hull of the trajectory. Since the convex hull of the trajectory for a linear dynamical system is forward closed, it is also the attainable region.

We now turn our attention to linear chemical reaction networks. In the following theorems we give a sufficient condition on the Laplacian of the graph such that the convex hull of the trajectory is a spectrahedral shadow.

Proposition 2.1.9. *For a linear chemical reaction network if non-zero eigenvalues of the Laplacian are in rational ratio then the convex hull of the trajectory is a spectrahedral shadow.*

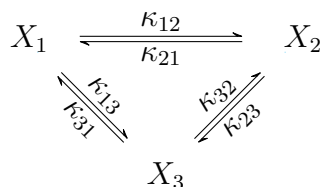
Proof. Consider a rational curve $\mathcal{C} : I \rightarrow \mathbb{R}^s$ given by $t \mapsto (t^{a_1}, t^{a_2}, \dots, t^{a_s})$ in \mathbb{R}^s over an interval $I \subset \mathbb{R}$ where a_i are positive rational numbers for $i \in \{1, 2, \dots, s\}$. For $0 \leq t \leq 1$ the image is a semialgebraic set S of dimension 1. By Theorem 2.1.7, the closure of the convex hull of S is a spectrahedral shadow.

For a linear chemical reaction network, let r be the number of eigenvalues of the Laplacian equal to 0. Let a_1, \dots, a_r be equal to 0 and a_{n-r}, \dots, a_n be in rational ratio same as the ratio of non-zero eigenvalues of the Laplacian. The trajectory of the dynamical system is the image of S under the map $\phi : S \rightarrow \mathbb{R}^n$ for $0 \leq t \leq 1$, given by the matrix whose i -th column vector is given by the transpose of the row vector $((x_0 \cdot r_i) l_i)$.

The convex hull of the trajectory of a linear chemical reaction network is the linear image of convex hull of S and therefore, it is a spectrahedral shadow. \square

We now give an example for a linear CRN such that the Laplacian has non-zero eigenvalues in rational ratio.

Example 2.1.10. The following graph illustrates the linear system of three species.



Let now $\kappa_{12} = 6, \kappa_{21} = 1, \kappa_{32} = 6, \kappa_{23} = 1, \kappa_{13} = 3, \kappa_{31} = 3$. From (3), we can express the dynamics of this system as

$$\begin{bmatrix} \dot{x}_1 & \dot{x}_2 & \dot{x}_3 \end{bmatrix} = \begin{bmatrix} x_1 & x_2 & x_3 \end{bmatrix} \cdot \begin{bmatrix} -9 & 6 & 3 \\ 1 & -2 & 1 \\ 3 & 6 & -9 \end{bmatrix}$$

The solution to such a system by equation (5) is

$$\begin{bmatrix} x_1 & x_2 & x_3 \end{bmatrix} = \begin{bmatrix} 9/4e^{-8t} - 3/2e^{-12t} + 5/4 \\ -9/2e^{-8t} + 15/2 \\ 9/4e^{-8t} + 3/2e^{-12t} + 5/4 \end{bmatrix}^\top$$

with $x_0 = [2 \ 3 \ 5]$ as the starting vector. For $t = 0$, we see that $[x_1 \ x_2 \ x_3] = [2 \ 3 \ 5]$ and as $t \rightarrow \infty$, this system tends to the stationary point $[5/4 \ 15/2 \ 5/4]$. We can replace e^{-t} by variable u such that u varies from 0 to 1 and get the parametric equation in u . After eliminating the variable u we obtain:

$$x_1 + x_2 + x_3 - 10 = 0 \text{ and } 8x_2^3 - 99x_2^2 + 324x_2x_3 + 324x_3^2 - 270x_2 - 3240x_3 + 4725 = 0. \quad (8)$$

These two equations cut out a curve. The trajectory of the linear system from x_0 to the stable point on the plane cut out by $x_1 + x_2 + x_3 - 10 = 0$ is part of that curve. This linear equation is the conservation law for the system.

Using Theorem 2.1.8 and Proposition 2.1.9, in the theorem below, we can characterise the class of linear system for which the attainable region is a spectrahedral shadow.

Theorem 2.1.11. *The attainable region of linear chemical reaction networks for which the Laplacian has non-zero eigenvalues in rational ratio is a spectrahedral shadow.*

Proof. By Proposition 2.1.9 the convex hull of the trajectory of a linear chemical reaction network for which the Laplacian has non-zero eigenvalues in rational ratio is a spectrahedral shadow. Also, for linear dynamical systems the convex hull is forward closed by Theorem 2.1.8. Therefore, the attainable region is the convex hull of the trajectory and is a spectrahedral shadow. \square

This result enables us to employ the techniques from real algebraic geometry that were originally developed to understand spectrahedral shadows to the applications associated with chemical reaction networks for the first time. In particular, we can use those techniques to understand the geometry of attainable regions. In the next subsection we discuss some experiments conducted on weakly reversible chemical reactions to understand their attainable region.

2.1.4 Weakly Reversible Chemical Reaction Networks

Following [35], a chemical reaction network is called *weakly reversible* if each connected component of the underlying graph is strongly connected. Following the usual terminology from graph theory, a directed graph is strongly connected if there is a directed path between any two of its vertices. In this section we will restrict ourselves to weakly reversible systems whose underlying graph has only one strongly connected component. These are called *one linkage class* systems. The following question naturally arises:

Question 2.1.12. *Consider a weakly reversible systems with one linkage class, and a trajectory that approaches a positive stable point. Is the convex hull of this trajectory forward closed?*

In the first version of the paper [71], we conjectured that the answer to this is affirmative. This was supported by computations in **SAGE** [108] that is explained below.

We generate a random digraph with s vertices. This graph is usually not strongly connected. Next add edges randomly between the strongly connected components to make the graph strongly connected. To each vertex associate a monomial in s indeterminates of degree $\leq d$. This represents the chemical complex as in Subsection 2.1.1. These monomials are the entries of a matrix $\Psi(x)$ and the powers in the monomials give the matrix Y in (3). We obtain the matrix A_κ by assigning random positive edge weights. These three matrices now fully specify a random dynamical system for a weakly reversible CRN.

We numerically integrate the obtained dynamical system in **SAGE** using the Runge-Kutta 4 method. In order for it to effectively integrate we keep the degree of monomials below 5. For higher values of d , one may use a higher order Runge-Kutta method for integration. This integration gives us points that lie on the trajectory C of the system. Because we want to make a statement about the convex hull of the trajectory, we construct a polytope in dimension n which is the convex hull of the points obtained. **SAGE** uses the `cdd` library for this.

In our computations, we computed 10,000 points per trajectory. The tailing points are closer to each other than the initial points, so we tailored the set of points for which we compute the convex hull C . Using a random point c in C as the initial point, for the same system we integrate again to get a new set of points on the new trajectory C' and ask if C contains the points on C' . This was done for various trajectories in \mathbb{R}^n for $n = 2, 3, 4, 5, 6$.

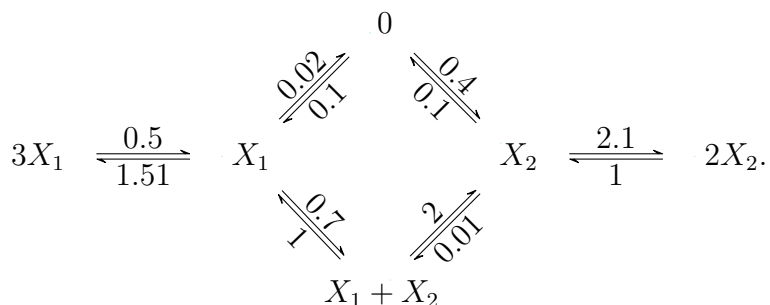
During these computations we faced various challenges. Most of these pertained to the fact that the computations were numerical, and also, to the large number of points. In particular, the computations were not always feasible in dimensions higher than $n = 6$.

It was proven in [38] and elaborated upon again in [16] that every weakly reversible chemical reaction network has at least one positive steady state. During our experiments in step one, all systems converged to a steady state. Moreover, the trajectories starting from any interior point also converged to the *same* point. This may, however, be due to the fact that the random graph we generated almost always had single stationary point. Since the computations were numerical, in higher dimensions it was difficult to compute the polytope for more than 200 points. We then double checked the points which in step one of the computations were found to not be in the convex hull, possibly due to error while

integration or computing the convex hull of floating point numbers. This led to the inclusion of additional points from \mathcal{C}' , and to a new polytope that was often larger than the first one.

In our subsequent work [30], we developed an improved algorithm (Algorithm 2.2.18) for the above procedure. This was implemented in the software **Bensolve Tools** [31]. We then found in [30, Example 8.4] that the answer to Question 2.1.12 is negative. This example is explained later in Subsection 2.4. The counterexample is in dimension three. After the posting of [30], Gheorghe Craciun and Yida Ding found another counterexample in dimension two. We thank them for their permission to include this example here.

Example 2.1.13. We consider the following reaction network



The dynamics corresponding to this network is

$$\begin{aligned}
 \dot{x}_1 &= \frac{dx_1}{dt} = 3x_1 - x_1^3 - 2x_1x_2 + 0.01x_2 + 0.1 \\
 \dot{x}_2 &= \frac{dx_2}{dt} = 2x_2 - x_2^2 - x_1x_2 + 0.7x_1 + 0.4.
 \end{aligned} \tag{9}$$

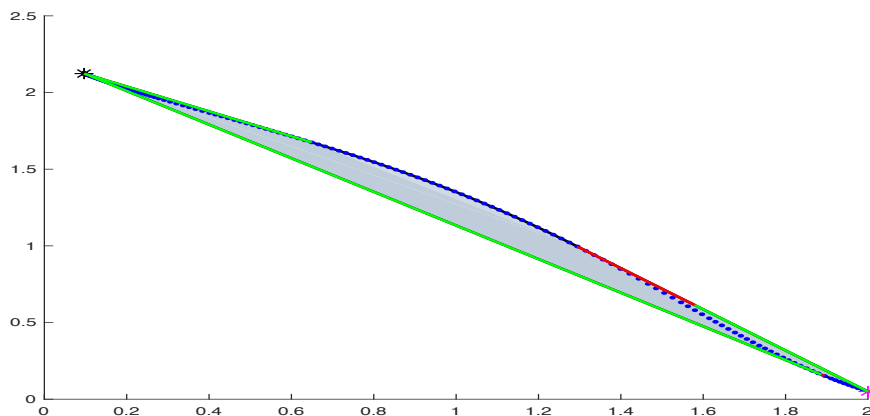


Figure 2: Trajectory and its convex hull

For the initial point $(x_0, y_0) = (2, 0.05)$, the figure above shows the trajectory in blue. The grey region is its convex hull bounded by the curve and segments coloured red and

green. We computed this using the implementation of algorithms in [30]. The red segment is the boundary of the convex hull where the vector field is pointing outwards. Any trajectory starting from a point on the line will go outside the convex hull and therefore, the convex hull is not forward closed.

2.1.5 Facial Structure

Let C be a convex set. Then $F \subset C$ is a face of C if for all points $p \in F$ whenever p is written as convex combination of points in C , those points must belong to F [118, Definition 1.1.2]. To understand convex objects using convex algebraic geometry it is imperative to study their *faces*. For parametrised curves, one such approach was suggested by Cynthia Vinzant in Section 5.2 of her PhD dissertation [118]. We give the details of this below.

Let \mathcal{C} be a parametrised curve given by $\mathbf{g} = (g_1(t), \dots, g_m(t))$ for $t \in \mathcal{D}$. Here, $\mathcal{D} \subseteq \mathbb{R}$ is a closed interval and $g_i(t)$ are univariate polynomials in t for $i \in \{1, 2, \dots, m\}$. The r -th *face-vertex set* $\text{Face}(r)$ of the curve \mathcal{C} is defined to be

$$\{(d_1, \dots, d_r) \in \mathcal{D}^r \mid \mathbf{g}(d_1), \dots, \mathbf{g}(d_r) \text{ are the vertices of a face of the convex hull of } \mathcal{C}\}.$$

For $k \leq r$, let $\{d_1, \dots, d_k\} \in \text{int}(\mathcal{D})$ be interior and $\{d_{k+1}, \dots, d_r\} \in \partial\mathcal{D}$ be the boundary points. As d_i varies in \mathcal{D} , the face-vertex set $\text{Face}(r)$ is always contained in the variety cut out by

$$\text{minors} \left(n + 1, \begin{pmatrix} 1 & \dots & 1 & 0 & \dots & 0 \\ \mathbf{g}(d_1) & \dots & \mathbf{g}(d_r) & \mathbf{g}'(d_1) & \dots & \mathbf{g}'(d_k) \end{pmatrix} \right). \quad (10)$$

This describes a variety in \mathcal{D}^r that contains the set $\text{Face}(r)$ for the convex hull of \mathcal{C} .

We apply this approach to the dynamical systems and illustrate them in the examples below. This method has not been previously used to understand the convex hulls. For any curve \mathcal{C} , let c_1, \dots, c_r be the points on the curve such that they define the vertex set of some face of the convex hull of \mathcal{C} . The equations given by

$$\text{minors} \left(n + 1, \begin{pmatrix} 1 & \dots & 1 & 0 & \dots & 0 \\ c_1 & \dots & c_r & c'_1 & \dots & c'_p \end{pmatrix} \right) \quad (11)$$

vanish where c'_i denote the tangent vector at the point c_i . We will exploit this fact and give a representation of the faces.

In our case, we only had points on the curve and this makes it difficult to express faces as a variety. For a curve in n dimension we were able to look at the following cases:

- $\text{Face}(\frac{n+1}{2})$ if n is odd.
- $\text{Face}(\frac{n}{2} + 1)$ if n is even.

The above two conditions make the matrix in (11) a square matrix and the corresponding faces are then given by the vanishing of the determinant. We used the software `Mathematica` [92] to plot the sign of the determinant for all combinations of points on the curve. We illustrate this for curves in dimensions 3, 4 and 5 below. These curves are given by the ODE's which satisfy the condition in the following lemma due to [60].

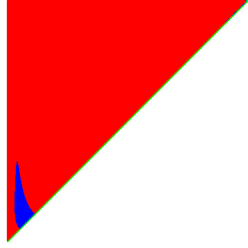


Figure 3: Face(2) of a curve in 3-space.

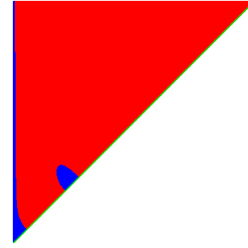


Figure 4: Face(3) with initial point as one vertex of the 3-face for a curve in 4-space.

Lemma 2.1.14. *A dynamical system $\dot{x} = f(x)$ where each f_i is a polynomial in n variables arises from a CRN with mass-action kinetics if and only if every monomial in f_i with negative coefficient is divisible by x_i for all $i \in \{1, 2, \dots, n\}$.*

By this lemma there exists a chemical reaction network for each of the systems in the examples below.

Example 2.1.15. Consider the following system with initial point as $x_0 = (10, 8, 9, 2)$,

$$\begin{aligned} \dot{x}_1 &= -2x_1^2 - 6x_1x_4 + 10x_3x_4 \\ \dot{x}_2 &= x_1^2 - 8x_2x_3 \\ \dot{x}_3 &= x_1^2 + 6x_1x_4 - 9x_3x_4 \\ \dot{x}_4 &= 8x_2x_3 - x_3x_4. \end{aligned} \tag{12}$$

The trajectory of this system lies in the stoichiometry subspace of dimension 3 and hence the convex hull has dimension 3. To find the curve of Face(2), we consider the matrix given by

$$\begin{pmatrix} 1 & 1 & 0 & 0 \\ c_{3i} & c_{3j} & c'_{3i} & c'_{3j} \end{pmatrix} \tag{13}$$

as in (11) for $i, j \in \{2, 3, \dots, 2000\}$ and $i \leq j$. We plot this in Fig. 3 where blue and red represents that the sign of the determinant is negative and positive, respectively. The separating boundary of the red and blue area represents the Face(2) of this system. \square

Next, we consider a curve with a 4-dimensional convex body.

Example 2.1.16. Consider the following system with initial point as $x_0 = (5, 8, 6, 2)$,

$$\begin{aligned} \dot{x}_1 &= -10x_1^2 + 12x_2x_3 + 6x_3^2 + 4x_3x_4 - 5x_1 \\ \dot{x}_2 &= 2x_1^2 - 8x_2x_3 + x_1 \\ \dot{x}_3 &= 8x_1^2 - 8x_2x_3 - 6x_3^2 + 5x_1 \\ \dot{x}_4 &= -8x_3x_4 + 4x_1. \end{aligned} \tag{14}$$

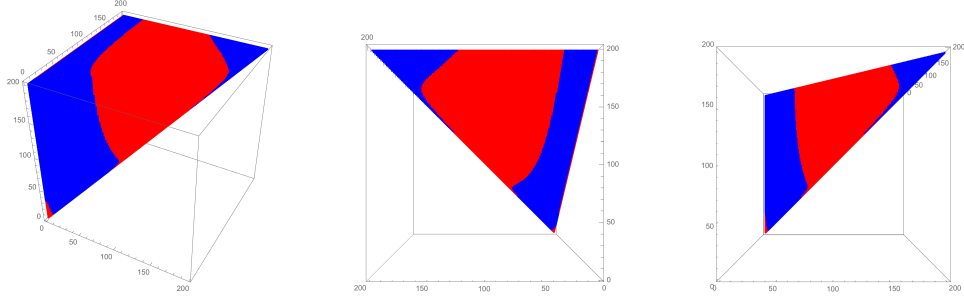


Figure 5: Face(3) of a 5-dimensional convex body

For this system we consider the representation of faces that has initial point as always one of the vertex. This is given by considering the matrix in Eq. (15) with the initial point as the boundary point

$$\begin{pmatrix} 1 & 1 & 1 & 0 & 0 \\ c_{3i} & c_{3j} & x_0 & c'_{3i} & c'_{3j} \end{pmatrix} \quad (15)$$

for $i, j \in \{2, \dots, 2000\}$ and $i \leq j$. The boundary of the red and the blue area in Fig. 4 gives the curve describing the Face(3) of the system such that every point on this curve represents the face of the convex hull such that initial point is one of the three vertices of that face. \square

The following example will depict the Face(3) of a trajectory in 5 dimensional space.

Example 2.1.17. The system given by

$$\begin{aligned} \dot{x}_1 &= 4x_3x_4x_6 - 8x_1x_6^2 + 2x_2^2 + 4x_3x_5 \\ \dot{x}_2 &= -10x_2^2x_4 + 4x_3x_4x_6 + 4x_1x_6^2 - 12x_2^2 + 6x_6^2 \\ \dot{x}_3 &= 5x_2^2x_4 - 6x_3x_4x_6 + 6x_1x_6^2 - 4x_3x_5 + 2x_6^2 \\ \dot{x}_4 &= -4x_2^2x_4 - 4x_3x_4x_6 + 2x_1x_6^2 + 2x_6^2 \\ \dot{x}_5 &= 4x_2^2x_4 + 4x_1x_6^2 - 4x_3x_5 \\ \dot{x}_6 &= x_2^2x_4 + 2x_3x_4x_6 - 14x_1x_6^2 + 12x_2^2 + 8x_3x_5 - 8x_6^2 \end{aligned} \quad (16)$$

has stoichiometry space of dimension 5. The Fig. 5 shows the sign of determinant of

$$\begin{pmatrix} 1 & 1 & 1 & 0 & 0 & 0 \\ c_{5i} & c_{5j} & c_{5k} & c'_{5i} & c'_{5j} & c'_{5k} \end{pmatrix} \quad (17)$$

for $i, j, k \in \{2, \dots, 200\}$ and $i < j < k$. \square

Using this adaptation for understanding the convex hulls is not sufficient. This approach when applied to the trajectories could not be used to give a representation of all the faces and therefore, for the curves coming from a dynamical system this adaptation could not give a general description. In the next section we develop another method to give a representation for the convex hull of trajectories. We present an algorithm and give its implementation in lower dimensions

2.2 Representing Convex Hulls

The main aim of this chapter has been to describe the geometric set which is the attainable region for a given system of ODE with respect to some initial starting point. For linear systems, the attainable region is the convex hull of the trajectory. With some assumptions we could describe this convex hull in Theorem 2.1.11 as a spectrahedral shadow. However, for non-linear system ODE it is a nontrivial task to represent the convex hull of a trajectory.

In this section we work towards representing the convex hull of a trajectory. This problem is also of general interest in convex algebraic geometry. We consider a general polynomial dynamical system as in equation (4)

$$\frac{d}{dt}x(t) = f(x(t)),$$

where $x : \mathbb{R} \rightarrow \mathbb{R}^n$ is an unknown function, and $f : \mathbb{R}^n \rightarrow \mathbb{R}^n$ is a given polynomial map. By the Picard-Lindelöf theorem, each initial value problem for (4) has a unique solution on a local interval. Although f is assumed to be polynomial, for most of the techniques we develop it suffices for f to be locally Lipschitz continuous. Any starting point $x(0)$ in \mathbb{R}^n gives rise to a unique trajectory $\mathcal{C} := \{x(t) \mid t \in [0, a) \text{ for } a > 0\}$. This curve may or may not converge to a stationary point, and its dynamics can be chaotic. We are interested in $\text{conv}(\mathcal{C})$. The convex hull of the trajectory need not be bounded and even if it is bounded, it need not be closed. In the latter case, we usually replace $\text{conv}(\mathcal{C})$ by its topological closure so that the convex hull of the trajectory becomes a compact convex body.

Since the trajectory is typically an analytic curve, we adopt numerical methods to approximate the actual convex hulls by polyhedra. We numerically integrate the equation (4) using solver `ode45`[103] in `Matlab`[93]. Using this we get the set of points \mathcal{A} on the actual trajectory.

Let $A = \text{conv}(\mathcal{A})$ be the convex hull of the points on the trajectory. The finer the sample set \mathcal{A} , the better is the approximation A to the actual convex hull $C = \text{conv}(\mathcal{C})$.

Let us first consider the planar case, i.e. when $n = 2$ in (4). We consider the pair of polynomials $f = (f_1, f_2)$ along with a starting point $y = (y_1, y_2)$ in \mathbb{R}^2 . The resulting trajectory of (4) is a plane curve \mathcal{C} that is parametrised by time t .

The boundary ∂C of the convex hull C consists of arcs on the curve \mathcal{C} and of edges that connect them. Each edge of C is a line segment between two points on \mathcal{C} . These are either points of tangency or the endpoints of the curve. This partitions ∂C into *patches*, described in general in Subsection 2.2.3. Here, k -patches are edges (for $k = 1$) and arcs (for $k = 0$).

If we had an exact algebraic representation of the curve \mathcal{C} then we could use symbolic methods to compute its bitangents and derive from this a description of ∂C . For instance, if \mathcal{C} is an algebraic curve of degree four, as in Example 2.3.2, then it has 28 bitangent lines (over \mathbb{C}) which can be computed using Gröbner bases. But, such algebraic representations are not available when we study dynamical systems. Each trajectory is an analytic curve $t \mapsto x(t)$. This parametrisation is given indirectly, namely by the differential equation (4) it satisfies.

We now assume that a polygonal approximation is given for the curve \mathcal{C} . Our input is a finite list \mathcal{A} of points $x(t_i)$ on \mathcal{C} . In our computations we solve (4) numerically using the

versatile solver `ode45` in `Matlab`. This generates the sample points \mathcal{A} which we assume to be reliably accurate. Using `ode45` also allows us to control the quality of the approximation.

Algorithm 2.2.1 computes a representation of the boundary ∂C of the convex hull C of the trajectory from a polygonal approximation \mathcal{A} of the trajectory \mathcal{C} . The key idea is the identification of long edges in A . In Subsection 2.2.3 we generalise to curves in \mathbb{R}^n . Algorithm 2.2.1 is a special case of Algorithm 2.2.18. It takes the set of points on the curve and $\delta > 0$ as the input. In step 1 it computes the convex polytope of those points. We use `Bensolve` [85] to compute the polytope in step 1 and returns the V -representation and H -representation of $A = \text{conv}(\mathcal{A})$. In the next step, a graph G is constructed with vertices as an element in the set of edges \mathcal{H} . The vertices of G are connected if the corresponding edges H_1 and H_2 have length less than the input threshold δ and have a common vertex as an end point. In step 3, we get the number of long edges and the number of cluster of short ones. From step 4 to 6 outputs the short edges and vertices corresponding to their clusters. The long edges and the arcs represented by the cluster of short edges fully describe the convex hull in the plane.

Algorithm 2.2.1. (Detection of edges and arcs for $n = 2$)

input : A list \mathcal{A} of points on a curve \mathcal{C} in \mathbb{R}^2 ; a threshold value $\delta > 0$

output: The numbers $\#_0$ and $\#_1$ of arcs and edges of $C = \text{conv}(\mathcal{C})$

For each i : list of curve points that represent the i th arc of ∂C .

List of line segments that represent the edges of C .

- 1 Compute the vertices \mathcal{V} and edges \mathcal{H} of $A = \text{conv}(\mathcal{A})$
- 2 Build a graph G with node set \mathcal{H} such that two distinct edges H_1, H_2 of A form an edge of G if $H_1 \cap H_2 \neq \emptyset$ and both H_1 and H_2 have length $\leq \delta$.
- 3 Output the number $\#_1$ of isolated nodes of G and the number $\#_0$ of remaining connected components G_i .
- 4 **foreach** *nonsingleton connected component* G_i **do**
- 5 | Output a list of curve points that are endpoints of those edges of A , that belong to G_i . This represents the i th arc of ∂C .
- 6 **end**
- 7 The edges H_j of A that correspond to isolated nodes of G represent edges of C .

In the following subsection we develop a theory on approximating the convex hull of a curve by a family of polytopes generated by sampling points on the curve. We then use this theory to generalise the above algorithm in Subsection 2.2.3.

2.2.1 Limiting Faces

We want to compute the boundary structure of C using a sequence of inner approximations by convex polytopes, each obtained as the convex hull of a path that approximates \mathcal{C} . Let B_1 and B_2 be two compact sets in \mathbb{R}^n . The *Hausdorff distance* of two compact sets B_1 and B_2 in \mathbb{R}^n is defined as

$$d(B_1, B_2) = \max \left\{ \max_{x \in B_1} \min_{y \in B_2} \|x - y\|, \max_{y \in B_2} \min_{x \in B_1} \|x - y\| \right\}.$$

A sequence $\{B_\nu\}_{\nu \in \mathbb{N}}$ of compact sets is *Hausdorff convergent* to B if $d(B, B_\nu) \rightarrow 0$ for $\nu \rightarrow \infty$.

A point x of a compact convex set B is *extremal* if it is not a proper convex combination of elements of B , that is, $\{x\}$ is a zero-dimensional face of B . Extremal points of a polytope are called *vertices*. Even if $\{B_\nu\}_{\nu \in \mathbb{N}}$ is a sequence of polytopes that Hausdorff converges to a polytope B , the limit of a convergent sequence of vertices x_ν of B_ν is not necessarily a vertex of B . For instance, consider $B_\nu = \text{conv}(\{(0, 0), (1, \frac{1}{\nu}), (2, 0)\})$. However, the converse holds as shown by the following lemma.

Lemma 2.2.2. *Let $\{B_\nu\}_{\nu \in \mathbb{N}} \rightarrow B$ be a Hausdorff convergent sequence of compact convex sets in \mathbb{R}^n . For every extremal point x of B there exist extremal points x_ν of B_ν converging to x .*

Proof. Let x be an extremal point of the limit body B . By Hausdorff convergence, there exists a sequence $\{x_\nu\}_{\nu \in \mathbb{N}}$ with $x_\nu \in B_\nu$ that converges to x . By Carathéodory's Theorem, each x_ν is a convex combination of at most $n + 1$ extremal points $v_0^\nu, v_1^\nu, \dots, v_n^\nu$ of B_ν .

Fix some $\varepsilon > 0$. Assume there is an infinite subset N of \mathbb{N} such that

$$\forall \nu \in N \quad \forall i \in \{0, 1, \dots, n\} : \|x - v_i^\nu\| \geq \varepsilon.$$

By compactness, there is a subsequence N' of N such that, for each i , the sequence $\{v_i^\nu\}_{\nu \in N'}$ converges to some v_j . Hence x is a proper convex combination of $v_0, v_1, \dots, v_n \in B$. This contradicts x being extremal in B . Therefore, for every $\varepsilon > 0$ there exists $\nu_0 \in \mathbb{N}$ such that

$$\forall \nu \geq \nu_0 \quad \exists i \in \{0, 1, \dots, n\} : \|v_i^\nu - x\| < \varepsilon.$$

In this manner we obtain a sequence $\{x_\nu\}$ of extremal points x_ν of B_ν converging to x . \square

Definition 2.2.3 (ε -Approximation). *An ε -approximation of a given curve \mathcal{C} is a finite subset $\mathcal{A}_\varepsilon \subset \mathcal{C}$ such that*

$$\forall y \in \mathcal{C} \quad \exists x \in \mathcal{A}_\varepsilon : \|y - x\| \leq \varepsilon.$$

We consider a sequence $\{\mathcal{A}_\varepsilon\}_{\varepsilon \searrow 0}$ of ε -approximations, where $\varepsilon \searrow 0$ stands for a decreasing sequence $\{\varepsilon_\nu\}_{\nu \in \mathbb{N}}$ of positive real numbers ε_ν . The polytopes $A_\varepsilon = \text{conv}(\mathcal{A}_\varepsilon)$ can be described by their facets. Our goal is to study convergent sequences of facets F_ε of A_ε in order to get information about the facial structure of the convex hull C of the curve \mathcal{C} by developing an algorithm in the Subsection 2.2.3.

Proposition 2.2.4. *Let $\{F_\varepsilon\}_{\varepsilon \searrow 0}$ be a Hausdorff convergent sequence of proper faces F_ε of the polytopes A_ε . Then its limit F is contained in an exposed face of C .*

Proof. We write the face F_ε of the polytope A_ε in the form $F_\varepsilon = \{x \in A_\varepsilon \mid y_\varepsilon^T x = \gamma_\varepsilon\}$, where $\|y_\varepsilon\| = 1$ and $y_\varepsilon^T x \leq \gamma_\varepsilon$ for $x \in A_\varepsilon$. Since \mathcal{C} is compact, the sequence $\{\gamma_\varepsilon\}$ is bounded. Choose accumulation points y and γ , respectively, of $\{y_\varepsilon\}_{\varepsilon > 0}$ and $\{\gamma_\varepsilon\}_{\varepsilon > 0}$. Since $y \neq 0$, $H := \{x \in \mathbb{R}^n \mid y^T x = \gamma\}$ is a hyperplane. By Lemma 2.2.2, any extremal point x of F is the limit of a sequence $\{x_\varepsilon\}_{\varepsilon \searrow 0}$ for x_ε a vertex of F_ε . Every vertex of F_ε belongs to C . Thus F is contained in $C \cap H$. It remains to show that C is contained in the halfspace $H_- := \{x \in \mathbb{R}^n \mid y^T x \leq \gamma\}$. Assume there exists $x \in C$ with $d := y^T x - \gamma > 0$. Then there exists a sequence $\{x_\varepsilon\}$ with $x_\varepsilon \in \mathcal{A}_\varepsilon$ converging to x and such that $\{y_\varepsilon^T x_\varepsilon - \gamma_\varepsilon\}$ converges to d . This contradicts that the halfspace $\{x \in \mathbb{R}^n \mid y_\varepsilon^T x \leq \gamma_\varepsilon\}$ contains A_ε . \square

The limit F in Proposition 2.2.4 may not be a face of C . This is shown in Figure 6 on the left. The following genericity assumptions on C will ensure that a Hausdorff convergent sequence of proper faces F_ε of the polytopes A_ε converges to a proper face F of the body C :

- (H1) Every point on the curve \mathcal{C} that is in the boundary of C is an extremal point of C .
- (H2) Every polytope face of C is a simplex.
- (H3) Intersecting the curve \mathcal{C} with a hyperplane always results in a finite set.

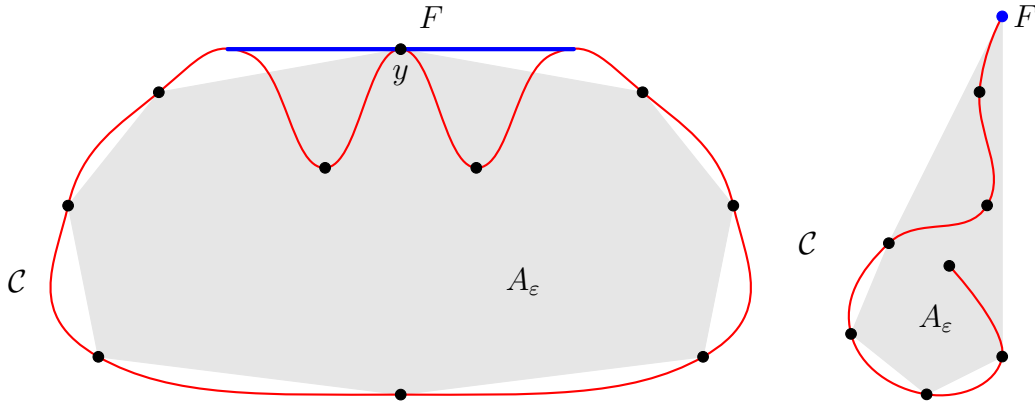


Figure 6: A Hausdorff convergent sequence of facets F_ε of A_ε need not converge to a face F of C . The face F in the left diagram contains a curve point $y \in \mathcal{C}$ which is not extremal in C . The endpoint F of the curve \mathcal{C} on the right is an exposed face of C but it is not uniquely exposed. There is no sequence of facets F_ε of A_ε that Hausdorff converges to exposed face F .

We now give a sufficient condition that proper faces of C are polytopes.

Proposition 2.2.5. *If \mathcal{C} satisfies assumption (H3), then every proper face of C is a polytope.*

Proof. A proper face F of C belongs to some hyperplane. By (H3), the set $\mathcal{C} \cap F$ is finite. Since F is a face of C , an extremal point of F is also an extremal point of C . All extremal points of C belong to \mathcal{C} , since they cannot be expressed as a proper convex combination of curve points. Thus, F is a polytope as it has only finitely many extremal points. \square

Proposition 2.2.6. *Suppose that (H1), (H2) and (H3) hold. Let $\{F_\varepsilon\}_{\varepsilon \searrow 0}$ be a Hausdorff convergent sequence of proper faces F_ε of A_ε . Then its limit F is a proper face of C .*

Proof. By Proposition 2.2.4, F is contained in an exposed face G of C , in particular, in a proper face of C . Let G be the smallest face of C containing F . By assumption (H3) and Proposition 2.2.5, G is a polytope. The extremal points of F belong to \mathcal{C} . The subset F of G is in the boundary of C . By assumption (H1), the extremal points of F are extremal points of C . Since $F \subset G \subset C$, they are also extremal points of G . Thus either $F = G$ or F is a sub-simplex of G by assumption (H2). The latter case contradicts the minimality of G . \square

Let F be a proper face of C . We seek a sequence F_ε of facets of A_ε that is Hausdorff converging to F . In general, such a sequence does not exist, even under the assumptions (H1), (H2) and (H3). We need to additionally require the face F to be *uniquely exposed*, that is, there is a uniquely defined halfspace H^+ such that $C \subset H^+$ and $F = C \cap -H^+$. For a counter example see Figure 6 (right).

Theorem 2.2.7. *Let assumption (H1) be satisfied and let F be a simplex which is a uniquely exposed face of C . Then F is the Hausdorff limit of a sequence $\{F_\varepsilon\}_{\varepsilon \searrow 0}$ of facets of A_ε .*

Proof. For $k \leq n$, denote by v_0, \dots, v_k the vertices of F . Without loss of generality, $\frac{1}{k+1} \sum_{i=0}^k v_i = 0$. The halfspace which defines F has the form $H_\gamma^+ := \{x \in \mathbb{R}^n \mid h^T x \geq \gamma\}$, where $\gamma = 0$ and $h \in \mathbb{R}^n$ with $\|h\| = 1$ is unique. We claim that for every $\delta > 0$ there exists $\gamma > 0$ such that

$$\forall y \in \mathcal{C} \setminus H_\gamma^+ \quad \exists i \in \{0, 1, \dots, k\} : \|y - v_i\| < \delta. \quad (18)$$

We prove this by contradiction. Suppose there exists $\delta > 0$ such that for all $\gamma > 0$ there exists $y \in \mathcal{C} \setminus H_\gamma^+$ with $\|y - v_i\| \geq \delta$ for all vertices v_i of F . Thus we can construct a sequence of curve points approaching $-H^+ = -H_0^+$ but maintain a distance of at least δ from each v_i . By compactness of \mathcal{C} , this sequence can be assumed to converge to some $z \in -H^+ \cap \mathcal{C} \subset F$. Since the curve point z belongs to the boundary of C , assumption (H1) ensures that z is an extremal point of C . Hence, z is a vertex of F different from v_0, \dots, v_k , a contradiction.

For $\varepsilon > 0$, we consider the linear program

$$\min \mu \quad \text{s.t.} \quad \mu h \in A_\varepsilon. \quad (19)$$

We claim that the following holds for sufficiently small $\varepsilon > 0$:

$$\text{span } h \cap \text{int } A_\varepsilon \neq \emptyset \quad (20)$$

Assume the contrary. Then, for all $\varepsilon > 0$, $\text{span } h$ and A_ε can be separated weakly by a hyperplane $H(\varepsilon) = \{x \in \mathbb{R}^n \mid h_\varepsilon^T x = \gamma_\varepsilon\}$ with $\|h_\varepsilon\| = 1$. By a compactness argument, a subsequence of $\{(h_\varepsilon, \gamma_\varepsilon)\}_{\varepsilon \searrow 0}$ converges to $(\bar{h}, \bar{\gamma})$ with $\|\bar{h}\| = 1$. The hyperplane $\bar{H} = \{x \in \mathbb{R}^n \mid \bar{h}^T x = \bar{\gamma}\}$ weakly separates $\text{span } h$ and C . Since 0 is contained in both C and $\text{span } h$, we have $\bar{\gamma} = 0$. Since 0 is a relative interior point of F , we must have $F \subset \bar{H}$. Hence, F is exposed with respect to a halfspace $\bar{H}^+ := \{x \in \mathbb{R}^n \mid \bar{h}^T x \geq \bar{\gamma}\}$ corresponding to \bar{H} . Since $H^+ \neq \bar{H}^+$, this contradicts the assumption that F is uniquely exposed with respect to H^+ .

Let μ_ε be the optimal value of (19). We have $\{\mu_\varepsilon\}_{\varepsilon \searrow 0} = 0$. We will use linear programming duality to show that, for $\varepsilon > 0$ sufficiently small, $\mu_\varepsilon h$ belongs to some facet of A_ε of the form

$$F_\varepsilon = A_\varepsilon \cap \{x \in \mathbb{R}^n \mid y_\varepsilon^T x = \mu_\varepsilon\} \quad \text{where } h^T y_\varepsilon = 1.$$

Indeed, the linear program dual to (19) is

$$\max \eta \quad \text{s.t.} \quad M_\varepsilon^T y - e\eta \geq 0 \quad \text{and} \quad h^T y = 1, \quad (21)$$

where M_ε is the matrix with columns \mathcal{A}_ε and $e = (1, \dots, 1)^T$ is the all-one vector. Let $(y_\varepsilon, \eta_\varepsilon)$ denote an optimal solution of (21). By duality, $\mu_\varepsilon = \eta_\varepsilon$. We conclude that F_ε is a face of A_ε .

To see that F_ε is even a facet of A_ε , we replace (19) and (21) by the pair of dual problems

$$\min 0\mu \quad \text{s.t.} \quad \mu h \in A_\varepsilon, \quad (22)$$

$$\max \eta \quad \text{s.t.} \quad M_\varepsilon^T y - e\eta \geq 0 \quad \text{and} \quad h^T y = 0. \quad (23)$$

Using complementary slackness, we conclude from (20) that $(y, \eta) = (0, 0)$ is the unique optimal solution of (23). Hence the set of optimal solutions of (21) is bounded, and we can choose $(y_\varepsilon, \eta_\varepsilon)$ to be a vertex. At least n linearly independent inequalities in (21) hold with equality at $(y, \eta) = (y_\varepsilon, \eta_\varepsilon)$. These correspond to n affinely independent points in \mathcal{A}_ε , all belonging to the hyperplane $\{x \in \mathbb{R}^n \mid y_\varepsilon^T x = \mu_\varepsilon\}$. This shows that F_ε is a facet of A_ε .

From (18), we conclude that, for sufficiently small $\varepsilon > 0$, the point $\mu_\varepsilon h \in F_\varepsilon$ (which approaches the mean of the vertices of F) can be represented only by elements $y \in \mathcal{A}_\varepsilon$ with $\|y - v\| < \delta$ for some vertex v of F . Since F is a simplex, each vertex v of F is used in this representation. Hence, for each vertex v of F there exists a vertex y of F_ε with $\|y - v\| < \delta$.

We claim that, if $\varepsilon > 0$ is sufficiently small then for every vertex y of F_ε there exists a vertex v of F with $\|y - v\| < \delta$. Assume the contrary. Then, by (18), for any small $\varepsilon > 0$, there is a vertex y_ε of F_ε with $y_\varepsilon \in \mathcal{C} \cap H_\gamma^+$. By compactness of \mathcal{C} , we may assume that $\{y_\varepsilon\}_{\varepsilon \searrow 0}$ converges to some $\bar{y} \in \mathcal{C} \cap H_\gamma^+$. By Proposition 2.2.4, $\text{conv}(F \cup \{\bar{y}\})$ belongs to an exposed face of C . Since $\bar{y} \notin -H^+$, this contradicts the assumption that F is uniquely exposed.

We conclude that for every $\delta > 0$ we find $\varepsilon_0 > 0$ such that $d(F_\varepsilon, F) < \delta$ for all $0 < \varepsilon \leq \varepsilon_0$. Hence, the simplex face F of C is the Hausdorff limit of the sequence $\{F_\varepsilon\}_{\varepsilon \searrow 0}$, as desired. \square

Remark 2.2.8. In the proof of Theorem 2.2.7, we construct a sequence $\{F_\varepsilon\}_{\varepsilon \searrow 0}$ of facets of A_ε whose vertices converge to the vertices of F . This is stronger than Hausdorff convergence.

2.2.2 Convex Hulls in Bensolve

To represent the convex hull of the curve we compute the convex hull of an ε -approximation of a curve \mathcal{C} . There are many methods and implementations for convex hulls. We used the software `Bensolve Tools` [31]. We next discuss this software, its underlying methodology, and how we apply it. `Bensolve` [85] is a solver for multiple objective linear programs (MOLP). In `Bensolve Tools` it is utilised to perform many polyhedral calculus operations, among them convex hull. The key insight behind this is that multiple objective linear programming is equivalent to polyhedral projection [84]. Convex hull computation is a special case of polyhedral projection. This follows from [124, Chapter 1]:

Lemma 2.2.9. *The convex hull of a finite set $\mathcal{V} = \{v^1, v^2, \dots, v^k\}$ in \mathbb{R}^n is the polytope*

$$\text{conv}(\mathcal{V}) = \{y \in \mathbb{R}^n \mid \exists \lambda \in \mathbb{R}^k : \lambda \geq 0, e^T \lambda = 1, y = V\lambda\},$$

where $V \in \mathbb{R}^{n \times k}$ is the matrix with set of columns \mathcal{V} and $e = (1, \dots, 1)^T$ denotes the all-one vector of length k . Hence, the convex hull of \mathcal{V} is a projection into \mathbb{R}^n of the polytope

$$Q = \{(y, \lambda) \in \mathbb{R}^n \times \mathbb{R}^k \mid \lambda \geq 0, e^T \lambda = 1, y = V\lambda\}.$$

To understand the computation of $\text{conv}(\mathcal{V})$ from Q , let us turn to an arbitrary polyhedral projection problem. By Fourier-Motzkin Elimination, every linear projection of a polyhedron is a polyhedron. This leads to the concept of a *P-representation* of a polyhedron. Let $M \in \mathbb{R}^{n \times k}$, $B \in \mathbb{R}^{m \times k}$, $a \in \mathbb{R}^m$ be given. The triple (M, B, a) represents the polyhedron

$$P = \{Mx \mid Bx \geq a\} = \{y \in \mathbb{R}^n \mid \exists x \in \mathbb{R}^k : y = Mx, Bx \geq a\}. \quad (24)$$

In what follows, we restrict to polytopes (bounded polyhedra). Given a P-representation (24) of a polytope, the polyhedral projection problem is to compute an irredundant *V-representation*, i.e. a representation as convex hull of finitely many points, and an irredundant *H-representation*, i.e. a representation by finitely many linear inequalities (cf. [124]).

Given a triple (M, B, a) as above, the associated *multiple objective linear program* is

$$\min Mx \quad \text{s.t.} \quad Bx \geq a \quad (\text{MOLP})$$

The *upper image* of the program (MOLP) is the polyhedron

$$\mathcal{P} = \{y \in \mathbb{R}^n \mid \exists x \in \mathbb{R}^k : y \geq Mx, Bx \geq a\}. \quad (25)$$

A solution of (MOLP) consists of both an irredundant V- and H-representation of \mathcal{P} . This concept of solution can be used to address the polyhedral projection problem as follows:

Proposition 2.2.10 (cf. [84, Theorem 3]). *The solution of the MOLP*

$$\min \begin{pmatrix} M \\ -e^T M \end{pmatrix} x \quad \text{s.t.} \quad Bx \geq a, \quad (26)$$

yields an irredundant V- and H-representation of the P-represented polyhedron (24).

The upper image of the MOLP in (26) is the polyhedron

$$\bar{\mathcal{P}} = \{(y, z) \in \mathbb{R}^n \times \mathbb{R} \mid y \geq Mx, z \geq -e^T Mx, Bx \geq a\}. \quad (27)$$

Corollary 2.2.11. *The polytope $P = \{Mx \mid Bx \geq a\}$ is obtained from $\bar{\mathcal{P}}$ by setting*

$$P = \{y \in \mathbb{R}^n \mid \exists z : (y, z) \in \bar{\mathcal{P}}, e^T y + z = 0\}.$$

An irredundant V-representation of P derives from the set of vertices of $\bar{\mathcal{P}}$ by deleting their last components. An H-representation of $\bar{\mathcal{P}}$ gives an H-representation of P by adding the equation $z = -e^T y$.

Bensolve computes a V-representation and an H-representation of the upper image (27) using Algorithm 2.2.12. This is a version of *Benson's algorithm*. It applies to upper images satisfying $\mathcal{P} \subseteq y + \mathbb{R}_{\geq 0}^n$ for some $y \in \mathbb{R}^n$. This version suffices for handling projections of polytopes including the representation of the convex hull of finitely many points. Since the algorithm is numerical, we work with a prescribed tolerance $\varepsilon > 0$. The output is an ε -*approximation* to the upper hull \mathcal{P} , i.e. it is a polyhedron \mathcal{O} satisfying $\varepsilon e + \mathcal{O} \subseteq \mathcal{P} \subseteq \mathcal{O}$.

Algorithm 2.2.12. (Benson’s algorithm)

input : (MOLP) given by the matrices M , B and vector a ; a tolerance $\varepsilon \geq 0$.

output: ε -approximated V-representation \mathcal{V} and H-representation \mathcal{H} of \mathcal{P} in (25).

```

1  $T \leftarrow \emptyset$ 
2 Compute the H-representation  $\mathcal{H}$  of a polyhedral outer approximation of  $\mathcal{P}$  having
   the same recession cone as  $\mathcal{P}$ . Also compute the corresponding V-representation  $\mathcal{V}$ 
3 while  $(\mathcal{V} \setminus T) \neq \emptyset$  do
4   | Choose a vertex  $v \in \mathcal{V} \setminus T$ 
5   | Compute the solution  $t^*$  of the linear program  $\min \{t \mid v + te \in \mathcal{P}\}$ 
6   | Compute the solution  $(u^*, w^*)$  of the dual linear program
   |    $\max \{a^T u - v^T w \mid B^T u = M^T w, e^T w = 1, w \geq 0, u \geq 0\}$ 
7   | if  $t^* \geq \varepsilon$  then
8   |   | Refine  $\mathcal{H}$  by adding  $\{y \mid (w^*)^T y \geq a^T u^*\}$  to the description
9   |   | Update  $\mathcal{V}$  by performing vertex enumeration on  $\mathcal{H}$ 
10  | else
11  |   |  $T \leftarrow T \cup \{v\}$ 
12  | end
13 end

```

One starts with an initial outer polyhedral approximation of \mathcal{P} . Both an H-representation and a V-representation are stored. Until the tolerance ε is reached, each iteration adds a linear inequality to refine the outer approximation of \mathcal{P} . An iteration step starts by choosing a vertex v of the current polyhedron. The V-representation is updated after adding an inequality. From v one moves in direction $e = (1, \dots, 1)^T$ to the boundary point $y = v + t^*e$ of \mathcal{P} . To this end, a linear program has to be solved. The solution of the dual linear program yields the desired linear inequality which cuts off v and holds with equality in y . Algorithm 2.2.12 terminates and computes both V- and H-representation of an ε -approximation of \mathcal{P} . For the computations we use the *dual Benson algorithm* [44]. It is related to Benson’s algorithm by duality and provides an inner approximation scheme for the upper hull \mathcal{P} .

We employ **Bensolve** for computing a polyhedral approximation of the convex hull of a smooth curve \mathcal{C} in \mathbb{R}^n . This is done by computing the convex hull of a sufficiently large finite subset \mathcal{A} of \mathcal{C} . The output gives both an irredundant H- and V-representation of an inner ε -approximation $\mathcal{C}_{\mathcal{A}}$ of $\text{conv}(\mathcal{A})$, and this is our approximation to $\text{conv}(\mathcal{C})$. All facets and all vertices of $\mathcal{C}_{\mathcal{A}}$ are known after such a computation. The output also contains the *incidence matrix* $I_{\mathcal{A}}$ for facets and vertices of $\mathcal{C}_{\mathcal{A}}$ and the *adjacency matrix* $A_{\mathcal{A}}$ for vertices of $\mathcal{C}_{\mathcal{A}}$.

The algorithm is output sensitive. This means that the runtime is mainly dependent on the number of facets and vertices of the P-represented polytope and the projection dimension. In particular, the number of sampled points in the interior of $\mathcal{C}_{\mathcal{A}}$ only marginally influences the computation time. Another advantage of Benson’s algorithm is the possibility to set the parameter ε . This feature enables the approximative representation of highly complex convex hulls in a reasonable amount of time. In addition, the process can be aborted at any point while still providing an outer approximation. For sufficiently small values of ε , we

obtain exact solutions, up to numerical inaccuracy of the vertex enumeration routine.

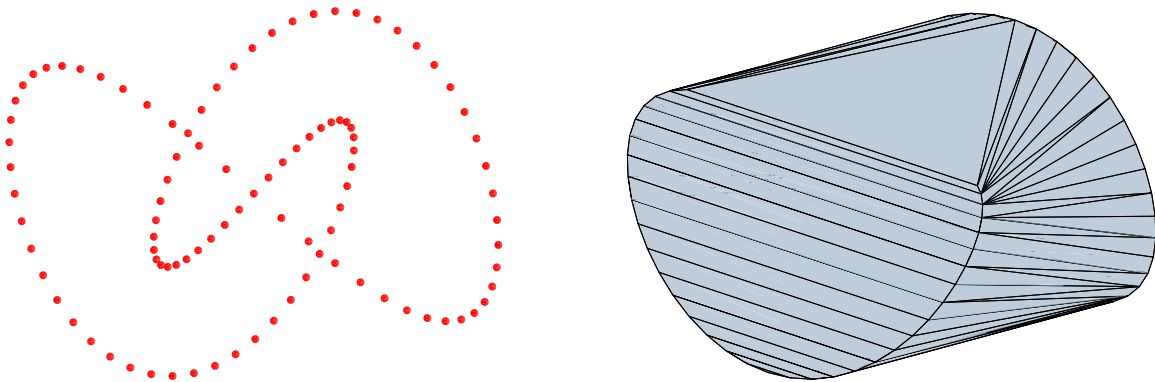


Figure 7: A sample of points (left) from a space curve and its convex hull (right)

Example 2.2.13. Let \mathcal{C} be the trigonometric space curve parametrically given by

$$\theta \mapsto (\cos(\theta), \sin(2\theta), \cos(3\theta)). \quad (28)$$

Its convex hull $C = \text{conv}(\mathcal{C})$ is shown in [102, Figure 1]. We select N sample points by taking

$$\mathcal{A} = \left\{ \left(\cos\left(\frac{2k\pi}{N}\right), \sin\left(\frac{4k\pi}{N}\right), \cos\left(\frac{6k\pi}{N}\right) \right) \mid k = 0, \dots, N-1 \right\}. \quad (29)$$

Using `Bensolve`, as described above, we can compute irredundant V- and H-representations of the inner approximation $\mathcal{C}_{\mathcal{A}}$ of the polytope $\text{conv}(\mathcal{A})$ for various values of N and with specified accuracy ε . For instance, let $N = 100$ and $\varepsilon = 10^{-9}$. The sample (29) is shown on the left in Figure 7. Its convex hull is the polytope $\mathcal{C}_{\mathcal{A}}$ on the right in Figure 7. It has 70 vertices and 102 facets, so, by Euler's relation, it has 170 edges. Thus the incidence matrix $I_{\mathcal{A}}$ is of size 102×70 and has 340 nonzero entries. The 70×70 adjacency matrix $A_{\mathcal{A}}$ also has 340 nonzero entries. The polytope $\mathcal{C}_{\mathcal{A}}$ in Figure 7 already looks like [102, Figure 1] and Figure 8. The picture of $\mathcal{C}_{\mathcal{A}}$ reveals the edge surfaces of C and the two triangles in ∂C . The identification of such patches from the `Bensolve` output is our theme in the next subsection.

2.2.3 Boundary of Convex Hulls

Let C be a full-dimensional compact convex body in \mathbb{R}^n . The boundary of ∂C is an $(n-1)$ -dimensional set whose subset ∂C_{sm} of smooth points is dense. We shall stratify ∂C_{sm} into finitely many manifolds we call *patches*. Each patch is an $(n-k-1)$ -dimensional family of k -faces of C . For a typical convex body of dimension $n = 3$, the boundary is comprised of surfaces of extreme points ($k = 0$), curves of edges ($k = 1$), and finitely many facets ($k = 2$).

For the general definition, we use the concept of the normal cycle of a convex body. Let \mathbb{S}^{n-1} denote the unit $(n-1)$ -sphere. Following [53, eqn (10)], the *normal cycle* of C equals

$$N(C) = \left\{ (u, v) \in \mathbb{R}^n \times \mathbb{S}^{n-1} : v \cdot (u - u') \geq 0 \text{ for all } u' \in C \right\}.$$

If ∂C is smooth then $N(C)$ is a Legendrian submanifold of dimension $n - 1$. If C is not smooth then we can approximate C by nearby smooth convex bodies C_ε , for $\varepsilon > 0$. By [53, Theorem 3.1], the normal cycle $N(C)$ is the Hausdorff limit of the manifolds $N(C_\varepsilon)$ for $\varepsilon \rightarrow 0$. The normal cycle $N(C)$ is pure $(n - 1)$ -dimensional, and its smooth points are dense.

There are several other ways of defining the normal cycle. The one we like best uses the dual convex body C^\vee . Assuming the origin is in the interior of C , we make the identification

$$N(C) = \{ (u, v) \in \partial C \times \partial C^\vee : v \cdot (u - u') \geq 0 \text{ for all } u' \in C \}. \quad (30)$$

The normal cycle comes naturally with two surjective maps

$$\pi_1 : N(C) \rightarrow \partial C, (u, v) \mapsto u \quad \text{and} \quad \pi_2 : N(C) \rightarrow \partial C^\vee, (u, v) \mapsto v. \quad (31)$$

Let $\mathcal{E} \subseteq \partial C^\vee$ be the set of exposed points of C^\vee . We have $v \in \mathcal{E}$ if and only if there exists $u \in C$ such that $\pi_1^{-1}(u) = \{(u, v)\}$.

Definition 2.2.14 (Patches). *A subset ψ of $N(C)$ with $\pi_2(\psi) \subset \mathcal{E}$ is called a patch if ψ is a connected differentiable manifold, $\dim(\pi_1(\psi)) = n - 1$, the fibers of π_2 vary continuously in the Hausdorff metric, and ψ is maximal with these properties.*

Definition 2.2.15 (k -Patches). *Let $\psi \subset N(C)$ be a patch. We say that ψ is a k -patch if $\dim(\pi_2(\psi)) = n - k - 1$.*

This means that $\pi_2(\psi)$ is an $(n - k - 1)$ -dimensional manifold of exposed points of C^\vee , and these exposed points support continuously varying k -faces of C .

Remark 2.2.16. If the trajectory \mathcal{C} is algebraic then its convex hull C is semialgebraic. Also the normal cycle $N(C)$ and all its patches ψ are semialgebraic. This follows from Tarski's theorem on quantifier elimination, and we find that the number of patches of C is finite.

We believe that finiteness holds more generally for compact trajectories. But we do not yet know the precise statement. Real analytic geometry is much more delicate than real algebraic geometry. For instance, the family of semianalytic sets is not closed under projection. We refer to [4] for a recent account. The concept of \mathbb{C} -semianalytic sets, introduced in [4] and named after Cartan, could be the appropriate one for our setting. One might hope that the convex trajectories and their patches are \mathbb{C} -semianalytic when f in (4) is polynomial.

Example 2.2.17. Consider the dynamical system

$$\begin{bmatrix} \dot{x}_1 & \dot{x}_2 & \dot{x}_3 \end{bmatrix} = \begin{bmatrix} 2x_2 & 12x_1^3 - 5x_2 + x_3 & -24x_1^2x_2 + 6x_2 \end{bmatrix}$$

with the starting point at $[0, 0.1, 0]$. Its convex hull is shown in the Fig. 8. This convex body has six patches. There are two 2-patches, namely the two triangles. Each of these 2-patches are surrounded by the four 1-patches. The 1-dimensional patches are separated by the curve in blue and the plane.

We now come back to the problem of computing the convex hull boundary in general. The planar case was dealt with Algorithm 2.2.1. We start with the ε -approximation of the actual curve. For the algorithm we assume the conditions (H1), (H2) and (H3) on the curve. Such a curve is called simplicial. Our goal is to identify the patches of the convex hull of the curve \mathcal{C} . The following algorithm computes the patches for $n \geq 3$.

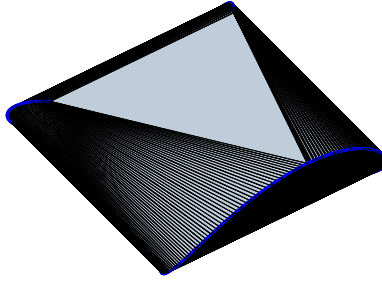


Figure 8: Patches on the convex hull.

Algorithm 2.2.18. (Detection of patches for $n \geq 3$)

input : Finite list \mathcal{A} of points on a curve \mathcal{C} in \mathbb{R}^n ; a threshold value $\delta > 0$

output: For each $k \geq 1$: the expected number $\#_k$ of k -patches of $C = \text{conv}(\mathcal{C})$

For each i : list of k -polytopes that represent the k -patch G_i

- 1 Compute vertices \mathcal{V} , facets \mathcal{H} , incidence list $I_{\mathcal{A}}$ and adjacency list $A_{\mathcal{A}}$ of $\text{conv}(\mathcal{A})$
- 2 Build a graph G with node set \mathcal{H} as follows: two facets H_1, H_2 form an edge if their unit normals $v(H_i)$ have distance $\leq \delta$, $\dim(H_1 \cap H_2) = n - 2$, and $d(H_1, H_2) \leq \delta$.
- 3 **foreach** *connected component* G_i *of the graph* G **do**
- 4 **foreach** *facet* $H \in G_i$ **do**
- 5 Find representatives $U = \{u_0, \dots, u_k\}$ of the δ -proximity clusters
- 6 of vertices of H such that $F = \text{conv}(U)$ is a k -face of $\text{conv}(\mathcal{A})$
- 7 Associate the tuple $(u_0, \dots, u_k; v)$ with that node of G_i
- 8 **end**
- 9 G_i represents a k -patch of C if k is the largest index encountered in the loop above
- 10 Adjust all tuples with smaller indices found in step 7 to that common value of k
- 11 **end**
- 12 Output $(\#_1, \dots, \#_{n-1})$, where $\#_k$ is the number of graphs G_i representing k -patches

The Algorithm 2.2.18 takes the ε -approximation of the curve \mathcal{C} , and a positive δ as the input. It uses **Bensolve Tools** to compute the convex hull of the points. In the next step, similar to Algorithm 2.2.1, it builds a graph G where vertices are the facets of the polytope $A = \text{conv}(\mathcal{A})$. Each facet H comes with its unit normal vector $v(H)$. Step 2 reflects the conditions in the definition of patches. For instance, the criterion $d(H_1, H_2) \leq \delta$, stating that H_1 and H_2 are close in Hausdorff distance, reflects the continuous variation of k -faces. The exposed points in $\pi_2(\psi) \subset \mathcal{E}$ are represented by the vectors $v(H_i)$. The requirement that they are δ -close along the edges of G is our discrete version of the smoothness of ψ . In step 3 we identify the connected components of G , and these represent the patches of C .

The inner loop in steps 5–7 reflects our results in Subsection 2.2.1. By Theorem 2.2.7, every k -face of C is approximated by a facet $H \in G$. Here, for each vertex of the k -face, the algorithm chooses a nearby vertex u_i of H . In the loop between steps 4 and 8, it can happen that a δ -proximity cluster corresponds to more than one vertex of the k -face. This happens

for k -faces with an edge shorter than δ . For that reason, we take the maximum in step 9. In a connected component of the graph not all facets may be classified as the same dimensional face after step 9. They represent k -faces of C , but step 5 identifies less than $k + 1$ proximity clusters at the fixed tolerance level δ . For such facets, step 10 adds additional points u_i from an existing cluster to get up to the correct value of k for that patch.

We implemented this algorithm for $n = 3$ and $n = 4$. A detailed theoretical analysis of this algorithm is left for future work. The task is to identify the precise conditions under which the output detects the true patches when applied to ε -approximations with $\varepsilon \rightarrow 0$. The code for dimensions 2, 3 and 4 is made available at

$$\text{http://tools.bensolve.org/trajectories.} \tag{32}$$

Example 2.2.19. We illustrate the output of Algorithm 2.2.18 when C is a random trigonometric curve of degree six in \mathbb{R}^4 and $\mathcal{A} \subset C$ is a finite approximation. Figure 9 shows the graph G . Each node in G is a face of the polytope $\text{conv}(\mathcal{A})$. We find $\#_3 = 0$. There are $\#_1 = 3$ patches for $k = 1$, represented by the three connected components of G on the right in Figure 9. These three connected graphs encode surfaces worth of edges. The number of patches for $k = 2$ is $\#_2 = 2$. These two components of G are shown on the left in Figure 9. Each node represents a triangle face of $\text{conv}(C)$. So, the picture on the left shows two curves worth of triangle faces in the boundary of our 4-dimensional convex body.



Figure 9: Two 2-patches (left) and three 1-patches (right) in the boundary of a 4-dimensional convex body, obtained as the convex hull of a trigonometric curve of degree six. The picture shows the graph G , with five connected components G_i , that is computed by Algorithm 2.2.18.

Trigonometric curves also arise from linear dynamical systems. Here (4) takes the form $\dot{x} = Ax$, where A is a real $n \times n$ -matrix. We tested our convex hull algorithms on linear systems for $n = 3, 4$. We sampled matrices A with no real eigenvalues. This ensures that the trajectories are bounded in \mathbb{R}^n . They can be written in terms of trigonometric functions. It was shown in Theorem 2.1.8 that convex hull of every trajectory of a linear dynamical system is forward-closed. Thus, computing the convex hull is equivalent to computing the attainable region.

Consider the *generalised moment curve*, whose convex hull was studied by Smilansky [114, Theorem 1]. Let $z = (1, 0, 1, 0)$ and consider the linear dynamical system given by

$$A = 2\pi \cdot \begin{pmatrix} 0 & -p & 0 & 0 \\ p & 0 & 0 & 0 \\ 0 & 0 & 0 & -q \\ 0 & 0 & q & 0 \end{pmatrix},$$

where p and q are relatively prime positive integers. The trajectory is the closed curve

$$x(t) = (\cos(2\pi pt), \sin(2\pi pt), \cos(2\pi qt), \sin(2\pi qt)).$$

We can restrict to $0 \leq t < 1$. The convex hull of the curve is a 4-dimensional convex body. By [114, Theorem 1], there are no 3-dimensional faces. Assuming $p, q \geq 3$, there are two 1-patches and two 2-patches. The explicit description in [114] makes this a useful test case.

Example 2.2.20 ($p = 3, q = 4$). The line segment $\text{conv}\{x(s), x(t)\}$ is an edge if and only if

$$\frac{1}{4} < |s - t| < \frac{1}{3} \quad \text{or} \quad \frac{2}{3} < |s - t| < \frac{3}{4}.$$

In addition to this surface of edges, there are two curves of 2-faces, namely the triangles

$$\text{conv}\left\{x(t), x\left(t + \frac{1}{3}\right), x\left(t + \frac{2}{3}\right)\right\} \quad \text{for } 0 \leq t < \frac{1}{3}$$

and the squares

$$\text{conv}\left\{x(t), x\left(t + \frac{1}{4}\right), x\left(t + \frac{1}{2}\right), x\left(t + \frac{3}{4}\right)\right\} \quad \text{for } 0 \leq t < \frac{1}{4}.$$

These are all the exposed faces of the convex hull of the trajectory. Even though the curve is not simplicial, Algorithm 2.2.18 works well, and we verified Smilansky's findings [114] using our software.

For a space curve, an *edge surface* is ruled irreducible surface that forms the boundary of the convex hull of the curve. It is the union of all stationary bisecants. A *tritangent plane* is a plane that is tangent to the curve at 3 or more points. In [102] the authors proved the following theorem for a smooth compact space curve.

Theorem 2.2.21. *Let \mathcal{C} be a general smooth compact curve of degree d and genus g in \mathbb{R}^3 . The algebraic boundary ∂C of its convex hull C is the union of the edge surface and the tritangent planes. The edge surface is irreducible of degree $2(d - 3)(d + g - 1)$, and the number of complex tritangent planes equals $8\binom{d+g-1}{3} - 8(d + g - 4)(d + 2g - 2) + 8g - 8$.*

We will now report on the experiments conducted using our implementation on random trigonometric space curves and compare our findings with the above result. The trigonometric space curves can be represented as:

$$x_j(t) = \sum_{k=1}^d A_{jk} \cdot \cos(2\pi kt) + \sum_{k=1}^d B_{jk} \cdot \sin(2\pi kt) + C_j \quad \text{for } j = 1, \dots, n.$$

The coefficients of \cos and \sin can be written as $n \times d$ matrices A and B . The matrix C is a column matrix of constants. If A , B , and C are general matrices then the resulting curve is algebraic curve of degree $2d$. We randomly sampled the matrices A , B , and C . We used our implementation on this sample of trigonometric curves for various degrees and computed the number of patches and tritangent planes. Table 1 records the data for curves of various degree. In the first row we record the maximum number of one dimensional patches observed for each degree. In the second row we record the maximum number of real tritangent planes observed in the boundary of the convex hull of the sampled trigonometric curves. For each degree the fourth and the fifth row gives the degree of the edge surface and number of complex tritangents for a generic curve computed using the previous theorem.

degree $2d$	6	8	10	12	14	16	18	20	22	24	26	28
max $\#_1$	10	16	24	26	30	32	35	38	41	44	46	50
max $\#_2$	6	10	16	17	20	21	24	26	28	30	34	34
edge surface	30	70	126	198	286	390	510	646	798	966	1150	1350
tritangents	8	80	280	672	1320	2288	3640	5440	7752	10640	14168	18400

Table 1: Census of random trigonometric curves in 3-space

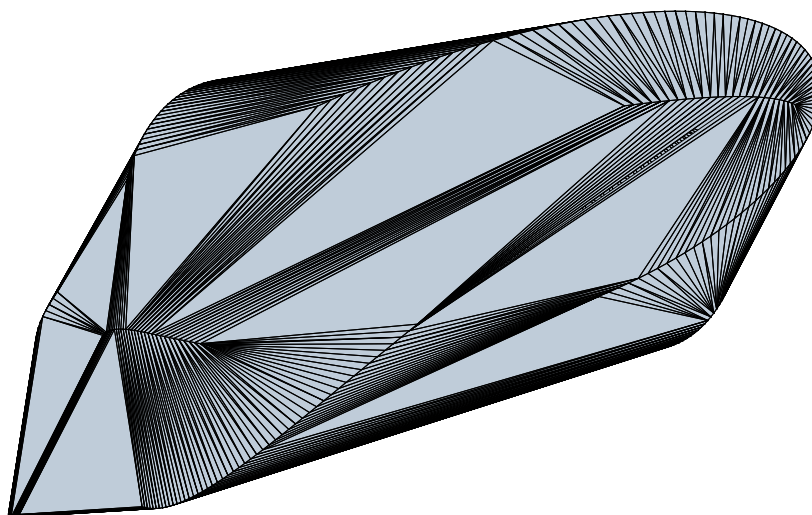


Figure 10: The convex hull of a trigonometric curve of degree 14 in 3-space. The boundary of this convex body consists of triangles and of 1-patches in a ruled surface of degree 286.

Example 2.2.22 ($2d = 14$). We consider the curve defined by the following 3×7 matrices

$$A = \begin{pmatrix} 0.28561 & -0.024204 & -0.07664 & 0.43593 & 0.15244 & -0.24464 & 0.41538 \\ -0.37439 & -0.30106 & 0.32118 & 0.38410 & 0.29990 & -0.14990 & -0.45481 \\ -0.17997 & -0.16046 & -0.23522 & 0.47912 & -0.08084 & 0.19628 & 0.46895 \end{pmatrix}$$

$$\text{and } B = \begin{pmatrix} -0.39109 & 0.06742 & -0.12451 & 0.44073 & -0.20822 & -0.03646 & -0.01034 \\ 0.48646 & 0.38580 & -0.13216 & 0.36184 & 0.30633 & -0.14131 & 0.48650 \\ -0.15326 & 0.32591 & 0.02569 & 0.23351 & -0.34972 & 0.04772 & 0.42441 \end{pmatrix},$$

along with the vector $C = (0.39768 \ 0.42346 \ 0.23797)^T$. The convex hull of this curve has 20 triangle facets. It is shown in Figure 10. The planes that define the triangles are tritangent planes. The curve is generic and has 1320 tritangent planes over \mathbb{C} . The nonlinear part of the boundary is the edge surface [102]. This is an irreducible ruled surface of degree 286.

2.3 Forward Closed Convex Sets

In previous section we numerically computed and represented the convex hulls of curves and trajectories. The attainable region is a convex hull that is also forward closed. In this section, we answer the question if the convex hull, given as the output of Algorithm 2.2.18, is forward closed. To do that we check if the vector field on the boundary of the convex hull points outside or inside. If it points inside at all points then the convex hull is forward closed. Let v be an outward pointing unit normal vector at the face of C containing the point u . We say that the right hand side of (4) *points inward* at $u \in \partial C$ if $f(u) \cdot v \leq 0$. It *points outward* otherwise.

First we note that every algebraic curve can be locally represented as a trajectory of a polynomial dynamical system. Let \mathcal{C} be an algebraic curve in \mathbb{R}^n and let y be a regular point on \mathcal{C} . We construct an appropriate vector field $f(x)$ on \mathbb{R}^n as follows. Let g_1, g_2, \dots, g_{n-1} be polynomials in $x = (x_1, x_2, \dots, x_n)$ that cut out the curve \mathcal{C} locally near its point y . Let J denote their Jacobian matrix. Thus, J is the $(n-1) \times n$ matrix whose entry in row i and column j is the partial derivative $\partial g_i / \partial x_j$. Let J_i be $(-1)^{i+1}$ times the determinant of the submatrix of J obtained by deleting the i th column. Fix the vector of polynomials $f = (J_1, J_2, \dots, J_n)^T$. Locally at y , the kernel of J is the line spanned by the vector f . This follows from Cramer's rule, and it implies that $f(y)$ is a tangent vector to the curve \mathcal{C} at its point y . The system then we are interested in is the dynamics given by $\dot{x} = f(x)$ when the starting point is $y \in \mathcal{C}$.

2.3.1 Planar Case

We now first look at the planar case, i.e $n = 2$. The boundary of the convex hull C is composed of arcs and long edges given by Algorithm 2.2.1. However, if the curve \mathcal{C} is algebraic, we can explicitly compute the boundary by computing the bitangents of the curve. For each point y on an arc of C , the vector $f(y)$ is tangent to the curve, so there is nothing to be checked at the arcs. To decide whether C is forward closed with respect to the dynamics (4), we must examine the edges of C . Consider the relative interior points of an edge joining the points p and q on the curve,

$$y = \lambda \cdot p + (1 - \lambda) \cdot q \quad \text{where } 0 < \lambda < 1. \quad (33)$$

The following 2×2 determinant is a polynomial in the parameter λ :

$$g(\lambda) = \det(f(y), p - q). \quad (34)$$

We compute all real zeros of the polynomial $g(\lambda)$ in the open interval $(0, 1)$. The zeros partition the edge of C into segments where $f(y)$ points either inward or outward, relative to the convex region C . If there are no zeros then the entire edge of C is either inward pointing or outward pointing. In this manner we partition ∂C . If there are no points that point outwards C is forward closed.

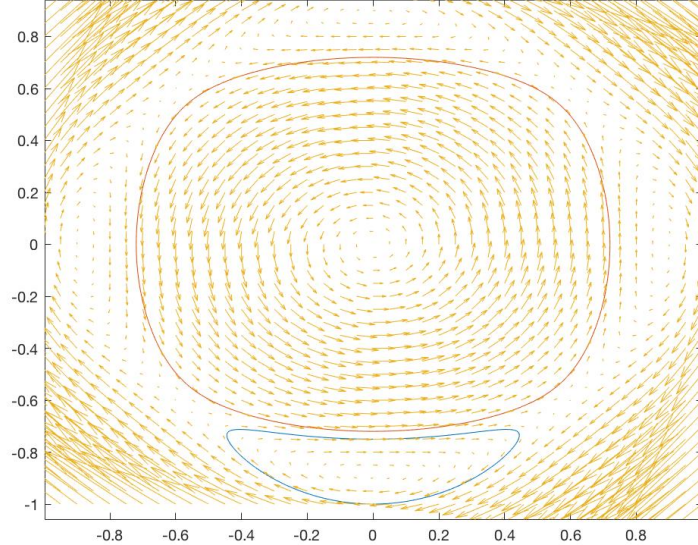


Figure 11: The Hamiltonian vector field defined by the Trott curve and two of its trajectories.

Let C be the curve in \mathbb{R}^2 defined by a polynomial equation $h(x, y) = 0$. The associated dynamics is given by

$$\dot{x} = \frac{\partial h}{\partial y}(x, y) \quad \text{and} \quad \dot{y} = -\frac{\partial h}{\partial x}(x, y). \quad (35)$$

For planar case this system is called *Hamiltonian system*. At any point that is not a critical point of h , the right hand side of (35) is orthogonal to the gradient vector of h . This means that the vector field is tangent to the *level curves* $h(x, y) = c$, where c ranges over \mathbb{R} . From this we infer the following well-known result.

Proposition 2.3.1. *Every trajectory of (35) is a piece of a level curve of the polynomial $h(x, y)$.*

We next illustrate a Hamiltonian system and compute the attainable region for a curve that is familiar in computational algebraic geometry.

Example 2.3.2 ($n = 2$). The *Trott curve* is the quartic curve in the plane \mathbb{R}^2 defined by

$$h(x, y) = 144(x^4 + y^4) - 225(x^2 + y^2) + 350x^2y^2 + 81.$$

This curve consists of four non-convex ovals, which implies that it has 28 real bitangents.

The vector field for the Hamiltonian system (35) is shown in Figure 11, along with two of its trajectories. Fix any point (u, v) in \mathbb{R}^2 and set $c = h(u, v)$. Then the trajectory of (35) that starts at (u, v) travels on the quartic curve defined by $h(x, y) = c$. Consider the starting point $(0, -1)$, which lies on the original Trott curve $h(x, y) = 0$. Its trajectory is one of the four ovals, namely the oval at the bottom that is red in Figure 12 (left) and blue in Figure 11.

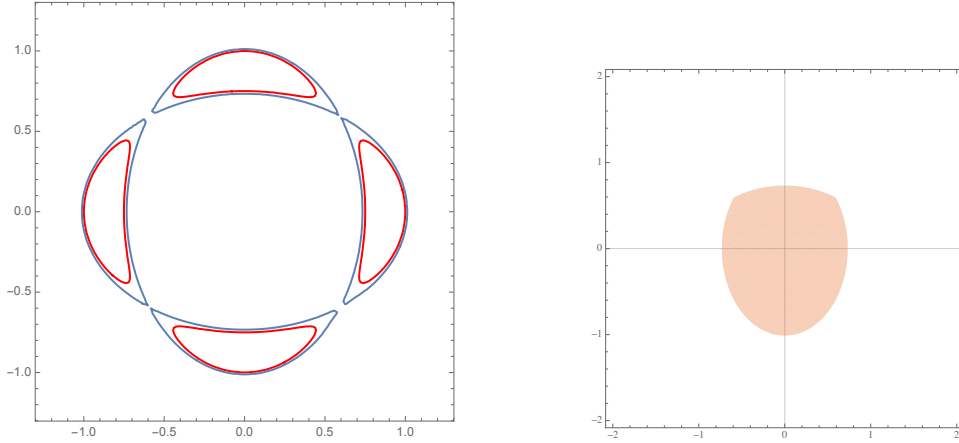


Figure 12: A pair of ellipses encloses the Trott curve and bounds the attainable region.

The region bounded by that oval is not convex. Its convex hull has one bitangent edge, namely the segment from $(-a, b)$ to (a, b) where

$$a = 0.4052937596229429488 \quad \text{and} \quad b = -0.7125251813139792270.$$

This convex hull is not forward closed. This can be seen by taking any starting point (x, b) where $0 < x < 0.239173943$. The resulting trajectory is a convex curve that lies above the original oval. It is shown in red in Figure 11. The set of all trajectories as x ranges from 0 to a sweeps out the attainable region for $(0, -1)$. This region is a semialgebraic set. Its boundary consists of parts of two ellipses. Their union is the zero set of $h(x, y) - \frac{1053}{638}$.

The containment of the Trott curve in the ellipse is shown on the left in Figure 12. The attainable region of the lower oval in the Trott curve is the convex set of the right in Figure 12.

2.3.2 General Case

We will now discuss the case when the convex hull is given as the output of Algorithm 2.2.18. We partition the boundary ∂C into two regions. The region where the vector field points outwards is coloured red and where it points inwards is coloured green. From equation (31) the set $\{u \in \mathbb{R}^n \mid \pi_2(\pi_1^{-1}(u)) = \{v\}\}$ is dense in ∂C and the boundary between inward and outward pointing vectors $f(y)$ is the image under the projection $\pi_1 : N(C) \rightarrow \partial C$ of the set $\{(u, v) \in N(C) : \phi(u) \cdot v = 0\}$. This is an analytic set of dimension $n - 2$ inside the $(n - 1)$ -dimensional normal cycle $N(C)$.

The output of Algorithm 2.2.18 represents a k -patch by a connected graph G_i . We refer back to the Definition 2.2.15 for the definition of ψ as a k -patch. Each node of G_i is a face $F = \text{conv}\{u_0, \dots, u_k\}$ along with a normal vector v at C . We are interested in the restriction of the boundary above to the patch of interest:

$$\pi_1(\{(u, v) \in \psi : f(u) \cdot v = 0\}). \quad (36)$$

Algorithm 2.3.3 computes a partition of the approximation computed by Algorithm 2.2.18 into inward and outward pointing regions.

Algorithm 2.3.3. (Partitioning the boundary of the convex hull of a trajectory)

input : The graphs G_i representing the patches of the convex hull of a trajectory of
(4)
output: Partition of the boundary into inward and outward pointing regions
1 **foreach** *connected graph* G_i *in the output of Algorithm 2.2.18* **do**
2 **foreach** *node* $(\{u_0, \dots, u_k\}, v)$ *of the graph* G_i **do**
3 Set $u = \sum_{i=0}^k \lambda_j u_j$ where λ_j are nonnegative unknowns satisfying $\sum_{j=0}^k \lambda_j = 1$
4 Compute the $(k - 1)$ -dimensional hypersurface in Δ_k defined by $f(u) \cdot v = 0$
 and identify inward and outward pointing regions
5 **end**
6 **end**

For each node of the connected component G_i , we have the approximated k vertices of the face represented by the node. Inner loop of the above algorithm then computes the zero set of the polynomial that separates the face into regions where vector field points inwards and the regions where it points outwards. This is done for each face. This zero set is given by $f(u) \cdot v = 0$ where v is the normal vector of the face which is also given as the output of Algorithm 2.2.18.

When the curve is an algebraic curve, recall that the associated dynamical system is locally given by $\dot{x} = f(x) = (J_1, J_2, \dots, J_n)^T$. Analogous to Proposition 2.3.1 we have the following result:

Proposition 2.3.4. *The trajectory of the dynamical system $\dot{x} = f(x)$ that starts at a point y on the algebraic curve \mathcal{C} remains on the curve \mathcal{C} . It either cycles around one nonsingular oval of \mathcal{C} , or it diverges towards infinity in \mathbb{R}^n , or it converges to a singular point of \mathcal{C} .*

In this case, we are solving the following polynomial equation

$$f(u) \cdot v = \sum_{l=1}^n J_l(\lambda_0 u_0 + \dots + \lambda_k u_k) \cdot v_l = 0 \quad \text{for } l = 1, 2, \dots, n.$$

In some situations, we might know the equation $g = 0$ that holds on the hypersurface $\pi_1(\psi)$ in \mathbb{R}^n . Here g is analytic or polynomial, depending on the instance. With this, we can write

$$v_l = \frac{\partial g}{\partial x_l}(\lambda_0 u_0 + \dots + \lambda_k u_k) \quad \text{for } l = 1, 2, \dots, n.$$

This formula allows us to solve the equation $f(u) \cdot v = 0$ simultaneously on the entire and exact k -patch, and not just on each approximated k -face of ψ individually, as it is done in line 4 of Algorithm 2.3.3.

Example 2.3.5 ($n = 3$). We partition the boundary of the convex body of the curve given by $z - 4x^3 + 3x = 0$ and $x^2 - y^2 - xz = 0$. The associated dynamical system is then given by

$$\dot{x} = -2y \quad \text{and} \quad \dot{y} = 12x^3 - 5x + z \quad \text{and} \quad \dot{z} = -24x^2y + 6y. \quad (37)$$

Its edge surface has two irreducible components, of degrees 3 and 16, each of which contributes two patches. The cubic is $g_2 = z - 4x^3 + 3x$, same as one of the defining polynomials. The degree 16 polynomial g_1 is displayed in [102, §1]. On the cubic patches, the equation $\nabla g_2 \cdot f = 0$ holds identically, so these patches are not partitioned. Hence, every trajectory that starts on a cubic patch remains in that patch. The two degree 16 patches are partitioned by a curve of degree 262, obtained by intersecting the patches with the surface defined by $\nabla g_1 \cdot f = 0$. The two triangle facets lie in the planes $z = \pm 1$. They are partitioned by the lines $y = 0$ and $x = \pm 1/2$.

2.4 Applications

Given an arbitrary polynomial dynamical system (4), it is natural to ask whether it arises from some chemical reaction network G . The solution to this inverse problem was given by Hárs and Tóth [60]. They showed that $f = (f_1, \dots, f_n)$ is realised by a graph G as above if and only if each monomial with negative coefficient in f_i is divisible by x_i , for $i = 1, 2, \dots, n$.

We discussed Hamiltonian systems in Subsection 2.3.1. The following result characterises chemical reaction dynamics in \mathbb{R}^2 that is Hamiltonian. It would be interesting to study such reaction networks, along with the higher-dimensional versions arising from Proposition 2.3.4.

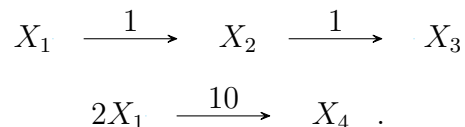
Proposition 2.4.1. *Let $h(x, y)$ be a polynomial in two variables. The Hamiltonian system (35) can be realised as a mass action system (3) if and only if the coefficients of all powers of y in $h(x, y)$ are non-negative and the coefficients of all pure powers of x are non-positive, i.e.*

$$h(x, y) = xy \cdot a(x, y) - b(x) + c(y), \quad \text{where } b \text{ and } c \text{ have nonnegative coefficients.}$$

Proof. This is immediate from Theorem 3.2 in [60]. □

We now apply the algorithms in Subsection 2.2.3 and Subsection 2.3.2 to two interesting chemical reaction networks.

Example 2.4.2 ($n = 4, m = 5$). We revisit the *Van de Vusse reaction* which has been studied extensively in the chemistry literature (cf. [95, Chapter 6]). The network equals



The rate constants κ_{ij} are written over the edges. The mass action system in (3) equals

$$f(x) = [x_1 \ x_2 \ x_3 \ x_1^2 \ x_4] \cdot \begin{bmatrix} -1 & 1 & 0 & 0 & 0 \\ 0 & -1 & 1 & 0 & 0 \\ 0 & 0 & 0 & 0 & 0 \\ 0 & 0 & 0 & -10 & 10 \\ 0 & 0 & 0 & 0 & 0 \end{bmatrix} \cdot \begin{bmatrix} 1 & 0 & 0 & 0 \\ 0 & 1 & 0 & 0 \\ 0 & 0 & 1 & 0 \\ 2 & 0 & 0 & 0 \\ 0 & 0 & 0 & 1 \end{bmatrix}, \quad (38)$$

where x_i is the concentration of species X_i . Explicitly, this is the dynamical system (4) with

$$f(x_1, x_2, x_3, x_4) = [-x_1 - 20x_1^2, x_1 - x_2, x_2, 10x_1^2].$$

Computations of the critical reactors of this system are discussed in [95, Section 5.3].

Fix the starting point $y = (1, 0, 0, 0)$. The trajectory starting at y converges to the steady state $y^* = (0, 0, 0.1522, 0.4238)$. The dynamics takes place in \mathbb{R}^4 , but the stoichiometry space has dimension 3. In our analysis we use the projection onto the first three coordinates. With this, the trajectory is an arc in a 3-dimensional space, shown in blue in Figure 13.

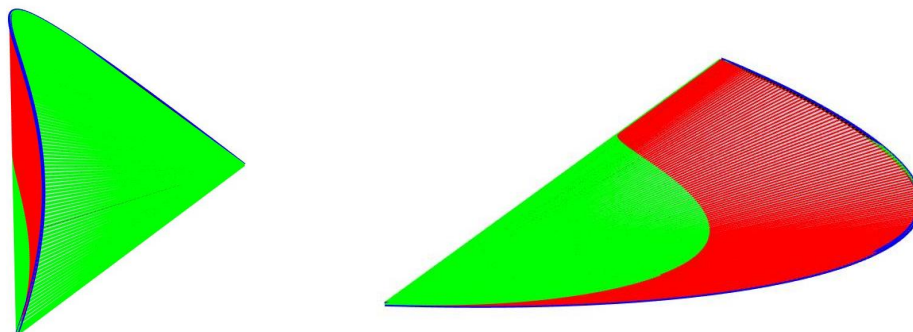


Figure 13: Convex hull of a trajectory of the Van de Vusse reaction and the partition of its boundary

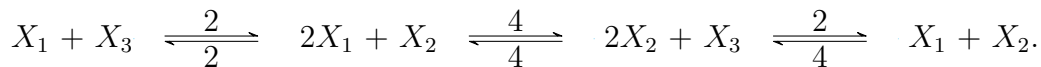
We computed the convex hull of the trajectory starting at y for (3) using Algorithm 2.2.18, and we then partitioned its boundary using Algorithm 2.3.3. The result is shown in Figure 13. The convex body has two 1-patches, obtained by joining each of the two endpoints with each point on the curve. One of the patches is entirely green. This means that the vector field is pointing inward on that patch. The other patch is partitioned into a green region and a red region, as shown on the right in Figure 13. Red color indicates that the vector field points outward. In particular, the convex hull of the trajectory is strictly contained in the attainable region.

The mass action system (3) is called *weakly reversible* if every connected component of the underlying directed graph is strongly connected in G , i.e. there is a directed path from any node in the component to any other node. It was conjectured in the first version of [71] that convex trajectories of weakly reversible systems are forward closed. We here numerically disprove that conjecture.

Proposition 2.4.3. *Not all convex trajectories of weakly reversible systems are forward closed.*

The proof is by direct computation using our algorithms. Here is the counterexample:

Example 2.4.4 (Weakly Reversible System). Consider the following weakly reversible network



The three coordinates for (4) are explicitly given by

$$\begin{aligned} f_1 &= -10x_1^2x_2 + 10x_2^2x_3 - 4x_1x_2 + 2x_1x_3, \\ f_2 &= 2x_1^2x_2 - 6x_2^2x_3 + 4x_1x_2 + 2x_1x_3, \\ f_3 &= 6x_1^2x_2 - 6x_2^2x_3 + 4x_1x_2 - 2x_1x_3. \end{aligned}$$

This system has deficiency zero, and it is a toric dynamical system [35]. There are no conservation relations and therefore, the trajectories are curves that span the ambient space \mathbb{R}^3 .

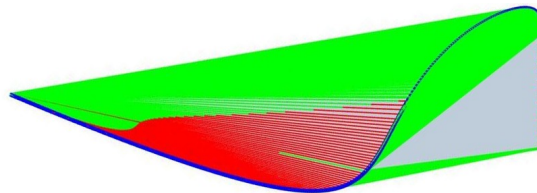


Figure 14: Convex hull of a trajectory of a weakly reversible system that is not forward closed

Let $y = (4, 4, 2)$. The convex body $C = \text{convtraj}(y)$ was computed using Algorithm 2.2.18 and is shown in Figure 14. The triangle shown in gray is a 2-patch of C . The vector field given by (f_1, f_2, f_3) points inward at all points on that triangle facet. We also show the partition of the 1-patches of C , as computed by Algorithm 2.3.3. One of the patches is partitioned into a green region and a red region. As before, the vector field points outward at each red point. We conclude that the convex hull C of the trajectory that starts at y is not forward closed.

3 Optimisation and Real Algebraic Geometry

The contents in this chapter is based on [72, 73]. Section 3.1 is a joint work with Mario Kummer, Daniel Plaumann, Mahsa Sayyary, and Bernd Sturmfels published online in *Experimental Mathematics*. Section 3.2 is an ongoing joint work with Yue Ren, Mohab Safe El Din, and Johannes W. R. Martini. It tackles an optimisation problem relevant to biology.

3.1 Sixty Four Curves

A classical theme in real algebraic geometry is the topological classification of algebraic curves in the real projective plane $\mathbb{P}_{\mathbb{R}}^2$. Hilbert's 16th problem asks for the *topological types* of smooth curves of a fixed degree d . In this section we denote a curve by C , unlike the last chapter where it was denoted by \mathcal{C} . Two curves C and C' have the same type if some homeomorphism of $\mathbb{P}_{\mathbb{R}}^2 \rightarrow \mathbb{P}_{\mathbb{R}}^2$ restricts to a homeomorphism $C_{\mathbb{R}} \rightarrow C'_{\mathbb{R}}$. This problem has been solved upto $d = 7$, thanks to contributions by many mathematicians, including Hilbert [61], Rohn [106], Petrovsky [100], Rokhlin [105], Gudkov [59], Nikulin [97], Kharlamov [76], and Viro [119, 120, 121]. We particularly focus on the case $d = 6$.

For a smooth curve C in plane $\mathbb{P}_{\mathbb{R}}^2$, each of its connected component C_0 is homeomorphic to a circle. If the complement $\mathbb{P}_{\mathbb{R}}^2 \setminus C_0$ is disconnected, then C_0 is called an *oval*, otherwise a *pseudoline*. An odd degree curve always has exactly one pseudoline. If C has even degree, then all connected components are ovals. The two connected components of the complement of an oval are called the *inside* and the *outside*. The former is homeomorphic to a disk, the latter to a Möbius strip. An oval C_0 *contains* another oval C_1 if C_1 lies in the inside of C_0 . In that case, we refer to C_0 and C_1 together as *nested ovals*. We call an oval *empty* if it contains no other oval. The topological type of the curve C is determined by the number of ovals together with the information of how these ovals contain each other. We denote the type of a smooth plane sextic C in the real projective plane $\mathbb{P}_{\mathbb{R}}^2$ by

- k if C consists of k empty ovals;
- $(k1)l$ if C consists of an oval C_0 containing k empty ovals and of l further empty ovals lying outside C_0 ;
- (hyp) if C consists of three nested ovals (where 'hyp' stands for 'hyperbolic').

Consider the set of non real points $C_{\mathbb{C}} \setminus C_{\mathbb{R}}$ on the Riemann surface given by the irreducible curve C . If this set has two connected components then the curve C is said to be of *dividing type*, else *non-dividing*. A finer notion of equivalence of types of curves comes from the *discriminant* Δ . This is an irreducible hypersurface of degree $3(d - 1)^2$ in the projective space $\mathbb{P}_{\mathbb{R}}^{d(d+3)/2}$ of curves of degree d . Points on Δ are singular curves. The *rigid isotopy classes* are the connected components of the complement $\mathbb{P}_{\mathbb{R}}^{d(d+3)/2} \setminus \Delta$. If two curves C and C' are in the same rigid isotopy class, then they have the same topological type. The converse is not true in general, as shown by Kharlamov [76]. The rigid isotopy type of a smooth plane sextic determines whether it is dividing or not. The following is the well known classification of sextics, found in Viro's survey article [120, §7].

Theorem 3.1.1 (Rokhlin–Nikulin). *The discriminant of plane sextics is a hypersurface of degree 75 in $\mathbb{P}_{\mathbb{R}}^{27}$ whose complement has 64 connected components. The 64 rigid isotopy types are grouped into 56 topological types, with the number of ovals ranging from 0 to 11. The distribution is shown in Table 2. The 56 types form the partially ordered set in Figure 15.*

The 64 types in Theorem 3.1.1 were known to Rokhlin [105]. The classification was completed by Nikulin. It first appeared in his paper [97] on the arithmetic of real K3 surfaces.

Number of ovals	0	1	2	3	4	5	6	7	8	9	10	11	total
Count of rigid isotopy types	1	1	2	4	4	7	6	10	8	12	6	3	64
Count of topological types	1	1	2	4	4	5	6	7	8	9	6	3	56

Table 2: Rokhlin–Nikulin classification of smooth sextics in the real projective plane

Figure 15 is a refinement of Viro’s diagram in [121, Figure 4]. It shows all possible topological types of degree six planar curves. These form a partially ordered set with cover relations corresponding to either fusing two ovals together or shrinking an oval until it vanishes (cf. Theorem 3.1.6). We know from [97, p. 107] that all but eight of the 56 topological types correspond to exactly one rigid isotopy class. The types shown in red in Figure 15 are topological types that always divide their corresponding Riemann surface. The top row contains the three types with 11 ovals. These are denoted (91)1, (51)5 and (11)9. Any degree 6 curve with 11 ovals always divides the Riemann surface into two connected components. Any curve of the type shown in blue in Figure 15 is of non dividing nature. The following eight types consist of two rigid isotopy classes:

$$(41) \quad (21)2 \quad (51)1 \quad (31)3 \quad (11)5 \quad (81) \quad (41)4 \quad 9. \quad (39)$$

These are shown in purple in the figure. Note that the maximal elements in the poset of sextics are necessarily of dividing type:

$$(91)1 \quad (51)5 \quad (11)9 \quad (61)2 \quad (21)6 \quad (\text{hyp}). \quad (40)$$

In summary, of the 56 topological types of smooth plane sextics, precisely 42 types are non-dividing. The six types in (40) are dividing, and the eight types in (39) can be dividing or non-dividing. Hence, there are 14 rigid isotopy types that are dividing. The subset of $\mathbb{P}_{\mathbb{R}}^{27}$ consisting of all dividing sextics is the closure of the union of these 14 rigid isotopy types. This accounts for all 64 rigid isotopy types (connected components of $\mathbb{P}_{\mathbb{R}}^{27} \setminus \Delta$) in the census of Theorem 3.1.1.

Many new results and questions can be derived by the computational framework developed in this section. We give an example concerning reducible sextic curves that consists of six distinct lines. This 12-dimensional family in $\mathbb{P}_{\mathbb{R}}^{27}$ is the *Chow variety* of factorisable forms.

Proposition 3.1.2. *Configurations of six general lines appear in the closure of precisely 35 of the 64 rigid isotopy classes. These are the classes that meet the Chow variety in a generic point. These 35 classes are marked with an asterisk in Table 8, in the column on eigenvectors.*

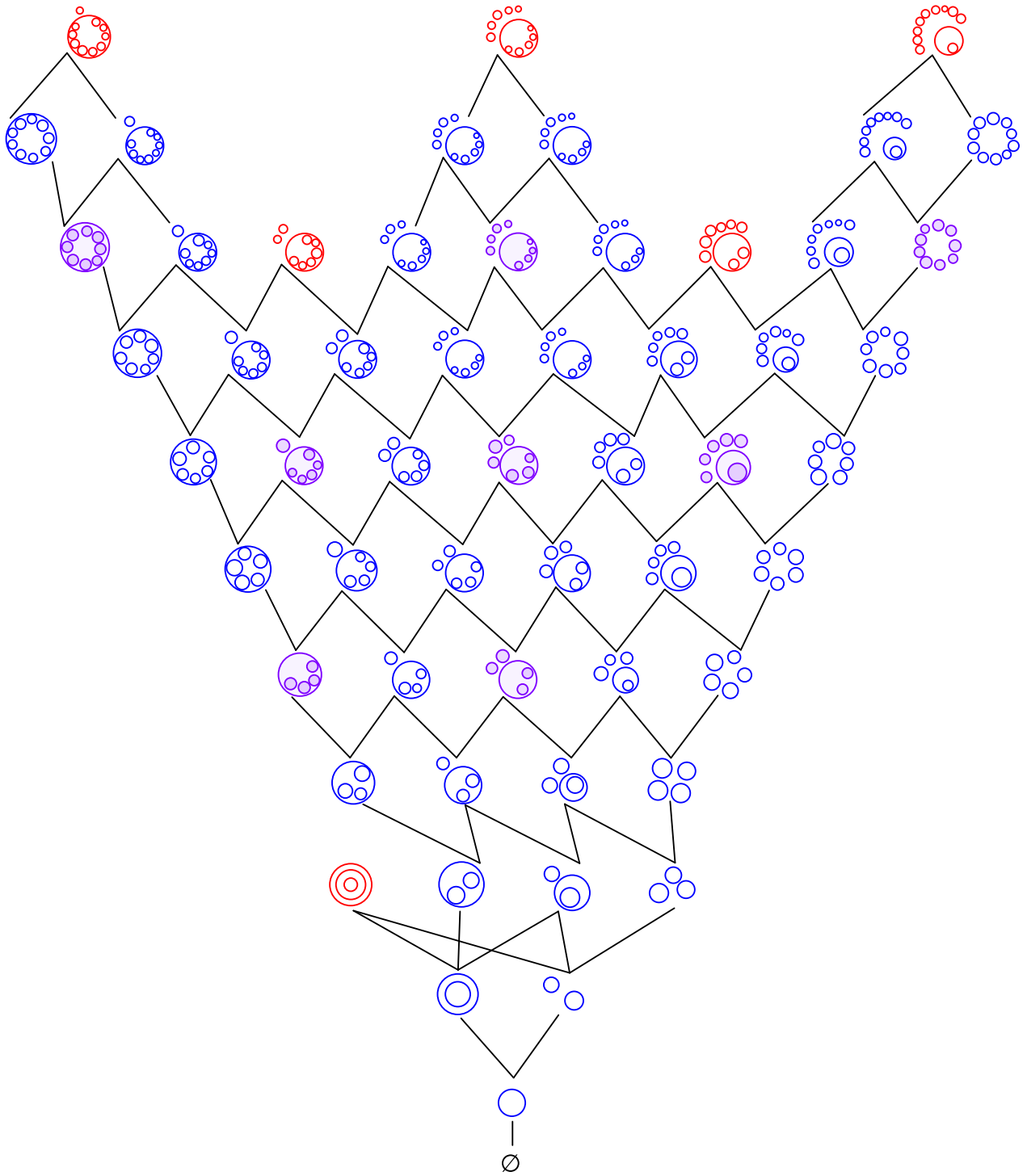


Figure 15: The 56 types of smooth plane sextics form a partially ordered set. The colour code indicates whether the real curve divides its Riemann surface. The red curves are dividing, the blue curves are non-dividing, and the purple curves can be either dividing or non-dividing.

3.1.1 Discriminantal Transitions

Ternary sextics are written as

$$f = \sum_{i+j+k=6} c_{ijk} x^i y^j z^k. \quad (41)$$

The discriminant Δ of f is an irreducible hypersurface of degree 75 in $\mathbb{P}_{\mathbb{R}}^{27}$. We identify Δ with its defining irreducible polynomial over \mathbb{Z} in the 28 unknowns c_{ijk} . Each point on Δ corresponds to a singular curve of degree 6. Each connected component of the complement $\mathbb{R}[x, y, z]_6 \setminus \Delta$ corresponds to one of our 64 types. For all systematic constructions, it is then imperative to work with the discriminant.

We evaluate Δ using *Sylvester's formula*, as stated by Gelfand, Kapranov and Zelevinsky [55, Theorem 4.10, Chapter 3]. This expresses Δ as the determinant of a 45×45 -matrix \mathcal{S}_f . Each entry in the first 30 columns of \mathcal{S}_f is either 0 or one of the coefficients c_{ijk} . The entries in the last 15 columns are cubics in the c_{ijk} . So, the degree of $\det(\mathcal{S}_f)$ is 75, as required. The *Sylvester matrix* \mathcal{S}_f is the representation in monomial bases of an \mathbb{R} -linear map

$$\mathcal{S}_f : (\mathbb{R}[x, y, z]_3)^3 \oplus \mathbb{R}[x, y, z]_4 \longrightarrow \mathbb{R}[x, y, z]_8$$

that is defined as follows. On the first summand, it maps a triple of cubics to an octic via

$$\mathcal{S}_f : (a, b, c) \mapsto a \frac{\partial f}{\partial x} + b \frac{\partial f}{\partial y} + c \frac{\partial f}{\partial z}.$$

On the second summand, the map \mathcal{S}_f takes a quartic monomial $x^r y^s z^t$ to the octic $\det(M_{rst})$, where M_{rst} is any 3×3 -matrix of ternary forms that satisfies the homogeneous identity

$$\begin{pmatrix} \partial f / \partial x \\ \partial f / \partial y \\ \partial f / \partial z \end{pmatrix} = M_{rst} \cdot \begin{pmatrix} x^{r+1} \\ y^{s+1} \\ z^{t+1} \end{pmatrix}.$$

The entries of M_{rst} are linear in the c_{ijk} , so $\det(M_{rst})$ is an octic in x, y, z whose coefficients are cubics in the c_{ijk} . These are the entries in the column of \mathcal{S}_f that is indexed by $x^r y^s z^t$.

Proposition 3.1.3. *The discriminant Δ equals the determinant of the 45×45 -matrix \mathcal{S}_f .*

Proof. We use Sylvester's formula for the resultant of three ternary quintics. This is [55, Theorem III.4.10] for $d = 5$ and $k = 4$. If we take the three quintics to be the three partial derivatives of f , then we get the matrix \mathcal{S}_f above. That resultant equals our discriminant because both are non-zero homogeneous polynomials of the same degree 75 in the c_{ijk} . \square

A general point in the discriminant is curve f that has precisely one ordinary node. If f is in the real locus $\Delta_{\mathbb{R}}$, then that node is a point in the real plane $\mathbb{P}_{\mathbb{R}}^2$. Two of the 64 types are connected by a *discriminantal transition* if there is a curve in the closure of both of the components having only one singular point which is an ordinary node. These transitions form the cover relations of the poset in Figure 15. There are three different

types of discriminantal transitions. If the singular curve has an isolated real point (acnode), defined locally by $x^2 + y^2 = 0$, then the transition corresponds to removing one of the empty ovals. We call this operation *shrinking of ovals*. Itenberg [69] uses the term *contraction*. The inverse operation is adding an empty oval.

By the way of the following lemma and the subsequent theorem, well-known to the experts, we make observations regarding the adjacencies of different connected components in the complement of the Δ .

Lemma 3.1.4. *Shrinking an oval always leads to a curve of non-dividing type.*

Proof. Consider a real plane curve C with only one singularity p that is an acnode. Since being of non-dividing type is an open condition, we can assume that C is of dividing type. Then p is in the closure of both connected components of $C_{\mathbb{C}} \setminus C_{\mathbb{R}}$. In particular, $(C_{\mathbb{C}} \setminus C_{\mathbb{R}}) \cup \{p\}$ is connected. Therefore, after shrinking an oval we get a curve of non-dividing type. \square

The other type of ordinary node consists of two crossing real branches (crunode), defined locally by $x^2 - y^2 = 0$. There are two possibilities: The connected component containing the node is either two ovals intersecting in one point, or two pseudolines intersecting in one point. The case of one oval and one pseudoline cannot occur in even degree. In the following we describe the topology of small perturbations of the nodal curve in each of these two cases. In the former case, the transition consists of two ovals coming together and forming one oval. This happens in one connected component of the complement of all other ovals. We call this transition *fusing of ovals*. Itenberg [69] uses the term *conjunction*. This operation reduces the number of ovals by one. In the case when two pseudolines intersect, every small perturbation of the nodal curve has the same number of ovals but the interior and exterior of one outermost oval are exchanged. We call this operation *turning inside out*. An example of turning inside out is shown in Figure 16. For plane conics, turning inside out is the only possibility. For quartics, all three transitions are possible. We summarise our discussion in the following theorem.

Theorem 3.1.5. *For curves of even degree, every discriminantal transition between rigid isotopy types is one of the following: shrinking of ovals, fusing of ovals, and turning inside out.*

Proof. Let C be a real plane curve of even degree with exactly one ordinary singularity p . If p is an acnode, then C corresponds to shrinking. Let p be a crunode. There are two subsets $C_1, C_2 \subset C_{\mathbb{R}}$, both homeomorphic to the circle, such that $C_1 \cap C_2 = \{p\}$. Let $\pi : \tilde{C} \rightarrow C$ be the normalisation map. The fiber $\pi^{-1}(p)$ consists of exactly two points $p_1, p_2 \in \tilde{C}_{\mathbb{R}}$.

Suppose that p_1 and p_2 belong to the same connected component of $\tilde{C}_{\mathbb{R}}$. If C_1 or C_2 does not disconnect $\mathbb{P}_{\mathbb{R}}^2$, there would be a small deformation of C to a smooth curve having (at least) one pseudoline as one of the connected components of its real part. Since this is not possible, both C_1 and C_2 disconnect $\mathbb{P}_{\mathbb{R}}^2$. This case corresponds to fusing of ovals.

Next suppose that p_1 and p_2 belong to different connected components of $\tilde{C}_{\mathbb{R}}$. For both bifurcations of the node, the number of connected components of the real part of the curve stays the same. If C_1 or C_2 disconnected $\mathbb{P}_{\mathbb{R}}^2$, then there would be another intersection point

of C_1 and C_2 besides p . Thus, $\mathbb{P}_{\mathbb{R}}^2 \setminus C_i$ is connected for $i = 1, 2$, and $\mathbb{P}_{\mathbb{R}}^2 \setminus (C_1 \cup C_2)$ has two connected components, both homeomorphic to an open disc. Depending on the bifurcation of the node, one of these connected components is still homeomorphic to an open disc after deformation and the other one is not. This corresponds to turning inside out. \square

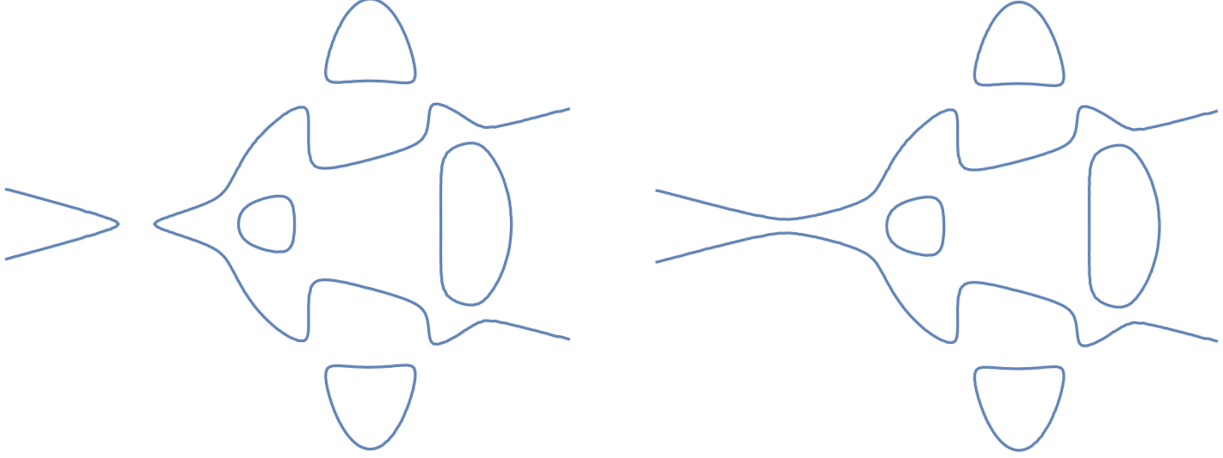


Figure 16: Type (21)2d transitions into Type (21)2nd by turning an oval inside out.

It is instructive to examine the diagram in Figure 15 from the perspective of discriminantal transitions. The edges in the poset correspond to shrinking or fusing. There are three possibilities for what might be geometrically possible: shrinking only, fusing only, or shrinking and fusing. For instance, Type (11) can become Type 1 by either shrinking the inner oval, or by fusing the two nested ovals. Both possibilities are geometrically realised by a singular curve with a single node that lies in the common boundary between the two types.

Theorem 3.1.6 (Itenberg). *Each of the edges in Figure 15 is realised by shrinking an empty oval, except the one between (hyp) and (2). Not every edge is realised by fusing two ovals.*

Proof. The first statement is [69, Prop. 2.1]. Furthermore, it was shown in [69] that the transition from (11)9 to 10 cannot be realised by fusing. \square

One possible way of explicitly realising edges by fusing is to use Gudkov's constructions [59] and the following lemma which is a special case of a theorem due to Brusotti [25].

Lemma 3.1.7. *Let $C_1, C_2 \subset \mathbb{P}^2$ be two smooth real curves of degrees 2 and 4 (resp. 1 and 5) intersecting transversally. By a small perturbation, we can fix any one of the real nodes of the sextic curve $C_1 \cup C_2$ and perturb all the others independently in any prescribed manner.*

Proof. Let $q, p_1, \dots, p_7 \in \mathbb{P}_{\mathbb{R}}^2$ be eight distinct real points lying on the smooth quadric C_1 . We claim that for every tuple $\epsilon \in \{\pm 1\}^7$, there is a sextic which is singular at q and whose sign at p_i is ϵ_i . Let L be the linear system of all sextic curves that are singular at q . The

pull-back of L to $C_1 \cong \mathbb{P}^1$ is the set of all bivariate forms of degree 12 having a double root at q . Since for any distinct 7 points in \mathbb{R} there is a polynomial of degree 10 that vanishes on all but one of these points, the claim follows. The other case (degrees 1 and 5) is analogous. \square

Let us now examine our third discriminantal transition. Turning inside out preserves the number of ovals, so it is an operation that acts on each of the rows in Figure 15 separately.

Proposition 3.1.8. *If we turn an outermost oval of a smooth sextic inside out, then the topological type of the resulting curve is the mirror image of the original curve when reflected along the vertical axis in Figure 15. If the curve was dividing, then it is non-dividing after turning inside out. Curves that are non-dividing can become either dividing or non-dividing.*

Proof. Let C be a real plane curve with exactly one ordinary crunode p . In a neighborhood of p , the Riemann surface $C_{\mathbb{C}}$ is homeomorphic to the union of two discs D_1 and D_2 with $D_1 \cap D_2 = \{p\}$. The real part $C_{\mathbb{R}}$ divides D_1 and D_2 into two connected components D_1^+ , D_1^- and D_2^+ , D_2^- respectively. One of the two possible smoothenings of the node p connects D_1^+ with D_2^+ and the other one connects D_1^+ with D_2^- . Thus, if C is dividing then exactly one of the two deformations results in a dividing curve. Otherwise, both are non-dividing. \square

Not every vertical reflection in Figure 15 can be realised geometrically by a discriminantal transition. For instance, the types (91)1 and (11)9 are related by a vertical reflection. But both types are dividing, so Proposition 3.1.8 implies that they are not connected by turning inside out. Put differently, these two components of $\mathbb{P}_{\mathbb{R}}^{27} \setminus \Delta$ do not share a wall of codimension one. In fact, turning inside out can only happen for curves with at most 9 ovals. Indeed, consider a plane sextic curve with exactly one crunode and r connected components, one of which is the intersection of two pseudolines. The normalisation of such a curve has genus 9 and $r + 1$ connected components. By Harnack's inequality this implies that $r \leq 9$.

3.1.2 Construction of Representatives

In this subsection we elaborate on different techniques employed to come up with the 64 representatives. These are listed in Subsection 3.1.6. To construct our list of 64 representatives, we relied on various methodologies. Firstly, small coefficient size is a natural criterion for desirable representatives. We say that a sextic f as in (41) is *optimal* if its coefficients c_{ijk} are integers, its complex curve $V_{\mathbb{C}}(f)$ is smooth, and the largest absolute value $|c_{ijk}|$ is minimal among all such sextics in the same rigid isotopy class. For instance, the Fermat sextics $x^6 + y^6 \pm z^6$ are optimal. One approach to finding optimal sextics is to sample at random from sextics with $|c_{ijk}| \in \{0, 1, \dots, m\}$ with m very small. One might also do a brute force search that progressively increases the sum of the absolute values $|c_{ijk}|$. Such strategies work for some of the types seen with highest frequency in Table 3. For instance,

sampling with $m = 1$ yields these four optimal sextics:

$$\begin{aligned}
& 2 \quad \text{nd} \quad x^6 - x^5y - x^5z - x^4yz + x^3y^3 + x^3yz^2 - x^2y^4 - x^2y^2z^2 + xy^4z \\
& \quad \quad \quad -xy^3z^2 - xy^2z^3 - xyz^4 + y^6 + y^5z + y^4z^2 + y^3z^3 - yz^5 + z^6 \\
& 3 \quad \text{nd} \quad x^6 - x^5y - x^4y^2 + x^4z^2 + x^3y^3 + x^3y^2z + x^3yz^2 + x^2y^3z - x^2y^2z^2 + x^2yz^3 + x^2z^4 \\
& \quad \quad \quad +xy^4z + xy^3z^2 + xy^2z^3 + xyz^4 - xz^5 + y^6 + y^5z + y^4z^2 - y^2z^4 - yz^5 + z^6 \\
(11) \quad \text{nd} \quad x^5y + x^5z + x^4y^2 + x^4yz - x^3y^3 + x^3yz^2 - x^3z^3 - x^2y^4 + x^2y^3z + x^2y^2z^2 - x^2yz^3 \\
& \quad \quad \quad +x^2z^4 - xy^4z + xy^3z^2 - xyz^4 + xz^5 - y^5z - y^4z^2 + y^3z^3 + y^2z^4 - yz^5 - z^6 \\
& 4 \quad \text{nd} \quad -x^6 + x^5y + x^4y^2 - x^3y^3 + x^2y^4 + xy^5 - y^6 + x^5z + x^4yz + xy^4z \\
& \quad \quad \quad +y^5z + x^4z^2 + y^4z^2 - x^3z^3 - y^3z^3 + x^2z^4 + xyz^4 + y^2z^4 + xz^5 + yz^5 - z^6
\end{aligned}$$

However, this approach is not useful for constructing the vast majority of types, since these seldomly occur in a random sample, and never appear for small m .

Next, we used an established and powerful technique for constructing real varieties with prescribed topology is Viro's *patchworking method* [121]. All 56 topological types of smooth sextics can be realised by a version of patchworking known as *combinatorial patchworking*, which can also be interpreted in the language of tropical geometry [121]. In that guise, one records the signs of the 28 coefficients c_{ijk} and represents their magnitudes by a regular triangulation of the Newton polygon. However, transitioning from that representation to actual polynomials in $\mathbb{Z}[x, y, z]_6$ yields integer coefficients c_{ijk} whose absolute values tend to be very large. We experimented with some of these sextics, but in the end we abandoned them for all but three types, because symbolic computation became prohibitively slow. This method was particularly helpful for sextics with larger number of ovals. For example, we employed Viro's method in [119, §3.2] and built a curve of type (51)5 using patchworking on three touching ellipses.

We then employed geometric constructions that are described in the literature on topology of real algebraic curves. Such constructions are found in many of the articles, from Harnack and Hilbert to Gudkov and Viro. Many types, especially the sextics with 3 to 7 ovals, can be found by perturbing the union of three quadrics intersecting transversally. This process is shown in Figure 17. Some of the types with 8 and 9 components could also be constructed in a similar fashion. This is reflected in our representatives in Subsection 3.1.6.

For most other types, we carried out the classical constructions of Harnack and Hilbert, as explained by Gudkov [59]. We start with two quadrics intersecting in four real points, pick eight points on the curves, and perturb the reducible quartic with the product of four lines through these points. The smooth quartic is intersected with one of the original quadrics and perturbed again to get a smooth sextic. The different ways in which the original curves and the points on them are selected give the different types. This method worked for almost all types. For larger numbers of ovals, these constructions led to polynomials whose integer coefficients were too big. In those cases, we needed to improve the coefficients. For the construction of type (51)5, Gudkov's method was too complicated to carry out explicitly.

Another approach is to start with especially nice, but possibly singular, ternary sextics seen in the literature. This method is exemplified by the *Robinson curve*. This is the symmetric sextic

$$\mathcal{R}(a, b, c) = a(x^6 + y^6 + z^6) + bx^2y^2z^2 + c(x^4y^2 + x^4z^2 + x^2y^4 + x^2z^4 + y^4z^2 + y^2z^4), \quad (42)$$

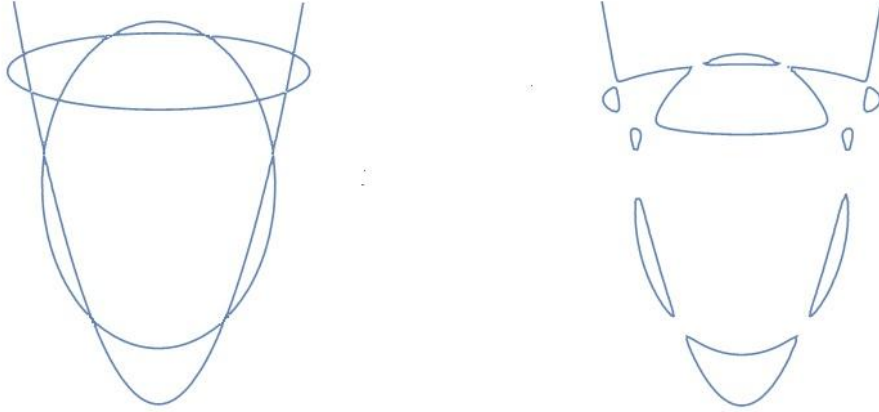


Figure 17: A sextic of Type (11)7 is constructed by perturbing the union of three quadratics.

where $(a : b : c)$ is any point in $\mathbb{P}_{\mathbb{R}}^2$. For $(a : b : c) = (19 : 60 : -20)$, this degree six curve is smooth and its real locus consists of ten non-nested ovals. The curve $\mathcal{R}(19, 60, -20)$ is listed as representative for the Type 10 nd in Subsection 3.1.6.

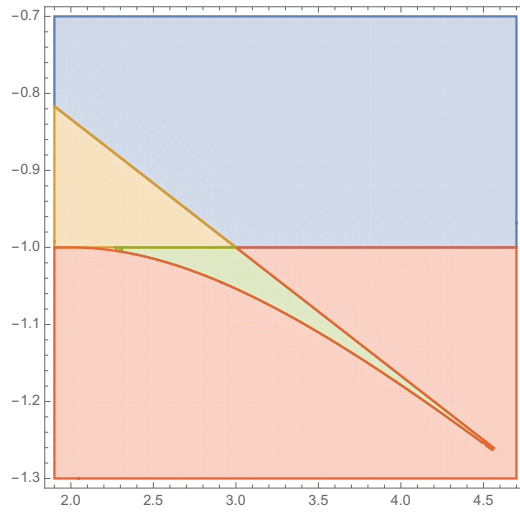


Figure 18: The discriminant divides the Robinson net (42) into 15 components that realise four topological types. The green region represents smooth sextics with 10 non-nested ovals.

We named this net of sextics after R.M. Robinson, who showed in 1973 that the special sextic $\mathcal{R}(1, 3, -1)$ is non-negative but is not a sum of squares. The reason is geometric: its real locus consists of 10 isolated singular points in $\mathbb{P}_{\mathbb{R}}^2$, given by the columns of the matrix

$$\begin{pmatrix} 1 & -1 & 1 & 1 & 0 & 0 & 1 & -1 & 1 & 1 \\ 1 & 1 & -1 & 1 & 1 & 1 & 0 & 0 & 1 & -1 \\ 1 & 1 & 1 & -1 & 1 & -1 & 1 & 1 & 0 & 0 \end{pmatrix}. \quad (43)$$

To understand how the topology of $\mathcal{R}(a, b, c)$ varies with $(a : b : c)$, we examine the com-

plement of the discriminant in $\mathbb{P}_{\mathbb{R}}^2$. The discriminant is given by the following reducible polynomial of degree 75:

$$a^3(a+c)^6(3a-c)^{18}(3a+b+6c)^4(3a+b-3c)^8(9a^3-3a^2b+ab^2-3ac^2-bc^2+2c^3)^{12} \quad (44)$$

The complement of the discriminant in $\mathbb{P}_{\mathbb{R}}^2$ has 15 connected components. These realise the following topological types of smooth sextics: 10, 4, 3 and 0. These types are found in 1, 3, 5 and 6 connected components respectively. The most interesting part of the partition is shown in Figure 18. The green region is the component corresponding to curves with 10 ovals. Smooth curves in the orange, red and blue region have 0, 3 and 4 ovals respectively.

Figure 18 is a two-dimensional slice of the partition of a 27-dimensional real projective space into 64 connected components by an irreducible hypersurface of degree 75.

These constructions enabled us to find representatives for the 56 topological types. What remained was the issue of distinguishing between dividing and non-dividing curves. In particular, we needed to find two representatives for the pairs of rigid isotopy types in the eight Nikulin cases (39). To construct those, we considered dividing curves of degree d_1 and d_2 , with prescribed orientations, that intersect in $d_1 \cdot d_2$ real points. The singular points of the reducible curve can be made smooth in two ways, shown in red in Figure 19. According to Fiedler [49, §2], if *all* intersections are perturbed either using only A or using only B then it is dividing. However, if the smoothening is done via A at some crossings and via B at other crossings, then the resulting smooth curve does not divide its Riemann surface. In particular, for the construction of types (41)4d and (41)4nd we followed [54, page 273].

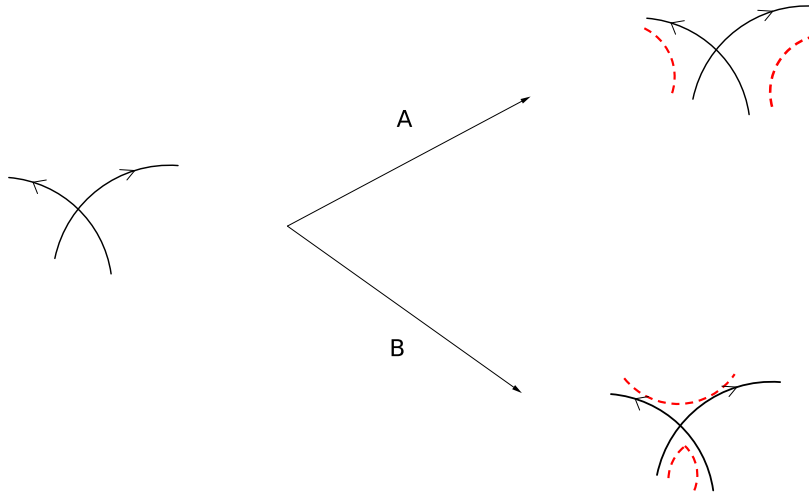


Figure 19: Using local perturbations to create sextics that are dividing or non-dividing

At this point, we had 64 representative sextics, and each of them was certified by our code `SexticClassifier`. However, the coefficient size for most of them was still unsatisfactory. To improve the representatives, and to arrive at the list that is displayed in Subsection Section 3.1.6, Sylvester’s formula for the discriminant (Proposition 3.1.3) proved again to be very helpful.

A pencil of sextics is a line $\{f + tg\}$ in the space \mathbb{P}^{27} of all sextics. Its discriminant $\Delta(f + tg)$ is a univariate polynomial in t of degree 75. We can compute that polynomial as the determinant of the Sylvester matrix \mathcal{S}_{f+tg} . For two sextics f and g in $\mathbb{Z}[x, y, z]_6$ with reasonable coefficients, we obtain the discriminant $\Delta(f + tg)$ in a few seconds. This method works, in principle, also for evaluating Δ on families with more than one parameter. For instance, we get the output (44) from the input (42) in under one second. However, that output (44) factors and is small. In our experience, the symbolic evaluation of the 45×45 determinant in Proposition 3.1.3 works well for pencils of sextics, but generally fails for nets of sextics. We use the discriminant $\Delta(f + tg)$ to shrink the absolute value of each coefficient separately of a given representative as far as possible without crossing the discriminant locus. The other way to reduce the coefficient size is to choose a prime number p and vary the polynomial without crossing the discriminant locus so that every coefficient of the resulting polynomial is divisible by p . In our experience, a combination of the two methods yields the best results.

3.1.3 Identifying the Type

Determining the topology of a real plane curve from its equation is a well-studied problem in computational geometry. The main idea is to ascertain the topology of plane curves by constructing isotopic graphs whose nodes are the critical points (singular and extreme). Authors who studied this problem include Jinsan Cheng, Sylvain Lazard, Luis Peñaranda, Marc Pouget, Fabrice Rouillier, Elias Tsigaridas, Laureano González-Vega, Ioana Necula, M’hammed El Kahoui, Hoon Hong, Raimund Seidel, and Nicola Wolpert. See [29, 45, 57, 111].

The algorithm in [29] is called `ISOTOP`. It is implemented in `Maple` using certain packages written in `C`. We refer to [29, Table 1, page 28] for comparisons between `ISOTOP` and `Top`, as well as with `INSULATE`, `AlciX` [45], and `Cad2d` [23]. The latter two are implemented in `C++`.

After initial experiments with these packages, we came to the conclusion that it is preferable for us to have our own specialised implementation for curves of degree six in $\mathbb{P}_{\mathbb{R}}^2$. In particular, all of the mentioned packages compute the topology of the curve in the affine chart $\{z = 1\}$. It was not obvious how to extract the topological type of the curve in the projective plane from the output with a reasonable amount of coding effort.

We wrote a program in `Mathematica` called `SexticClassifier`. It relies heavily on the built-in quantifier elimination techniques of `Mathematica`. The code can be obtained from our supplementary materials website (48). The input to `SexticClassifier` is a ternary sextic with integer coefficients, $f \in \mathbb{Z}[x, y, z]_6$. The code checks whether f defines a non-singular curve in $\mathbb{P}_{\mathbb{C}}^2$. If not, then the output is “singular”. Otherwise, our program identifies which of the 56 topological types the real curve $V_{\mathbb{R}}(f)$ belongs to. We next explain how it works.

First we compute a *Cylindrical Algebraic Decomposition* (CAD; see e.g. [12, 23]) of the curve $V_{\mathbb{R}}(f)$ in the affine chart $z = 1$. From this we build a graph whose nodes are the critical points of the projection along the y -axis. Two nodes are connected by an edge if an arc of the curve connects the corresponding points. We also keep track of the relative

positions of these arcs. In order to get the correct topology in $\mathbb{P}_{\mathbb{R}}^2$, we add further edges corresponding to arcs crossing the line at infinity. We end up with a graph whose connected components are in one-to-one correspondence with the connected components of the curve. Finally, for each pair of connected components of the graph, we have to check whether one of the corresponding ovals lies in the inside of the other. This is done by first deciding whether the center of projection lies inside the ovals or not. Knowing this, detecting a nesting of two ovals only amounts to looking at the parity of the number of branches of one oval lying above the other oval. The program terminates correctly in less than four seconds for all sextics in Subsection 3.1.6. If the coefficients are between -10^8 and 10^8 , then it takes less than one second.

Example 3.1.9. Here is an instance that will be of interest in Subsection 3.1.5. Let f be the sextic

$$7(x+y+2z)(x+2y+z)(2x+y+z)(x-2y+3z)(y-2z+3x)(z-2x+3y)+xyz(x^3+y^3+z^3).$$

After checking that the complex curve $V_{\mathbb{C}}(f)$ is smooth, our code reveals that the real curve $V_{\mathbb{R}}(f)$ consists of three separate non-nested ovals. Thus, the input to `SexticClassifier` is the polynomial f and the output is the label 3. In particular, $V_{\mathbb{R}}(f)$ is non-dividing.

The sextic f has the property that every real line in \mathbb{P}^2 meets $V_{\mathbb{C}}(f)$ in at least one real point. Thus, $V_{\mathbb{R}}(f)$ is not compact in any affine chart of $\mathbb{P}_{\mathbb{R}}^2$, regardless of which line serves as the line at infinity. While such non-compact curves may cause difficulties in some of the other programs discussed above, `SexticClassifier` has been designed to handle them well.

Forty-eight of the fifty-six topological types determine whether the curve is dividing or not. However, the remaining eight were found by Nikulin [97] to split into two rigid isotopy types. Suppose that the output of `SexticClassifier` is one of the eight labels in (39). At present, we have no easy tool for deciding whether the given f is dividing or non-dividing. That decision requires us to build a model of the Riemann surface $V_{\mathbb{C}}(f)$ in order to ascertain whether $V_{\mathbb{C}}(f) \setminus V_{\mathbb{R}}(f)$ has one or two connected components. A method for making that decision was developed and implemented by Kalla and Klein [74], but presently their code is not suitable for curves of genus 10. One of our goals for the future is to extend `SexticClassifier` so that it decides rapidly between ‘d’ and ‘nd’ when the output is in (39).

3.1.4 Probability Distribution and Experiments

As a first application of `SexticClassifier`, we computed the empirical distributions of the topological types over the space of ternary sextics. In other words, we ask: what is the probability that a particular topological type arises when we pick a sextic curve at random? Of course, the answer will depend on the choice of a probability distribution on the sextics. A theoretical study for curves of large degree was carried out recently by Lerario and Lundberg [83], who employed the real Fubini-Study ensemble and the Kostlan distribution. The experiments below are meant to inform this line of inquiry with some empirical numbers.

The first distribution we consider is $U(3)$ -invariant. The 28 coefficients c_{ijk} are chosen independently from a univariate normal distribution, centered at 0, with variance equal to the multinomial coefficient $6!/(i!j!k!)$. According to [26, §16.1], this is the unique $U(3)$ -invariant probability measure on $\mathbb{R}[x, y, z]_6$. We selected 1,500,000 samples, ran `SexticClassifier` on these sextics, and then tallied the topological types. The result is shown in Table 3.

We see that the empirical distribution is very skewed. Only 14 of the 56 types were observed at all. Only six types had an empirical probability of $\geq 1\%$. No curve with more than six ovals was observed. In our sample, the average number of connected components is approximately 1.50. Another numerical invariant of the topological type of a smooth real plane curve introduced in [83, page 8] is the *energy*. This nonnegative integer measures the nesting of the ovals. For sextics, the maximal energy is 38 and attained by the Harnack-type curve (91)1. The average energy of the sextics in the sample above is approximately 2.99.

We experimented with several other distributions on $\mathbb{R}[x, y, z]_6$, each time drawing 500,000 samples and running `SexticClassifier`. In the following tables, we report percentages, and we only list topological types with empirical probability at least 0.01%.

If we naively sample our sextics having uniformly distributed integer coefficients, then the empirical distribution is even more skewed (Table 4). In Table 5 we see the empirical distribution obtained from sampling symmetric sextic polynomials. We do this by taking linear combinations of the monomial symmetric polynomials with coefficients being uniformly distributed integers between -10^{12} and 10^{12} . We see that the distribution now looks rather different from the two distributions considered before. For example, Type 7 appears with probability 0.01% whereas it did not appear among the 1,500,000 samples from the $U(3)$ -invariant distribution. The largest variation of types is observed when we sample sextics of the form $\det(xA + yB + zC)$ where A, B and C are symmetric 6×6 -matrices whose entries are uniformly distributed random integers between -1000 and 1000 (Table 6). This is also the only distribution we considered where the type with only one oval is not the most common type. Several types appear that did not show up among the 1,500,000 samples in Table 3.

Our most skewed distribution was from sampling signed sums (with the signs chosen uniformly at random) of ten sixth powers of linear forms whose coefficients are uniformly distributed integers between -1000 and 1000 . Thus, here we are restricting to sextics of real rank 10, the case considered in [94, §6]. Table 7 reveals that more than 90% of the samples have one oval. After passing to eleven summands, we observe more curves of Type 2 than empty curves. Going to sums of twelve sixth powers of linear forms increases this effect.

The experiments demonstrate that it is extremely rare to observe many ovals when sextic curves are generated at random. We never encountered a sextic with 8, 9, 10 or 11 ovals. Only few types occurred in our samples. This underscores the importance of having the explicit polynomials in $\mathbb{Z}[x, y, z]_6$ that are listed above, to serve as seeds for local sampling.

1	2	3	(11)	4	(11)1	(21)	5	\emptyset	(11)2	(21)1	6	(31)	(hyp)
875109	423099	97834	90316	7594	4360	1180	245	127	118	8	7	2	1

Table 3: Counts of topological types sampled from the $U(3)$ -invariant distribution

1	2	3	(11)	\emptyset	4
77.52%	18.19%	2.11%	1.46%	0.66%	0.06%

Table 4: Sextics with coefficients in $\{-10^{12}, \dots, 10^{12}\}$ uniformly distributed

1	\emptyset	3	(11)	4	6	(31)	(11)3	7	(hyp)
45.69%	28.38%	16.15%	7.40%	2.17%	0.13%	0.03%	0.03%	0.01%	0.01%

Table 5: Symmetric sextics with coefficients in $\{-10^{12}, \dots, 10^{12}\}$ uniformly distributed

2	3	1	4	(11)	(11)1	5	(21)	(11)2	6	(11)3	(21)1	(31)	7
29.12%	25.77%	16.44%	11.06%	8.02%	4.30%	2.46%	1.19%	0.98%	0.30%	0.13%	0.12%	0.07%	0.02%

Table 6: Sextics that are determinants of random symmetric matrices with linear entries

n	1	\emptyset	2	(11)	3
10	90.17%	5.14%	4.50%	0.09%	0.09%
11	89.95%	4.75%	5.06%	0.12%	0.12%
12	89.90%	4.28%	5.53%	0.15%	0.15%

Table 7: Sextics that are signed sums of n sixth powers of linear forms

We now report on the real properties of each of the topological type. We use Sylvester’s formula to sample from a fixed rigid isotopy class. Namely, we start with a representative f with $\Delta(f) \neq 0$, like one of the 64 sextics in Subsection 3.1.6. We then pick a random sextic g and we compute the univariate polynomial $\Delta(f+tg)$. This has 75 complex roots. We extract the real roots, and we identify the largest negative root and the smallest positive root. For any t in the open interval between these two roots, the sextic $f+tg$ has the same rigid isotopy type as f . Repeating this many times, we sample from the connected component of $\mathbb{R}[x, y, z]_6 \setminus \Delta$ that contains f . This gives us access to all sextics in the largest star domain with center f contained in that component. We call this process the *local exploration method*.

Certified samples were drawn in the vicinity of each of our current 64 representatives. For the sampled curves, Table 8 summarises experimental data on the numbers of real features associated with real sextics in $\mathbb{P}_{\mathbb{R}}^2$. Each row of Table 8 has five entries: the name of the rigid isotopy type, numbers of real inflection points, numbers of real eigenvectors, numbers of real bitangents, and one real rank. The numbers are ranges of integers that were observed in our experiments. For instance, for Type (11)1, we found numbers ranging between 20 and 66 of real bitangents among 324 complex ones. In some cases, all samples gave the same number of real solutions. For instance, all our Type (71) sextics had 108 real bitangents. Each entry in Table 8 can be regarded as a **conjecture**. For example, we conjecture that

every smooth sextic of Type (71) has exactly 108 real bitangents. For real inflection points and real eigenvectors we performed exact computations. That means that we are sure that all numbers listed in the table actually occur. However, we do not know whether there are more possible numbers. For bitangents the calculations are more involved and we applied numerical methods. This means that, for some instances, the number of real solutions might be undercounted. This can happen when two or more real bitangents lie very close to each other. The computations for estimating the real rank are even more delicate and were also accomplished numerically.

Bitangents and their applications are discussed in detail in Subsection 3.1.5. We now give the definitions needed to understand the other three columns in Table 8.

The second column concerns *inflection points* of a smooth sextic $V_{\mathbb{C}}(f) \subset \mathbb{P}^2$. There are $72 = 6 \cdot 12$ complex inflection points. They are computed as the solutions of the equations

$$f(x, y, z) = \det \begin{pmatrix} \frac{\partial^2 f}{\partial x^2} & \frac{\partial^2 f}{\partial x \partial y} & \frac{\partial^2 f}{\partial x \partial z} \\ \frac{\partial^2 f}{\partial x \partial y} & \frac{\partial^2 f}{\partial y^2} & \frac{\partial^2 f}{\partial y \partial z} \\ \frac{\partial^2 f}{\partial x \partial z} & \frac{\partial^2 f}{\partial y \partial z} & \frac{\partial^2 f}{\partial z^2} \end{pmatrix} = 0.$$

A curve of degree d has $3d(d-2)$ complex inflection points. A classical result due to Felix Klein states that the number of real inflection points is at most $d(d-2)$. Brugallé and López de Medrano [24] showed that this upper bound is tight for all degrees d . Hence, for a general sextic in $\mathbb{P}_{\mathbb{R}}^2$, the number of real inflection points is an even integer between 0 and 24. The column labeled “Flex” shows the empirical distribution on the 64 rigid isotopy types.

The third and fifth column pertain to the study of tensors in multilinear algebra. Here we identify the space $\mathbb{R}[x, y, z]_6$ of ternary sextics with the space of symmetric tensors of format $3 \times 3 \times 3 \times 3 \times 3 \times 3$. Such a symmetric tensor f has 28 distinct entries, and these are the coefficients c_{ijk} of the sextic. A vector $v \in \mathbb{C}^3$ is an *eigenvector* of f if v is parallel to the gradient of f at v . Thus the eigenvectors correspond to the solutions in $\mathbb{P}_{\mathbb{C}}^2$ of the constraint

$$\text{rank} \begin{pmatrix} x & y & z \\ \frac{\partial f}{\partial x} & \frac{\partial f}{\partial y} & \frac{\partial f}{\partial z} \end{pmatrix} = 1. \quad (45)$$

A general ternary form f of degree d has $d^2 - d + 1$ eigenvectors [3, Theorem 2.1]. The eigenvectors are the critical points of the optimisation problem of maximising f on the unit sphere $\mathbb{S}^2 = \{(x, y, z) \in \mathbb{R}^3 : x^2 + y^2 + z^2 = 1\}$. Since f attains a minimum and a maximum on \mathbb{S}^2 , the number of real eigenvectors is at least 2. We note that the upper bound $d^2 - d + 1$ is attained over \mathbb{R} . If f is a product of d general linear forms, then all its complex eigenvectors are real. This was shown in [3, Theorem 6.1]. For $d = 6$, we conclude that the number of real eigenvectors of a general ternary sextic is an odd integer between 3 and 31. The column labeled “Eigenvec” shows the empirical distribution on the rigid isotopy types. For many rigid isotopy types we found instances that attain the maximal number 31 of real eigenvectors. Among them are the 35 types that have unions of six real lines in general position in their closure. These types are marked with an asterisk next to the number 31. We found these by perturbing each of the four combinatorial types of arrangements of six

Type	Flex	Eigenvec	Bitang	Rank	Type	Flex	Eigenvec	Bitang	Rank
0	0	3–31	12	3	(11)5nd	6–16	29–31*	116–122	16
1	0–12	3–31*	12–56	3	(11)5d	8–16	25–31*	120–128	16
(11)	0–14	11–31*	12–66	10	7	4–14	25–31*	96–124	14
2	0–8	5–31*	12–52	13	(71)	20–24	29	108	16
(21)	0–10	7–31*	16–86	14	(61)1	20–22	25	104–214	15
(11)1	2–6	7–31*	20–66	15	(51)2	22	25–31	226–228	15
3	0–8	7–31*	24–94	13	(41)3	20	23–25	154–214	14
(hyp)	0–14	11–31*	12–52	13	(31)4	22	21	162–214	14
(31)	2–10	19–31*	24–90	13	(21)5	16–20	29–31	168	13
(21)1	0–6	11–31*	28–72	14	(11)6	12–14	27–31*	172–176	14
(11)2	0–4	11–31*	32–82	13	8	0–12	23–31*	124–142	13
4	0–2	11–31*	36–54	11	(81)nd	18–22	23	122–196	14
(41)nd	14–16	21–31*	48–90	16	(81)d	18–24	29	124–132	12
(41)d	12–14	27–31*	98–104	14	(71)1	14–18	21–31	104–240	13
(31)1	2–8	15–31*	40–86	14	(61)2	18–20	23–31	228–276	13
(21)2nd	10–16	17–31*	54–82	20	(51)3	22	25	192–254	13
(21)2d	8–16	19–31*	60–70	17	(41)4nd	14–16	25	188–220	9
(11)3	8–12	19–31*	48–94	14	(41)4d	18	25	194–230	11
5	2–10	19–31*	52–112	15	(31)5	20	25–31	198–260	13
(51)	12–16	21–31*	54–64	14	(21)6	20	23–31	242–258	15
(41)1	22	27–31*	90–104	14	(11)7	14–16	29–31	216	14
(31)2	14–18	27–31*	126–130	14	9nd	8–16	25–31*	162–172	15
(21)3	16	27–31*	112–116	14	9d	4–16	29–31*	156	15
(11)4	6–10	25–31*	76–106	15	(91)	18–22	23	124–236	13
6	10–12	23–31*	78–108	14	(81)1	16–20	23–31	162–240	14
(61)	16	27–31*	78–88	14	(51)4	20	27	232–234	10
(51)1nd	16	23–25	110–124	15	(41)5	18–20	27–31	232	10
(51)1d	20–24	29	136	16	(11)8	14–18	25–31	142–210	13
(41)2	16–20	29–31	126–128	14	10	0–24	21–31*	192	12
(31)3nd	12	25–31*	124–148	15	(91)1	18–22	25–31	200–284	14
(31)3d	20–22	29	132	16	(51)5	20–22	25–31	276–306	10
(21)4	14–20	27–31*	138–142	15	(11)9	16–20	25–31	174–250	14

Table 8: Computational results for the number of real solutions for inflection points, eigenvectors, bitangents and real rank among the 64 rigid isotopy classes of smooth sextics in $\mathbb{P}_{\mathbb{R}}^2$.

lines in general position in $\mathbb{P}_{\mathbb{R}}^2$. This search process resulted in 35 of the rigid isotopy types. This is the result stated in Proposition 3.1.2. The computation we described is the proof.

A theoretical study of real eigenvectors was undertaken by Maccioni in [86]. He proved that the number of real eigenvectors of a ternary form is bounded below by $2\omega + 1$, where ω is the number of ovals. Our findings in the third column of Table 8 confirm this theorem. Moreover, there are seven types where our computations prove the converse, namely that all values between this lower bound and the upper bound 31 are realised in these types.

Every tensor is a sum of rank one tensors. The smallest number of summands needed in such a representation is the *rank* of that tensor. This notion depends on the underlying field. Symmetric tensors of rank 1 are powers of linear forms (times a constant). Hence, the rank r of a ternary form f of degree d is the minimum number of summands in a representation

$$f(x, y, z) = \sum_{i=1}^r \lambda_i (a_i x + b_i y + c_i z)^d. \quad (46)$$

The exact determination of the real rank of a sextic f is very difficult. The task is to decide the solvability over \mathbb{R} of the equations in the unknowns λ_i, a_i, b_i, c_i obtained by equating coefficients in (46). This computation is a challenge for both symbolic and numerical methods. There is no known method that is guaranteed to succeed in practice. If f is a generic sextic in $\mathbb{R}[x, y, z]_6$ then the complex rank of f is 10, and the real rank of f is an integer between 10 and 19. This was shown in [94, Proposition 6.3]. This upper bound is probably not tight.

We experimented with the software `tensorlab` [117]. This is a standard package for tensors, used in the engineering community. This program furnishes a local optimisation method for the following problem: given f and r , find a sextic f^* of rank r that is closest to f , with respect to the Euclidean distance on the tensor space $(\mathbb{R}^3)^{\otimes 6}$. If the output f^* is very close to the input f , we can be confident that f has real rank $\leq r$. If f^* is far from f , even after many tries with different starting parameters, then we believe that f has real rank $\geq r + 1$. However, `tensorlab` does not furnish any guarantees. One needs to rerun the same instance many times to achieve a lower bound on the real rank with high confidence.

The last column of Table 8 suggests the real rank for each of the 64 sextics listed in Subsection 3.1.6. In each case, we report our best guess on the lower bound, based on numerical experiments with that instance. Obtaining these numbers with high confidence proved to be difficult. We had considerable help from Anna Seigal and Emanuele Ventura in carrying this out. Most puzzling is the real rank 20 we found for our representative of type (21)2nd, as this seems to contradict [94, Proposition 6.3]. This is either an error arising in our numerical method, or the sextic lies on some exceptional locus. Clearly, some further study is needed.

We did not yet attempt the same calculation for a larger sample of sextics in each rigid isotopy class. This would be a very interesting future project at the interface of numerics and real algebraic geometry. The guiding problem is to find the maximal generic real rank among sextics. To underscore the challenge, here is another open question: the real rank of the monomial $x^2 y^2 z^2$ is presently unknown. It is either 11, 12 or 13, by [94, Example 6.7].

We now shift gears and turn to the construction of real K3 surfaces. Two basic models of algebraic K3 surfaces are quartic surfaces in \mathbb{P}^3 and double-covers of \mathbb{P}^2 branched at a sextic curve. Thus, each of our ternary sextics in Subsection 3.1.6 represents a K3 surface over \mathbb{Q} . Suppose we can write $f = v_3^2 - v_2v_4$ where v_i is a form of degree i in x, y, z . Then $F = v_2w^2 + 2v_3w + v_4$ is a quartic in four variables that realises the K3 surface with one singular point at $(0 : 0 : 0 : 1)$. Blowing up that singular point gives the K3 surface encoded by f . Perturbing the coefficients of F gives a smooth quartic surface with similar properties.

The topology of the real surface $V_{\mathbb{R}}(F)$ is determined by the topological type of the real curve $V_{\mathbb{R}}(f)$ and its sign behavior. By perturbing F to a polynomial \tilde{F} , we can obtain a smooth quartic surface whose real part $V_{\mathbb{R}}(\tilde{F})$ has the desired topology. See [116] for details.

The construction methods in Subsection 3.1.2 reveal that many of the 64 types can be realised by adding a positive sextic to the product of a quartic and a conic. For such types, the sextic has the desired form $f = v_3^2 - v_2v_4$. The resulting quartic F has nice coefficients in \mathbb{Q} .

The real part of a smooth K3 surface is always an orientable surface. It has at most one connected component with nonpositive Euler characteristic — and therefore is determined (up to homeomorphism) by its total Betti number and its Euler characteristic — except when it is the union of two tori. If it is nonempty, by the Smith-Thom inequality, then its total Betti number ranges between 2 and 24. Furthermore, according to the Comessatti inequalities its Euler characteristic ranges between -18 and 20 . There are 64 possible combinations of these two numbers; they are displayed in [113, Table (3.3), page 189]. All these 64 possibilities can be realised as a quartic surface in \mathbb{P}^3 . These topological classifications were studied by G. Utkin in [116] and the isotopic, and rigid isotopic classifications were completed by V. Kharlamov ([75],[77]). For proofs and further information we refer to Silhol’s book [113, Section VIII.4]. We conclude by presenting two explicit quartic surfaces that realise the minimal and the maximal Euler characteristic.

Example 3.1.10. Consider the smooth quartic surface $V_{\mathbb{C}}(\bar{F}) \subset \mathbb{P}^3$ defined by the polynomial

$$\begin{aligned} \bar{F} = & 100w^4 - 12500w^2x^2 + 104x^4 - 12500w^2y^2 + 1640x^2y^2 + 1550y^4 + 12500w^2yz \\ & - 75x^2yz - 1552y^3z + 9375w^2z^2 - 487x^2z^2 - 1533y^2z^2 + 354yz^3 + 314z^4. \end{aligned}$$

Its real locus $V_{\mathbb{R}}(\bar{F})$ is a connected orientable surface of genus 10. The Euler characteristic of that surface is -18 . This is the smallest possible Euler characteristic for a real K3 surface.

We constructed the quartic \tilde{F} from a sextic f with ten non-nested ovals. Namely, $f = v_3^2 - v_2v_4$, where $v_4 = 33001x^4 + 131227x^2y^2 + 30980y^4 - 11842x^2yz - 62072y^3z - 155986x^2z^2 - 122652y^2z^2 + 56672yz^3 + 100672z^4$, $v_3 = 10^{-3}z^3$ and $v_2 = -4x^2 - y^2 + 2yz + 3z^2$. Our code `SexticClassifier` easily confirms that $V_{\mathbb{R}}(f)$ has Type 10. The quartic $F = v_2w^2 + 2v_3w + v_4$ has a node at $(0 : 0 : 0 : 1)$. The projection from this node is ramified at $V_{\mathbb{C}}(f)$. The K3 surface defined by $\tilde{F} = F + \epsilon w^4$ has the desired properties for $\epsilon = 10^{-10}$. Starting from \tilde{F} , we constructed \bar{F} using the techniques discussed in Subsection 3.1.2 for improving integer coefficients.

Our final example is dedicated to the algebraic geometer Karl Rohn, whose article [106]

inspired the work in [72]. Rohn was a professor at the University of Leipzig from 1904 until 1920.

Example 3.1.11. We start with Rohn’s imaginary symmetroid in [106, §9]. This is the quartic

$$G = \tau(s_1^2 - 6s_2)^2 + (s_1^2 - 4s_2)^2 - 64s_4,$$

where s_i is the i th elementary symmetric polynomial in x, y, z, w and $\tau = (16\sqrt{10} - 20)/135$. This is a nonnegative form with exactly 10 real zeros. Subtracting a positive definite form multiplied with a small positive scalar gives a quartic surface with ten connected components. Using the techniques in Subsection 3.1.2 we get the following quartic with nice integer coefficients:

$$\bar{G} = 6s_1^4 - 53s_1^2s_2 + 120s_2^2 - 320s_4.$$

The surface $V_{\mathbb{R}}(\bar{G})$ is the disjoint union of ten spheres, so it has Euler characteristic 20.

3.1.5 Avoidance Locus

Many software packages for plane curves, such as those discussed at the beginning of Subsection 3.1.3, work with affine coordinates. They often assume that the given curve is compact, so its closure in $\mathbb{P}_{\mathbb{R}}^2$ is disjoint from a distinguished line, namely, the line at infinity. We saw in Example 3.1.9 that no such line exists for some sextics. This motivates the concept of the avoidance locus, to be introduced and studied in this subsection. This will lead us naturally to computing dual curves and bitangent lines, and to investigating the reality of these objects.

Let C be a smooth real curve of even degree d in \mathbb{P}^2 . Its *avoidance locus* is the set \mathcal{A}_C of all lines in $\mathbb{P}_{\mathbb{R}}^2$ that do not intersect the real curve $C_{\mathbb{R}}$. Thus, \mathcal{A}_C is a semi-algebraic subset of the dual projective plane $(\mathbb{P}^2)_{\mathbb{R}}^{\vee}$. We write C^{\vee} for the curve of degree $d(d-1)$ in $(\mathbb{P}^2)^{\vee}$ that is dual to C . The points on C^{\vee} correspond to lines in \mathbb{P}^2 that are tangent to C . The real dual curve $C_{\mathbb{R}}^{\vee}$ divides the real projective plane $(\mathbb{P}^2)_{\mathbb{R}}^{\vee}$ into connected components.

Proposition 3.1.12. *Up to closure, the avoidance locus \mathcal{A}_C is a union of connected components of $(\mathbb{P}^2)_{\mathbb{R}}^{\vee} \setminus C_{\mathbb{R}}^{\vee}$. Each component appearing in \mathcal{A}_C is convex, when regarded as a cone in \mathbb{R}^3 .*

Proof. Points in $(\mathbb{P}^2)_{\mathbb{R}}^{\vee} \setminus C_{\mathbb{R}}^{\vee}$ correspond to real lines that intersect C transversally. Whether that intersection contains real points or not does not change unless the curve $C_{\mathbb{R}}^{\vee}$ is crossed. Hence $\mathcal{A}_C \setminus C_{\mathbb{R}}^{\vee}$ is a union of connected components of $(\mathbb{P}^2)_{\mathbb{R}}^{\vee} \setminus C_{\mathbb{R}}^{\vee}$. Each of these components is convex: it is the convex dual of the convex hull of $C_{\mathbb{R}}$ in the affine space $\mathbb{P}_{\mathbb{R}}^2 \setminus L$, where $L \in \mathcal{A}_C$. The prefix “up to closure” is needed because \mathcal{A}_C also contains some points in $C_{\mathbb{R}}^{\vee}$, corresponding to real lines that do not meet $C_{\mathbb{R}}$ but are tangent to C at complex points. \square

Example 3.1.13. Let $d = 4$ and consider the *Edge quartic* C , taken from [101, equation (1.5)]:

$$25(x^4 + y^4 + z^4) - 34(x^2y^2 + x^2z^2 + y^2z^2) = 0.$$

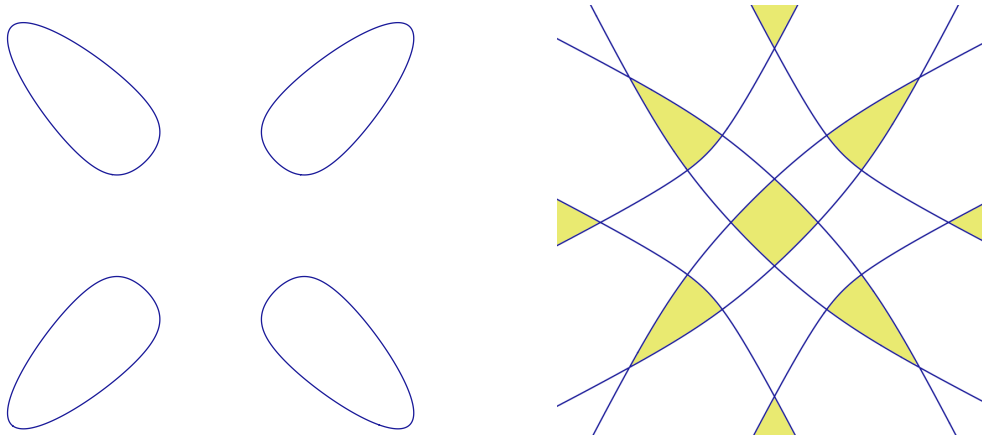


Figure 20: The Edge quartic C and its dual C^\vee ; the avoidance locus \mathcal{A}_C is coloured.

This curve $C \subset \mathbb{P}^2$ served as a running example in [101]. It is shown on the left in Figure 20. We choose coordinates $(u : v : w)$ for points in the dual projective plane $(\mathbb{P}^2)^\vee$. Such a point represents the line $L = \{ux + vy + wz = 0\}$ in the primal \mathbb{P}^2 . The dual curve C^\vee is given by

$$\begin{aligned}
& 10000u^{12} - 98600u^{10}v^2 - 98600u^{10}w^2 + 326225u^8v^4 + 85646u^8v^2w^2 + 326225u^8w^4 - 442850u^6v^6 \\
& - 120462u^6v^4w^2 - 120462u^6v^2w^4 - 442850u^6w^6 + 326225u^4v^8 - 120462u^4v^6w^2 + 398634u^4v^4w^4 \\
& - 120462u^4v^2w^6 + 326225u^4w^8 - 98600u^2v^{10} + 85646u^2v^8w^2 - 120462u^2v^6w^4 - 120462u^2v^4w^6 \\
& + 85646u^2v^2w^8 - 98600u^2w^{10} + 10000v^{12} - 98600v^{10}w^2 + 326225v^8w^4 - 442850v^6w^6 + 326225v^4w^8 \\
& - 98600v^2w^{10} + 10000w^{12} = 0.
\end{aligned}$$

The dual curve $C_{\mathbb{R}}^\vee$ divides $(\mathbb{P}^2)_{\mathbb{R}}^\vee$ into 21 open regions. Seven of the regions comprise the avoidance locus \mathcal{A}_C . They are coloured in Figure 20, and they represent the seven ways of bipartitioning the four ovals of $C_{\mathbb{R}}$ by a straight line. The convex body dual to the convex hull of $C_{\mathbb{R}}$, in our affine drawing on the left, is the innermost yellow region on the right.

The number seven of yellow regions seen in Figure 20 attains the following upper bound.

Proposition 3.1.14. *Let C be a smooth real curve of even degree d in \mathbb{P}^2 . The number of open convex sets in the dual plane that make up the avoidance locus \mathcal{A}_C is bounded above by*

$$\frac{9}{128}d^4 - \frac{9}{32}d^3 + \frac{15}{32}d^2 - \frac{3}{8}d + 1. \quad (47)$$

Proof. By Harnack's inequality, the real curve $C_{\mathbb{R}}$ can have at most $\binom{d-1}{2} + 1$ ovals in $\mathbb{P}_{\mathbb{R}}^2$. However, for our count we only care about the outermost ovals, i.e. those not contained inside any other oval. By a result of Arnold in [6], which is a more precise version of a classical inequality due to Petrovsky's [100], the number of outermost ovals of the curve $C_{\mathbb{R}}$ is at most

$$m = \frac{3}{8}d^2 - \frac{3}{4}d + 1.$$

Pick a generic point in each oval. Then the configuration of points has $\binom{m}{2} + 1$ bipartitions that can be realised by a straight line. Indeed, dually, this is the number of regions in the

complement of a general arrangement of m lines in the plane $\mathbb{P}_{\mathbb{R}}^2$. The quartic polynomial in (47) is simply $\binom{m}{2} + 1$ with Petrovsky's expression for m . It remains to be seen that this number is the desired upper bound. Indeed, every connected component of \mathcal{A}_C is uniquely labeled by a bipartition of the set of non-nested ovals. The number of such bipartitions that are realised by a straight line is bounded above by the said bipartitions of the points. \square

The upper bound in (47) evaluates to 46 for $d = 6$. Here is a sextic that attains the bound.

Example 3.1.15. Let t and ϵ be parameters, and consider the following net of sextics:

$$\begin{aligned} F_{t,\epsilon} = & 60x^6 - 750x^5z - 111x^4y^2 + 1820x^4z^2 + 700x^3y^2z - 2250x^3z^3 + 20x^2y^4 \\ & - 1297x^2y^2z^2 + 960x^2z^4 - 56xy^4z + 1440xy^2z^3 - y^6 - 576y^2z^4 \\ & + t(x^3 + xz^2 - y^2z)^2 + \epsilon(x^2z^4 + y^2z^4 + z^6) \end{aligned}$$

For $t_0 = -\frac{1645}{2} - 150\sqrt{34}$ and $\epsilon = 0$, the sextic $F_{t_0,0}$ has 10 isolated real singular points:

$$((3 - \sqrt{34})/5 : 0 : 1), (0 : 0 : 1), (1 : \pm\sqrt{2} : 1), (2 : \pm\sqrt{10} : 1), (3 : \pm\sqrt{30} : 1), (4 : \pm 2\sqrt{17} : 1).$$

No three of these 10 points lie on a line. For any sufficiently small $\epsilon > 0$ and t sufficiently close to t_0 , the sextic $F_{t,\epsilon}$ is smooth with 10 small ovals arranged around the singular points of $F_{t_0,0}$. When these ovals are small enough, the avoidance locus will have the maximum number 46 of connected components, by the argument given in the proof of Proposition 3.1.14. This example was found using the construction developed by Kunert and Scheiderer in [79].

We now describe an algorithm for computing the avoidance locus \mathcal{A}_C of a smooth curve C . The first step is to find all bitangents of C . A *bitangent* of C is a line L in \mathbb{P}^2 that is tangent to C at two points. Note that bitangents of C correspond to nodal singularities of the dual curve C^\vee . By the Plücker formulas, the expected number of bitangents is $(d-3)(d-2)d(d+3)/2$, which is 324 for $d = 6$. A bitangent L is called *relevant* if the real part of the divisor $L \cap C$ is an even divisor on the curve C . For generic curves C , this means that L has no real intersection points with C except possibly the two points of tangency. If these two points are real, then L is an extreme point of a convex connected component of \mathcal{A}_C .

Remark 3.1.16. Let C be a smooth curve in $\mathbb{P}_{\mathbb{R}}^2$ of degree $d \geq 4$. If C contains at least two outermost ovals or has a non-convex outermost oval, then every connected component of the avoidance locus \mathcal{A}_C has a relevant bitangent in its closure. If C does not satisfy this hypothesis then \mathcal{A}_C is connected; we do not know whether it always contains a real bitangent. In the case of quartics, this follows from the Zeuthen classification [123]. In that case, however, the number of bitangents only depends on the topological type. In higher degrees, when this is not the case, not much seems known. (See Conjecture 3.1.19 below.)

We now assume that C satisfies the hypothesis in Remark 3.1.16. Our algorithm for computing \mathcal{A}_C is as follows. First we compute linear forms representing all real bitangents of C , and we discard those that are not relevant. Next, we compute a graph \mathcal{G}_C whose nodes are the relevant bitangents, as follows: two linear forms L_1 and L_2 form an edge if and only if

- (a) $L_1 + L_2$ lies in the avoidance locus \mathcal{A}_C , and
- (b) the open line segment $\{tL_1 + (1-t)L_2 : 0 < t < 1\}$ is disjoint from the dual curve $C_{\mathbb{R}}^{\vee}$.

Here the sign of the linear forms L_1 and L_2 for the bitangents has to be chosen carefully.

Remark 3.1.17. The graph \mathcal{G}_C is a disjoint union of cliques, one for each connected component of \mathcal{A}_C . This follows from Remark 3.1.16 and convexity of the connected components.

In summary, given a smooth curve $C = V_{\mathbb{C}}(f)$ of even degree d , our algorithm computes the *avoidance graph* \mathcal{G}_C . We represent the avoidance locus \mathcal{A}_C by the connected components (cliques) of \mathcal{G}_C . Midpoints of the segments in (b) furnish sample points in the components.

We made a proof-of-concept implementation of this algorithm for the case of sextics. Its two main ingredients are computing the dual curve and computing the bitangents. For the former task we solve a linear system of equations in the $\binom{30+2}{2} = 496$ coefficients of C^{\vee} . The equations are derived by projecting C from random points $p \in \mathbb{P}^2$. The ramification locus of this projection reveals (up to scaling) the binary form of degree 30 that defines $C^{\vee} \cap p^{\perp}$.

To compute the bitangents, we employ the variety of binary sextics with two double roots. The prime ideal of this variety is defined by 13 forms of degree 7; see the row labeled 2211 in [81, Table 1]. Substituting the binary form $f(x, y, -\frac{1}{w}(ux + vy))$ into that ideal, and clearing denominators, yields the ideal in $\mathbb{Q}[u, v, w]$ that defines the 324 bitangents $(u:v:w) \in (\mathbb{P}^2)^{\vee}$.

Example 3.1.18. Let C be the representative for Type 8nd displayed in Subsection 3.1.6. This sextic curve has 324 distinct complex bitangents of which 124 are real. Of the real bitangents,

- 8 are tangent at non-real points and meet the curve in two more non-real points;
- 60 are tangent at real points and meet the curve in two more non-real points;
- 4 are tangent at non-real points and meet the curve in two more real points;
- 52 are tangent at real points and meet the curve in two more real points.

Only the first two types are relevant, so C has 68 relevant bitangents. The avoidance graph \mathcal{G}_C is found to consist of 14 cliques: four K_6 's, five K_5 's, four K_4 's and one K_3 . Hence \mathcal{A}_C consists of 14 convex components. The curve C together with its 68 relevant bitangents is shown in Figure 21. There are 14 ways to bipartition the 8 ovals by a line that avoids $C_{\mathbb{R}}$.

While the nodes on C^{\vee} are bitangents of C , the cusps on C^{\vee} are the *flex lines* of C . The number of *inflection points* is $3d(d-2)$ for a general curve of degree d . A classical result due to Felix Klein states that at most one third of the complex inflection points of a real plane curve can be real. Brugallé and López de Medrano [24] proved, using tropical methods, that Klein's upper bound $d(d-2)$ is attained for all $d \geq 3$. Hence, for smooth sextics, the number of real inflection points can be any even integer between 0 and 24. The distribution of the numbers of real bitangents and real inflection points over the 64 rigid isotopy types is presented in the previous subsection. Based on our experiments, we propose the following conjecture:

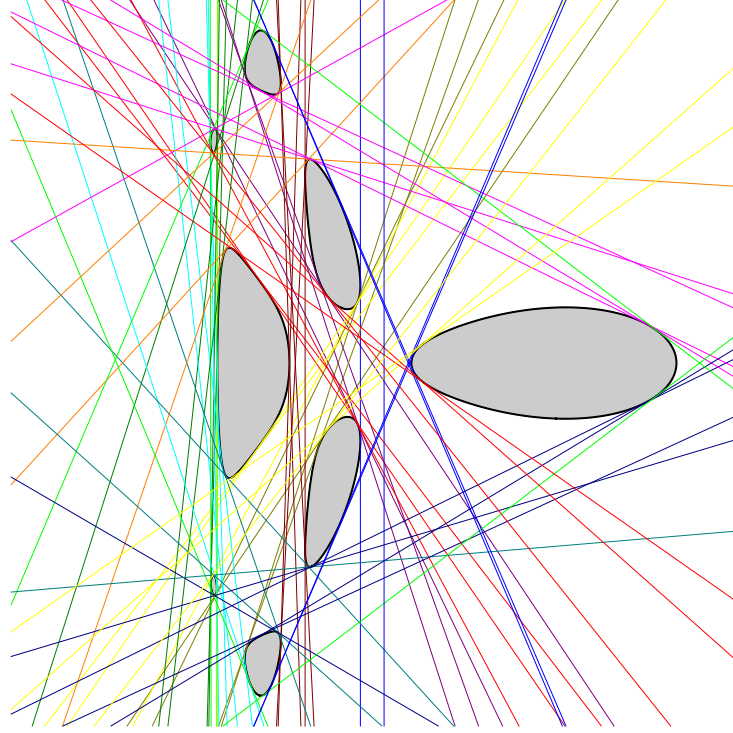


Figure 21: A sextic curve C with 8 non-nested ovals; its 68 relevant bitangents represent \mathcal{A}_C .

Conjecture 3.1.19. *The number of real bitangents of a smooth sextic in $\mathbb{P}_{\mathbb{R}}^2$ ranges from 12 to 306. The lower bound is attained by curves in the following four types: empty, 1, 2, (11) and (hyp). The upper bound is attained by certain 11-oval curves of Gudkov-type (51)5.*

The numbers of real inflection points and bitangents of a sextic C often change when passing through the discriminant hypersurface. However, they may also change within the same rigid isotopy type. If C is smooth then the total number of complex inflection points resp. bitangents drops below the bounds 72 resp. 324 in the following three exceptional cases:

- (411) C has an *undulation point*, in which the tangent meets C with multiplicity at least 4.
- (222) C has a *tritangent line*, i.e. a line that is tangent to C in three distinct points.
- (321) C has a *flex-bitangent*, i.e. a line that meets C with multiplicity 3 in one point and is tangent at another point.

In each case, the stated property defines a hypersurface in $V = \mathbb{R}[x, y, z]_6$. The number of real inflection points or bitangents changes only when passing through the discriminant or one of these hypersurfaces. When generic sextics approach these hypersurfaces, three lines come together: a bitangent and two flex lines for an undulation point (411), three bitangents for a tritangent line (222), and two bitangents and a flex line for a flex-bitangent (321).

Theorem 3.1.20. *Let \mathcal{T} be the Zariski closure in $\mathbb{P}V = \mathbb{P}^{27}$ of the set of smooth sextics with a tritangent line and let \mathcal{F} be the locus of smooth sextics with a flex-bitangent. Then:*

1. The loci \mathcal{T} and \mathcal{F} are irreducible hypersurfaces of degree 1224 and 306 respectively.
2. Their union $\mathcal{B} = \mathcal{T} \cup \mathcal{F}$ is the bitangent discriminant, i.e. the Zariski closure of the set of smooth sextics in $\mathbb{P}V$ having fewer than 324 bitangent lines.

Proof. The variety of binary sextics with three double roots is irreducible of codimension 3 in $\mathbb{R}[x, y]_6$. (It is defined by 45 quartics [81, Table 1].) Let \mathcal{X} be the incidence variety of all pairs (L, f) in $(\mathbb{P}^2)^\vee \times \mathbb{P}V$ where L is a tritangent of $V_{\mathbb{C}}(f)$. The locus \mathcal{T} is the projection of \mathcal{X} onto $\mathbb{P}V$. The intersection of \mathcal{X} with any subspace of the form $\{L\} \times \mathbb{P}V$ for $L \in (\mathbb{P}^2)^\vee$ has codimension 3 in $\mathbb{P}V$. Taking the union over all L , we conclude that \mathcal{T} has codimension 1. Since the projection of \mathcal{X} onto the first factor is surjective with irreducible fibers of constant dimension, \mathcal{X} is irreducible, hence so is \mathcal{T} . The same argument applies to \mathcal{F} . The degrees of the hypersurfaces \mathcal{F} and \mathcal{T} were computed for us by Israel Vainsencher with the Maple package `schubert`. The relevant theory is described by Colley and Kennedy in [32].

To prove (2), we first note that a tritangent splits into three bitangents, and a flex-bitangent into two bitangents and a flex line, for any smooth deformation of a sextic in \mathcal{T} or \mathcal{F} , respectively. This shows that \mathcal{T} and \mathcal{F} are both contained in the bitangent discriminant. For the reverse, we argue in the dual picture, with degenerations of singularities on C^\vee . \square

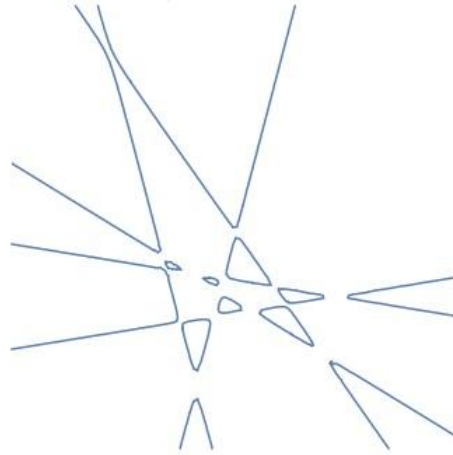


Figure 22: A smooth sextic with 10 non-nested ovals whose avoidance locus is empty

We conclude this subsection with the following result on the avoidance loci of plane sextics.

Corollary 3.1.21. *For any integer m between 0 and 46, there exists a smooth sextic C in $\mathbb{P}_{\mathbb{R}}^2$ whose avoidance locus \mathcal{A}_C comprises exactly m convex connected components.*

Proof. Let f_1 be a sextic of Type 10nd whose avoidance locus has 46 components, as in Example 3.1.15. Let f_0 be a sextic of Type 10nd with empty avoidance locus, for instance

$$f_0 = (20x^2 - (y+10z)^2 + z^2)(21y^2 - (x-10z)^2 + z^2)(20(x-5z+y)^2 - (y+10z)^2 + z^2) + z^6.$$

The real picture of such a curve is shown in Figure 22. Let U be the connected component of $\mathbb{P}_{\mathbb{R}}^{27} \setminus \Delta$ that contains both f_0 and f_1 . Consider the bitangent discriminant \mathcal{B} of Theorem 3.1.20. There is an open dense subset \mathcal{B}_0 of \mathcal{B} , whose points represent curves with a single tritangent line or a single flex-bitangent. The exceptional locus $Z = \mathcal{B} \setminus \mathcal{B}_0$ has codimension at least 2 in $\mathbb{P}_{\mathbb{R}}^{27}$, hence $V = U \setminus Z$ is path-connected. Fix a path $\gamma: [0, 1] \rightarrow V$ with $\gamma(0) = f_0$, $\gamma(1) = f_1$. Let $\{\gamma(t_1), \dots, \gamma(t_k)\}$ be its intersection points with \mathcal{B} . Since $\gamma(t_i)$ lies in \mathcal{B}_0 , the number of connected components of the avoidance locus of $V_{\mathbb{R}}(\gamma(t))$ cannot change by more than 1 in a neighborhood of t_i . Indeed, at a point where that number drops by one, exactly three relevant bitangents come together, giving a sextic with a single tritangent in \mathcal{B}_0 . Hence any number of convex avoidance components between 0 and 46 is realised along the path γ . \square

3.1.6 List of Representatives

We now give the explicit polynomial representatives and thence, proving the following result.

Proposition 3.1.22. *Each of the 64 rigid isotopy types can be realised by a ternary sextic in $\mathbb{Z}[x, y, z]_6$ whose integer coefficients have absolute value less than 1.5×10^{38} .*

We list 64 polynomials with integer coefficients that represent the 64 rigid isotopy types of smooth sextic curves in $\mathbb{P}_{\mathbb{R}}^2$. This list is available in a computer-algebra-friendly format at

$$\text{https://software.mis.mpg.de/planeSexticCurves/index.html} \quad (48)$$

Each of our sextics is labeled by its topological type and whether it is dividing (d) or non-dividing (nd) in its Riemann surface. We begin with the 35 types that have at most 7 ovals:

0	nd	$x^6 + y^6 + z^6$
1	nd	$x^6 + y^6 - z^6$
(11)	nd	$6(x^4 + y^4 - z^4)(x^2 + y^2 - 2z^2) + x^5y$
2	nd	$(x^4 + y^4 - z^4)((x + 4z)^2 + (y + 4z)^2 - z^2) + z^6$
(21)	nd	$16((x+z)^2 + (y+z)^2 - z^2)(x^2 + y^2 - 7z^2)((x-z)^2 + (y-z)^2 - z^2) + x^3y^3$
(11)1	nd	$((x + 2z)^2 + (y + 2z)^2 - z^2)(x^2 + y^2 - 3z^2)(x^2 + y^2 - z^2) + x^5y$
3	nd	$(x^2 + y^2 - z^2)(x^2 + y^2 - 2z^2)(x^2 + y^2 - 3z^2) + x^6$
(hyp)	d	$6(x^2 + y^2 - z^2)(x^2 + y^2 - 2z^2)(x^2 + y^2 - 3z^2) + x^3y^3$
(31)	nd	$(10(x^4 - x^3z + 2x^2y^2 + 3xy^2z + y^4) + z^4)(x^2 + y^2 - z^2) + x^5y$
(21)1	nd	$(10(x^4 - x^3z + 2x^2y^2 + 3xy^2z + y^4) + z^4)((x + z)^2 + y^2 - 2z^2) + x^5y$
(11)2	nd	$(10(x^4 - x^3z + 2x^2y^2 + 3xy^2z + y^4) + z^4)(x^2 + (y - z)^2 - z^2) + x^5y$
4	nd	$x^6 + y^6 + z^6 - 4x^2y^2z^2$
(41)	nd	$((x^2 + 3y^2 - 20z^2)(4x^2 + y^2 - 16z^2) + 18x^2z^2)(x^2 + y^2 - 10z^2) - 2z^6$
(41)	d	$10(((x^2 + 2y^2 - 16z^2)(2x^2 + y^2 - 16z^2) + x^2y^2)(10x + y + 5z) + xz^4)(10x - y - 8z) - xz^5$
(31)1	nd	$((x^2 + 3y^2 - 17z^2)(3x^2 + y^2 - 10z^2) + 15x^2z^2)(x^2 + 4(y + z)^2 - 25z^2) + x^3y^3$
(21)2	nd	$((x^2 + 3y^2 - 20z^2)(4x^2 + y^2 - 16z^2) + 18x^2z^2)((x + y)^2 + 20(x - y - 3z)^2 - 24z^2) + (y - x)z^5$
(21)2	d	$((x^2 + 3y^2 - 20z^2)(4x^2 + y^2 - 16z^2) + 18x^2z^2)(x^2 + 8y^2 - 16z^2) - 4z^6$
(11)3	nd	$((x^2 + 2y^2 - 30z^2)(3x^2 + y^2 - 20z^2) + 15x^2z^2)(x^2 + (4y + 16z)^2 - 15z^2) + x^3y^3$

5	nd	$4((x^2 + 2y^2 - 4z^2)(2x^2 + y^2 - 4z^2) + z^4)(x^2 + y^2 - z^2) + x^3y^3$
(51)	nd	$(3x^2 + 4xy + 2y^2 - 4z^2)(x^2 + 2(y - z)^2 - 8z^2)(2x^2 + y^2 - 3z^2) - z^6$
(41)1	nd	$(4x^2 + 6x(y - z) + 3(y - z)^2 - 14z^2)(x^2 + 5(y - 2z)^2 - 9z^2)(2x^2 + (y - z)^2 - 15z^2) - yz^5$
(31)2	nd	$((x + z)^2 + 4y^2 - 4z^2)(7(x + z)^2 + y^2 - 10z^2)((x + z)^2 + 4(2(x + y) + 3z)^2 - 8z^2) + xz^5$
(21)3	nd	$((x + z)^2 + 3y^2 - 4z^2)(7(x + z)^2 + y^2 - 12z^2)((x + z)^2 + 3(2(x + y) + 3z)^2 - 5z^2) + xz^5$
(11)4	nd	$((x^2 + 3y^2 - 20z^2)(4x^2 + y^2 - 16z^2) + 18x^2z^2)(8x^2 + y^2 - 16z^2) + (x + y)z^5$
6	nd	$(3x^2 + 5xy + 2y^2 - 7z^2)(x^2 + 2(y - z)^2 - 8z^2)(2x^2 + y^2 - 5z^2) - z^6$
(61)	nd	$(4x^2 + 4xy + 3y^2 - 4z^2)(x^2 + 3y^2 - 4z^2)(4x^2 + y^2 - 4z^2) - z^6$
(51)1	nd	$30(((x - z)^2 + 3y^2 - 5z^2)(3(x - z)^2 + y^2 - 5z^2) + xz^3)((x - z)^2 + y^2 - 2z^2) + (x - 2z)z^5$
(51)1	d	$7((x^2 + 3(y + z)^2 - 48z^2)(3(x + z)^2 + y^2 - 48z^2) - z^4)(x^2 + y^2 - 26z^2) + xz^5 + yz^5$
(41)2	nd	$15(4x^2 + y^2 - 3z^2)(x^2 + 3y^2 - 3z^2)((4x - z)^2 + 16y^2 - 22z^2) + (5xz^5 + (y - z)^3z^3)$
(31)3	nd	$34((3x^2 + y^2 - 3z^2)(x^2 + 8y^2 - 3z^2) + x^2y^2)(2x^2 - yz - 2z^2) + (x - 4z)yz^4$
(31)3	d	$((x^2 + 3y^2 - 28z^2)(4x^2 + y^2 - 20z^2) - z^4)((x + z)^2 + y^2 - 12z^2) - xz^5$
(21)4	nd	$27(2xz - 6y^2 + 2yz + 3z^2)(-(x + y)^2 - 4y^2 + 2z^2)(5(x + y)^2 + y^2 - 4z^2) - xz^5$
(11)5	nd	$((x^2 + 3y^2 - 20z^2)(4x^2 + y^2 - 16z^2) + 18x^2z^2)(16x^2 + y^2 - 20z^2) - (x + y)z^5$
(11)5	d	$((x^2 + 3y^2 - 20z^2)(4x^2 + y^2 - 16z^2) + 18x^2z^2)((x + y)^2 + 20(x - y - 3z)^2 - 24z^2) + (x + y)z^5$
7	nd	$2(4x^2 + y^2 - 4z^2)(x^2 + 4y^2 - 5z^2)(x^2 + y^2 - 4z^2) + 3x^4y^2 + xy^5$

Next, we have eight topological types with eight ovals, all of which are non-dividing:

(71)	nd	$2(x^2 + y^2 - 26z^2)(x^2 + 3(y + z)^2 - 48z^2)(3(x + z)^2 + y^2 - 48z^2) - z^6$
(21)5	nd	$40(3x^2 + y^2 - 3z^2)(x^2 + 8(y - z)^2 - 3z^2)(2x^2 - yz - 2z^2) - (y^3z^3 + 2xz^5 - 2z^6)$
(11)6	nd	$19(4x^2 + y^2 - 4z^2)(x^2 + 8(y - z)^2 - 3z^2)(2x^2 - yz - 2z^2) - (2y - 3z)z^5$
8	nd	$12(x^4 + 2x^2y^2 + y^4 - x^3z + 3xy^2z)(7(8x + 3z)^2 + 8y^2 - 10z^2) + x^5y + 2z^6$

(61)1	nd	$(160075(5yz - x^2)(8(xz + 15z^2) - (y - 12z)^2) + 109(17x + 5y + 72z)(13x + 5y + 42z)(9x + 5y + 20z)(2x + 5y))(5yz - x^2) - (x + 3z)z^5$
(51)2	nd	$(5435525((y + z)z - x^2)((x + 2z)z - 2(y - x)^2) + 5(25x - 25y - 31z)(5x - 50y - 49z)(15x + 25y + 27z)(35x + 25y + 37z))((y + z)z - x^2) + x^5y$
(41)3	nd	$(14460138((y + z)z - x^2)((x + 2z)z - 2(y - x)^2) + 5(25x - 25y - 31z)(5x - 50y - 49z)(15x + 25y + 27z)(37z + 35x + 25y))((y + z)z - x^2) + x^5y$
(31)4	nd	$(27867506((y + z)z - x^2)((x + 2z)z - 2(y - 2x)^2) + 61(6x + 8y + 9z)(64y + 63z)(15x - 25y - 27z)(35x - 25y - 37z))((y + z)z - x^2) + x^5y$

Among the 12 rigid isotopy types with 9 ovals, two are from (40) and three pairs are from (39):

(11)7	nd	$23(3x^2 + y^2 - 3z^2)(x^2 + 8(y - z)^2 - 3z^2)(2x^2 - yz - 2z^2) - (2y - 3z)z^5$
9	nd	$((x^2 + 3y^2 - 20z^2)(4x^2 + y^2 - 16z^2) + 18x^2z^2)((x + y)^2 + 20(x - y - 3z)^2 - 24z^2) + y^2z^4$
9	d	$((x^2 + 3y^2 - 20z^2)(4x^2 + y^2 - 16z^2) + 18x^2z^2)(16x^2 + y^2 - 20z^2) + z^6$
(81)	d	$((x^2 + 3y^2 - 28z^2)(4x^2 + y^2 - 20z^2) - z^4)(2x^2 + y^2 - 12z^2) - z^6$

(81)	nd	$(1920981(yz - x^2)(57(x + z)z - (6x - y + 6z)^2) + 48(10x + 7y + 3z)(11x + 25y + z)(11x - 23y - z)(10x - 8y - 3z))(x^2 - yz) + x^2y^4 - 61y^6$
(71)1	nd	$(529321083(yz - x^2)(53(x + z)z - (6x - y + 6z)^2) + 25(10x + 8y + 3z)(12x + 30y + z)(12x - 32y - z)(10x - 8y - 3z))(x^2 - yz) - y^6$
(61)2	d	$(19157935(5yz - x^2)(8(xz + 15z^2) - (y - 12z)^2) + 1185(17x + 5y + 72z)(13x + 5y + 42z)(9x + 5y + 20z)(2x + 5y))(5yz - x^2) - (x + 3z)z^5$
(51)3	nd	$(28920269((y + z)z - x^2)((x + 2z)z - 2(y - x)^2) + 10(25x - 25y - 31z)(5x - 50y - 49z)(15x + 25y + 27z)(35x + 25y + 37z))((y + z)z - x^2) + x^5y$
(41)4	nd	$6761249083262(68794627464(1095368(118(x^2 + y^2 - 3z^2)y + (x - 2z)(x - 12z)(x - 13z))y + (x - 4z)(x - 9z)(x - 10z)(x - 11z))y + (x - 3z)(x - 5z)(x - 6z)(x - 7z)(x - 8z))y - z^6$
(41)4	d	$13278270242890(52982089012(1610519(149(x^2 + y^2 - 4z^2)y + (x - 3z)(x - 13z)(x - 14z))y + (x - 5z)(x - 10z)(x - 11z)(x - 12z))y + (x - 4z)(x - 6z)(x - 7z)(x - 8z)(x - 9z))y - (x - 5z)z^5$
(31)5	nd	$(26894836459((y + z)z - x^2)((x + 2z)z - 2(y - 2x)^2) + 1880(6x + 8y + 9z)(64y + 63z)(15x - 25y - 27z)(35x - 25y - 37z))((y + z)z - x^2) + x^5y$
(21)6	d	$(93678589978((y + z)z - x^2)((x + 2z)z - 2(y - 2x)^2) + 50949(6x + 8y + 9z)(18x - 72y - 73z)(5x - 6y - 7z)(-27x + 18y + 28z))((y + z)z - x^2) + x^5y$

3.2 Biology and Optimisation

This section is based on an ongoing work with Yue Ren, Mohab Safey El Din, and Johannes Martini. We look at the interaction between components that is a key concept in the functionality of biological systems. In chemistry and biology, a *ligand* is a substance that purposefully binds to a *target molecule* inside a bigger system. Examples for ligands and their target molecules are oxygen and the hemoglobin in blood [13], nicotine and the nicotinic receptors inside the brain [19], or glutamate and the umami receptors on the tongue [18]. Usually target molecules have multiple *binding sites*, which means that multiple ligands may bind to a single molecule, and *cooperativity* is a phenomenon in which already bound ligands affect the chances of other ligands binding to the still open sites. We call cooperativity positive if the chances increase and negative if the chances decrease.

Cooperativity is ubiquitous in nature. It makes the molecule prefer the states in which either all or none of its sites are occupied, which is useful if its purpose is to transport or detect the ligand. This effect is best observed in the *binding curve*, which relates the ligand concentration Λ outside the system with the ligand saturation $\Psi(\Lambda)$ inside the system.

Figure 23 is taken from a classical work in biology [13]. It visualises the oxygen binding to hemoglobin in dog blood and horse blood. Binding curves reveal a distinct S-shape instead of a steady linear increase for systems with independent sites [7, 62]. In the figure, this shape indicates that more the sites are occupied by oxygen, it becomes likely for more oxygen to bind to the hemoglobin till all the sites are occupied.

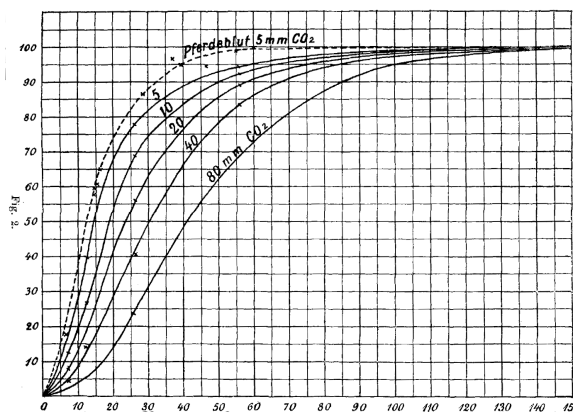


Figure 23: The effect of cooperativity on a binding curve

The most comprehensive model for ligand binding is based on the grand canonical ensemble of statistical mechanics [9, 122]. It describes the target molecule by assigning each site a variable which encodes the difficulty of binding to it and each subset of sites a variable which encodes the interaction between them. In this model, the binding curve arises from the Adair equation [5, 115]

$$\Psi(\Lambda) = \frac{na_n\Lambda^n + (n-1)a_{n-1}\Lambda^{n-1} + \dots + a_1}{a_n\Lambda^n + a_{n-1}\Lambda^{n-1} + \dots + a_1 + 1}.$$

The coefficients a_i depend on the variables of the molecule. The *binding polynomial* is the denominator of $\Psi(\Lambda)$, and it uniquely determines the shape of the binding curve. For the

characterisation of the binding behavior, the roots of the binding polynomial have been the objects of investigations [20, 21, 22, 98]. In particular, it has been pointed out that the criterion of having non-real roots is the generally relevant aspect indicating that a binding process relies on non-neglectable interactions [91].

Despite its prominence, there is no universal definition for cooperativity. It is well-studied for many important classes of molecules, usually molecules with some internal symmetry such as having indistinguishable binding sites [2, 107]. However, it has been shown that in the framework of the grand canonical ensemble of statistical mechanics, different definitions of cooperative binding do not coincide when general asymmetric systems with more than two binding sites are considered [91, 89]. For the case when the binding sites are not considered indistinguishable, it has been proposed to use the minimal absolute interaction between the sites which is required to generate the overall binding behavior as a general measure of cooperativity [90]. As cooperativity emerges from the individual interactions between the sites, it makes sense to study the internal interactions of molecules with the given binding curve. However, it has not been clear how to explicitly calculate this measure of cooperativity for larger systems.

In the following subsections, we show that looking for the minimal interaction required to generate a given overall titration behavior leads to an algebraic optimisation problem. In Subsection 3.2.1 we describe the mathematical problem and the software that can be used to address it. We will discuss the challenge of computing a target molecule with prescribed binding curve that globally minimises the overall interaction between its sites in Subsection 3.2.2. Our main focus is the classical system of hemoglobin with its four binding sites for oxygen or other ligands such as carbon monoxide. Hence, we usually consider the case when the molecule has four binding sites. In Subsection 3.2.3 we calculate the minimal interaction energies and hence, cooperativity for native hemoglobin and some of its modified variants [34]. For our examples, the minimal interaction reduces when the molecule structure, on which the cooperative mechanism relies, is disturbed. However, our results rank the degree of cooperativity in differently treated hemoglobin differently than other measures of cooperativity.

3.2.1 The Mathematical Framework

In this subsection, we briefly review the model for ligand binding based on the grand canonical ensemble of statistical mechanics and recall the notion of minimal absolute interaction from [90]. We refer the reader to the books [9, 122] for detailed exposition on the model.

Definition 3.2.1 (Molecule). *A molecule W with n sites is a positive real point, whose coordinates are indexed by the subsets of $[n] := \{1, \dots, n\}$ and with $w_\emptyset = 1$:*

$$W = (w_I)_{I \subseteq [n]} \in (\mathbb{R}_{>0})^{2^n}.$$

For the sake of brevity, we abbreviate $w_{\{i_1, \dots, i_r\}}$ to $w_{i_1 \dots i_r}$ such that $i_1 < \dots < i_r$ (see Fig. 24). We refer to w_I as *binding energy* if $|I| = 1$ and *interaction energy* if $|I| > 1$. The binding energies w_i encode the energy required to bind to the sites, and the interaction

energies $w_{i_1 \dots i_r}$ encode the discrepancy between the energy required for r ligands to bind to the sites i_1, \dots, i_r and the energies required to bind to its smaller subunits. Note that, contrary to their names, our binding energies are exponentials of the binding energies in [9, 122].

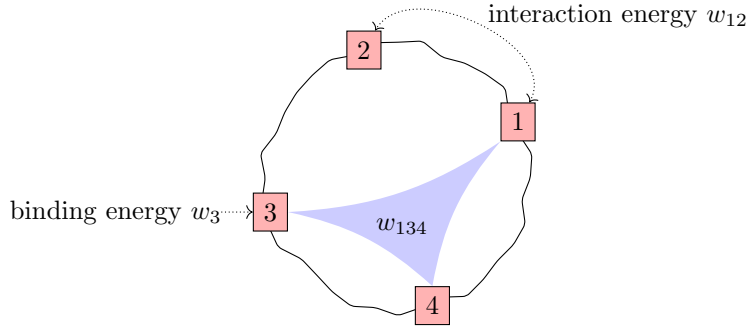


Figure 24: A molecule with 4 binding sites.

Definition 3.2.2 (Binding Polynomial). *Given a molecule $W = (w_I)$ with n sites, its binding polynomial $\Phi(W)$ is a univariate polynomial of degree n ,*

$$\Phi(W) := a_n \Lambda^n + \dots + a_1 \Lambda + a_0,$$

whose positive real coefficients a_k are given by

$$a_k := \sum_{|I|=k} \prod_{I' \subseteq I} w_{I'} \in \mathbb{R}_{>0}.$$

Example 3.2.3. Let $W = (w_I)_{I \subseteq [3]} \in (\mathbb{R}_{>0})^{2^3}$ be a molecule with 3 sites. The binding polynomial $\Phi(W) = a_3 \Lambda^3 + a_2 \Lambda^2 + a_1 \Lambda + a_0$ is a real univariate polynomial of degree 3 whose coefficients are given by

$$\begin{aligned} a_0 &= w_\emptyset = 1, \\ a_1 &= w_1 + w_2 + w_3, \\ a_2 &= w_1 w_2 w_{12} + w_1 w_3 w_{13} + w_2 w_3 w_{23}, \\ a_3 &= w_1 w_2 w_3 w_{12} w_{13} w_{23} w_{123}. \end{aligned}$$

Note that different molecules may have the same binding polynomial and thus, the same binding curve. Hence, the map Φ which maps a molecule with n sites to its binding polynomial is not injective.

Definition 3.2.4 (Absolute interaction). *The absolute interaction of a molecule $W = (w_I) \in (\mathbb{R}_{>0})^{2^n}$ is given by*

$$\|W\| := \prod_{|I|>1} \max(w_I, w_I^{-1}). \quad (49)$$

Definition 3.2.5 (Minimal absolute interaction). *Given a binding polynomial P of degree n , the minimal absolute interaction is*

$$\|P\| := \min \{ \|W\| \mid W \in (\mathbb{R}_{>0})^{2^n} \text{ with } \Phi(W) = P \}. \quad (50)$$

We call a molecule W a *minimal molecule*, if $\|W\| = \|\Phi(W)\|$.

In words, the minimal absolute interaction $\|P\|$ is the minimum of all absolute interactions of molecules with a fixed binding polynomial P , or equivalently with a fixed binding curve. This notion is well defined by the following proposition.

Proposition 3.2.6 ([90, §4]). *For any univariate polynomial P of degree n with positive coefficients there exists a molecule $W \in (\mathbb{R}_{>0})^{2^n}$ with n sites such that $\Phi(W) = P$ and $\|W\| = \|P\|$.*

Since cooperativity is an emerging property of the interaction between the sites and is usually deduced from the binding curve, the minimal absolute interaction of the binding polynomial is a natural candidate for quantifying cooperativity. In addition, [90, §4] shows that it has several properties that could be considered desirable in such a quantifier.

Remark 3.2.7. We view molecules as points in a Euclidean space. It is possible to interpret molecules as *hypergraphs* or *tensors*. In a different context, one can also draw a comparison between these molecules and biallelic n -loci genes [8]. In that setting cooperativity corresponds to *epistasis*.

Example 3.2.8. Consider the following binding polynomials:

$$\begin{aligned} P_1 &:= 4\Lambda^3 + 3\Lambda^2 + 2\Lambda + 1, \\ P_2 &:= 6\Lambda^3 + 7\Lambda^2 + 4\Lambda + 1 = (2\Lambda + 1)(3\Lambda^2 + 2\Lambda + 1), \\ P_3 &:= \Lambda^3 + 3\Lambda^2 + 3\Lambda + 1 = (\Lambda + 1)(2\Lambda + 1)(3\Lambda + 1). \end{aligned}$$

A brief computation reveals that the minimal absolute interactions are

$$\|P_1\| = 13.50, \quad \|P_2\| = 3, \quad \|P_3\| = 1.$$

The computation for $\|P_1\|$ is explicitly shown in Example 3.2.9. Figure 25 illustrates the minimal molecules for each binding polynomial. This figure can also be seen as the diagrammatic representation of $2 \times 2 \times 2$ tensors. Since P_3 factorises into three real linear factors, its minimal molecule has only trivial interactions.

3.2.2 The Algebraic Optimisation Problem

In this subsection we consider the computation of the minimal absolute interaction (50) as an optimisation problem. The absolute interaction is the objective function and the set of all molecules that share the same binding polynomial constitutes the feasible set:

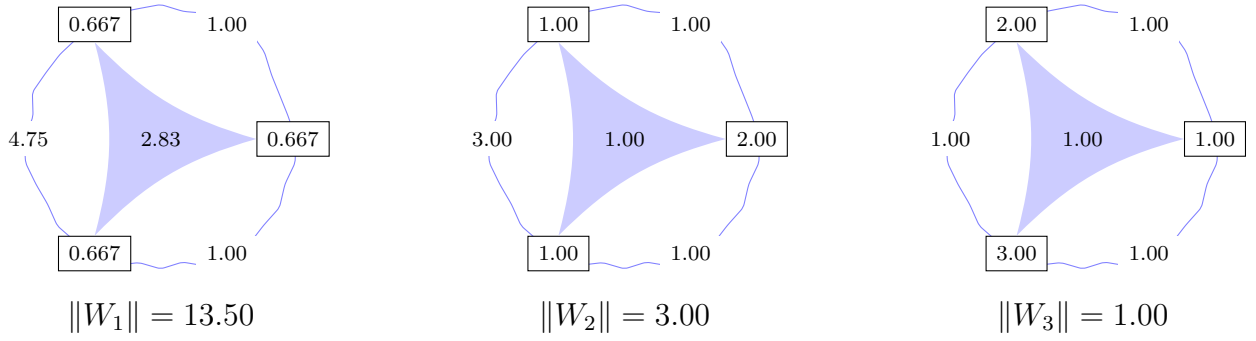


Figure 25: Minimal molecules for binding polynomial P_1, P_2, P_3

$$\begin{aligned} & \underset{\mathbf{W}}{\text{minimise}} && \|\mathbf{W}\| \\ & \text{subject to} && \Phi(\mathbf{W}) = P \end{aligned} \quad (51)$$

This problem seems simple and its concept can be understood easily. However, it becomes quickly complicated if larger systems are considered. For small n it can be worked out by methods of algebraic optimisation. For $n = 4$ explicitly, the problem for given $a_1, a_2, a_3, a_4 \in \mathbb{R}_{>0}$ is as follows:

$$\begin{aligned} & \underset{(w_I)}{\text{minimise}} && \prod_{|I|>1} \max(w_I, w_I^{-1}) \\ & \text{subject to} && a_1 = w_1 + w_2 + w_3 + w_4, \\ & && a_2 = w_1 w_2 w_{12} + w_1 w_3 w_{13} + w_1 w_4 w_{14} \\ & && \quad + w_2 w_3 w_{23} + w_2 w_4 w_{24} + w_3 w_4 w_{34}, \\ & && a_3 = w_1 w_2 w_3 w_{12} w_{13} w_{23} w_{123} + w_1 w_2 w_4 w_{12} w_{14} w_{24} w_{124} \\ & && \quad + w_1 w_3 w_4 w_{13} w_{14} w_{34} w_{134} + w_2 w_3 w_4 w_{23} w_{24} w_{34} w_{234}, \\ & && a_4 = w_1 w_2 w_3 w_4 w_{12} w_{13} w_{14} w_{23} w_{24} w_{34} w_{123} w_{124} w_{134} w_{234} w_{1234}. \end{aligned}$$

One intuitive way for computing the minimal absolute interaction $\|P\|$ is to decompose the space of molecules $(\mathbb{R}_{>0})^{2^n}$. We look at $2^{2^n - n - 1}$ regions on which for $|I| > 1$ either $w_I \geq 1$ or $w_I \leq 1$ holds. Each w_I with $I \subseteq [n]$ and $|I| > 1$ denotes an interaction. For each set of interactions $\mathcal{I} \subseteq \{I \subseteq [n]\}$, we can define a region

$$\begin{aligned} O_{\mathcal{I}} & := \{(w_I)_{I \subseteq [n]} \mid \text{for all } |I| > 1, w_I \geq 1 \text{ if } I \notin \mathcal{I} \text{ and } w_I \leq 1 \text{ if } I \in \mathcal{I}\} \\ (\mathbb{R}_{>0})^{2^n} & = \bigcup_{\mathcal{I} \subseteq \{I \subseteq [n]\}} O_{\mathcal{I}} \end{aligned} \quad (52)$$

On each region $O_{\mathcal{I}}$, the absolute interaction $\|W\|$ is a rational function in the interaction energies which we denote $f_{\mathcal{I}}(W)$,

$$\|W\| = \prod_{I \in \mathcal{I}} w_I^{-1} \prod_{\substack{|I|>1 \\ I \notin \mathcal{I}}} w_I =: f_{\mathcal{I}}(W) \quad \text{for } W \in O_{\mathcal{I}}. \quad (53)$$

Finding the minimal absolute interaction inside $O_{\mathcal{I}}$ is a straight-forward problem in polynomial optimisation:

$$\begin{aligned} & \underset{W \in \mathcal{O}_{\mathcal{I}}}{\text{minimise}} && f_{\mathcal{I}}(W) \\ & \text{subject to} && \Phi(W) = P. \end{aligned} \tag{54}$$

However, this approach requires solving $2^{2^n - n - 1}$ polynomial optimisation problems, one for each region $\mathcal{O}_{\mathcal{I}}$, which is simply not practical as n becomes large. Instead, we preprocess the optimisation problem. Note that we can rewrite (51) as the following minimax form:

$$\begin{aligned} & \underset{W}{\text{minimise}} && \max_{\mathcal{I} \subseteq \{I \subseteq [n] \mid |I| > 1\}} f_{\mathcal{I}}(W) \\ & \text{subject to} && \Phi(W) = P. \end{aligned} \tag{55}$$

On each region $\mathcal{O}_{\mathcal{I}}$ the function $f_{\mathcal{I}}(W)$, as defined in (53), dominates all other $f_{\mathcal{I}'}(W)$ with $\mathcal{I}' \neq \mathcal{I}$. Moreover, observe that (55) can be lifted to a problem with a linear objective function and non linear constraints.

$$\begin{aligned} & \underset{W}{\text{minimise}} && r \\ & \text{subject to} && \begin{cases} f_{\mathcal{I}}(W) \leq r & \text{for all } \mathcal{I} \subseteq \{I \subseteq [n] \mid |I| > 1\}, \\ \Phi(W) = P. \end{cases} \end{aligned} \tag{56}$$

Given a fixed binding polynomial P , the polynomial system $\Phi(W) = P$ poses a serious computational problem. To sidestep this issue we now introduce new coordinates $s_I := \prod_{I' \subseteq I} w_{I'}$. In [9, Section 2.2], the s_I are referred to as intrinsic binding constant if $|I| = 1$ or conditional binding constant if $|I| > 1$. On the positive orthant $(\mathbb{R}_{>0})^{2^n}$, this defines a bijection

$$\begin{array}{ccc} W = (w_I) & \xrightarrow{\varphi} & \left(\prod_{I' \subseteq I} w_{I'} \right) \\ \cap & & \cap \\ (\mathbb{R}_{>0})^{2^n} & \xleftrightarrow{\quad} & (\mathbb{R}_{>0})^{2^n} \\ \psi & & \psi \\ \left(\prod_{I' \subseteq I} s_{I'}^{(-1)^{|I \setminus I'|}} \right) & \xleftarrow{\varphi^{-1}} & (s_I) = S \end{array} \tag{57}$$

In the new coordinates, the formerly polynomial constraints $a_k = \sum_{|I|=k} \prod_{I' \subseteq I} w_{I'}$ are simplified to linear constraints $a_k = \sum_{|I|=k} s_I$ for $k = 1, \dots, n$. However, the functions $f_{\mathcal{I}}$ become more complicated. For example, for $n = 4$ and $\mathcal{I} = \{\{123\}\}$

$$f_{\mathcal{I}}(W) = w_{123}^{-1} \cdot \prod_{\substack{|I| > 1, \\ I \neq \{1,2,3\}}} w_I \quad \text{becomes} \quad f_{\mathcal{I}} \circ \varphi^{-1}(S) = \frac{s_{1234} s_{12}^2 s_{13}^2 s_{23}^2}{s_{123}^2 s_1^3 s_2^3 s_3^3 s_4} =: g_{\mathcal{I}}.$$

Since the $g_{\mathcal{I}}$ remain monomials (with possibly negative exponents), this complication is of little consequence for the resulting problem:

$$\begin{aligned} & \underset{S}{\text{minimise}} && r \\ & \text{subject to} && \begin{cases} f_{\mathcal{I}} \circ \varphi^{-1}(S) \leq r & \text{for all } \mathcal{I} \subseteq \{I \subseteq [n] \mid |I| > 1\}, \\ \sum_{|I|=k} s_I = a_k & \text{for all } k = 1, \dots, n. \end{cases} \end{aligned} \quad (58)$$

Example 3.2.9. Consider the binding polynomial P_1 of Example 3.2.8. We use SCIP [56] to solve the resulting polynomial optimisation problem (58), which is currently one of the fastest solvers for nonlinear programming. It uses branch and bound method to solve the optimisation problem with non-linear constraints.

Figure 26 shows the full input on the left and the partial output on the right. In the input, the first constraints **c1**, **c2**, **c3** enforce $\sum_{|I|=k} s_I = a_k$ for $i = 1, 2, 3$. The remaining constraints **c4** to **c19** enforce $f_{\mathcal{I}} \circ \varphi^{-1}(S) \leq r$. For example, **c19** states that $s_1 s_2 s_3 / s_{123} \leq r$ which is equivalent to $f_{\emptyset}(W) = (w_{123} w_{12} w_{13} w_{23})^{-1} \leq r$ in the coordinates w_I . The output states an approximate optimal value of $y = 13.5$ and clearly lists all values of s_I of the minimal molecules, which gave rise to the values of w_I in Example 3.2.8.

Since the number of constraints when $n = 3$ are less, SCIP works well. However, for $n = 4$ there are 2^{11} constraints which makes it a hard problem to solve directly. Therefore, we consider a relaxed problem with fewer constraints. We do that by exploiting the symmetry in our problem. We look at the natural action of the symmetric group S_n on the space of molecules $(\mathbb{R}_{>0})^{2^n}$ which permutes the binding sites and the corresponding interaction energies:

$$S_n \times (\mathbb{R}_{>0})^{2^n} \longrightarrow (\mathbb{R}_{>0})^{2^n}, \quad (\sigma, (w_I)) \longmapsto \sigma \cdot (w_I) := (w_{\sigma(I)}).$$

Proposition 3.2.10. *The binding polynomial and the absolute interaction of a molecule are invariant under the group action of S_n i.e., $\Phi(\sigma \cdot W) = \Phi(W)$ and $\|\sigma \cdot W\| = \|W\|$ for all $W \in (\mathbb{R}_{>0})^{2^n}$ and all $\sigma \in S_n$.*

We can consider this action on the regions $O_{\mathcal{I}}$. For example, for $1 \leq i < j \leq n$ the permutation $(1i)(2j) \in S_n$ induces a binding polynomial and absolute interaction preserving bijection $O_{\{1,2\}} \leftrightarrow O_{\{i,j\}}$, which is why we have

$$\begin{aligned} & \min\{\|(w_I)_{I \subseteq [n]}\| \mid (w_I)_{I \subseteq [n]} \in O_{\{1,2\}} \text{ with } \Phi(w_I) = P\} \\ & = \min\{\|(w_I)_{I \subseteq [n]}\| \mid (w_I)_{I \subseteq [n]} \in O_{\{i,j\}} \text{ with } \Phi(w_I) = P\}. \end{aligned}$$

To solve our problem and avoid the calculation of the 2^{11} different cases, we compute the upper bound b_+ and lower bound b_- for the minimal absolute interaction of a given binding polynomial. To compute the upper bound we minimise the absolute interaction in a single orthant. For the experiments in Subsection 3.2.3 we consider the orthant O_{\emptyset} . The result may not be the global minimum - since the minimum may lie in another orthant - but it gives an upper bound. For the lower bound, we consider the relaxed problem by looking at a problem with less constraints. We consider the S^n group action. We then pick a representative of the

```

Minimize
obj: r
Subject to
c1: s1+s2+s3=2
c2: s12+s13+s23=3
c3: s123=4
c4: s123-r*s1*s2*s3<=0
c5: s1*s2*s123-r*s3*s12^2<=0
c6: s1*s3*s123-r*s2*s13^2<=0
c7: s2*s3*s123-r*s1*s23^2<=0
c8: s12^2*s13^2*s23^2
-r*s1^3*s2^3*s3^3*s123<=0
c9: s1^3*s2*s3*s123-r*s12^2*s13^2<=0
c10: s1*s2^3*s3*s123-r*s12^2*s23^2<=0
c11: s13^2*s23^2-r*s1*s2*s3^3*s123<=0
c12: s1*s2*s3^3*s123-r*s13^2*s23^2<=0
c13: s12^2*s23^2-r*s1*s2^3*s3*s123<=0
c14: s12^2*s13^2-r*s1^3*s2*s3*s123<=0
c15: s1^3*s2^3*s3^3*s123
-r*s12^2*s13^2*s23^2<=0
c16: s1*s23^2-r*s2*s3*s123<=0
c17: s2*s13^2-r*s1*s3*s123<=0
c18: s3*s12^2-r*s1*s2*s123<=0
c19: s1*s2*s3-r*s123<=0

Bounds
0<s1<2
0<s2<2
0<s3<2
0<s12<3
0<s13<3
0<s23<3
4<=s123<=4
1<=r
End

SCIP version 6.0.0
Copyright (C) 2002-2018 ZIB Berlin

SCIP> read input.pip

SCIP> opt
SCIP Status : problem is solved
Solving Time : 2.32
Solving Nodes: 587
Primal Bound : +1.349997004816e+01
Dual Bound : +1.349997004816e+01
Gap : 0.00 %

SCIP> display solution
objective value: 13.4999700481621
y 13.4999700481621
s1 0.666630230040994
s2 0.66617295525322
s3 0.667196814705786
s12 0.444091987464541
s13 0.444773633975962
s23 2.1111343785595
s123 4
[...]
```

Figure 26: Computing cooperativity for a molecule with 3 sites using SCIP

orbits of \mathbb{R}^{2^n} and consider the corresponding region. We only consider the constraints given by functions $f_{\mathcal{I}}$ dominant in those regions. This new problem gives the lower bound on the true optimisation problem. Where the gap between upper and lower bound is sufficiently small, we assume to have found a molecule minimising the problem and also consider the respective molecule minimising the interaction magnitude.

Remark 3.2.11. Note that the number of orbits remains asymptotically large, which is why computing the minimal interaction magnitude remains a hard task. If we restrict to the case $w_I = 1$ for $|I| > 2$, each necessary case corresponds to a (unlabeled) graph on n nodes, whose numbers are known to be superexponential in n :

n	4	5	6	7	8	9	10	...
	11	34	156	1044	12346	274668	12005168	...

For general molecules, the number of necessary cases equals the number of (unlabeled) hypergraphs on n nodes with edges of cardinality 2 or higher.

3.2.3 Experimental Results

We now report on some computational experiments conducted on data from [68, 67] which is also summarised in [34]. The first data set [68] consists of eight binding polynomials of human adult hemoglobin both chemically treated and untreated and under two different environmental conditions. The second data set [67] contains five binding polynomials of native hemoglobin HbII of *Scapharca inaequivalvis*. Both works have studied cooperativity through the maximal slope of the Hill plot n_{max} , which relates the variance of the probability distribution on the macrostates $\{0, 1, 2, 3, 4\}$ at the respective ligand activity to the variance of a binomial distribution with the same mean [1, 63, 91]. Table 9 describes the experiments from which binding polynomials 1 to 8 were obtained and illustrates the relation of n_{max} . Table 10 describes the temperature conditions under which polynomials P_9 to P_{13} were obtained. The corresponding values of n_{max} have been reported to vary between 2.08 and 2.12 [67, Table 3].

Table 11 lists the coefficients a_1, a_2 and a_3 of all binding polynomials and a_4 is set to 1. We list upper b_+ and lower bounds b_- for the minimal absolute interaction $\|P_i\|$. Table 11 shows that for most binding polynomials our upper and lower bound allows for a sufficient approximation of the absolute minimal interaction. However, there remains a nontrivial gap between both bounds for P_2, P_3, P_4 , which makes a comparison of the degree of cooperativity according to the minimal absolute interaction difficult. Fig. 27 shows all molecules realising the upper bound of the minimal absolute interaction. For all but P_2, P_3, P_4, P_7, P_8 the molecules are minimal.

Let us assume that the correct value for P_2 is close to the upper bound which we determined. Then, nearly all relations of the degree of cooperativity described by the maximal slope of the Hill plot n_{max} (Table 9) are found again. The only exception is the very drastic difference between P_4 and P_6 . Whereas, P_4 describes a more cooperative system than P_6 according to n_{max} , we obtain a different image when using the minimal absolute interaction.

Human Hb	in the absence of 2mM DPG		in the presence of 2mM DPG	
untreated	P_1	\prec	P_2	
	Υ		Υ	
treated with iodoacetamide	P_3	\prec	P_4	
	Υ		Υ	
treated with N-ethylmaleimide	P_5	\prec	P_6	
	Υ		Υ	
treated with carboxypeptidase A	P_7	\prec	P_8	

Table 9: Binding polynomials 1 to 8 and the relation of their degree of cooperativity according to the maximal slope of the Hill plot n_{max} (\succ = bigger n_{max} , DPG = 2,3-diphosphoglycerate)

Clam HbII	at 10°	at 15°	at 20°	at 25°	at 30°
	P_9	P_{10}	P_{11}	P_{12}	P_{13}

Table 10: Binding polynomials 9 to 13

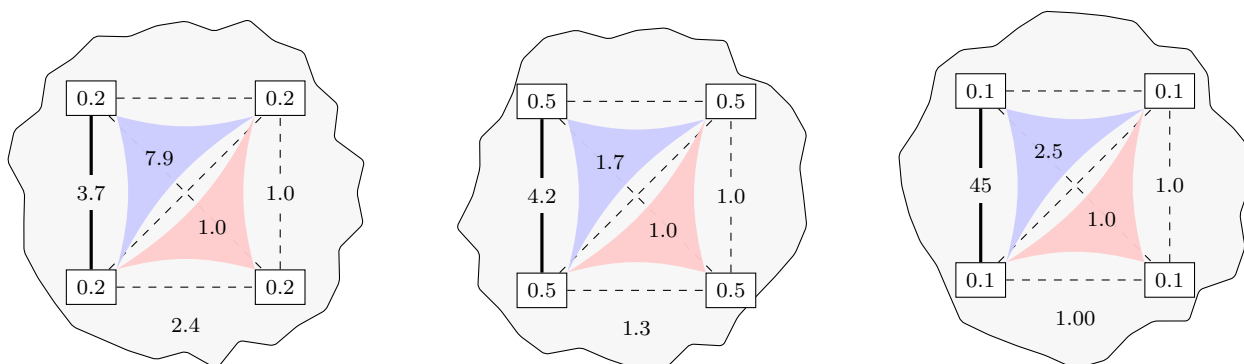


Figure 27: Minimal molecules for binding polynomials P_1 , P_5 , P_6

Among the polynomials P_9 to P_{13} , in the second data set, a small variation in the same coefficients of different binding polynomials leads to a relatively big difference in the minimal interaction magnitude. To interpret these differences, recall that w_{ij} are exponentials of interaction energies. Already small differences in the energies may lead to the observed differences on the level of interaction magnitude. Moreover, considering the behavior (66.60, 66.60, 123.00, 66.60, 175.0) for the temperatures (10°, 15°, 20°, 25°, 30°), there is a counter-intuitive fluctuation with increasing magnitude from 15°, 20°, decreasing interaction from 20°, 25° and increasing interaction from 25°, 30°. This observation suggests that the described variation is the result of measurement errors and rounding effects of the coefficients, which is also supported by the fact that the n_{max} criterion shows a similar pattern [67].

	a_1	a_2	a_3	b_+	b_-
P_1	0.835	0.379	0.541	527.00	527.00
P_2	0.789	0.154	0.0648	3320.00	1600.00
P_3	1.42	2.42	0.752	111.00	63.00
P_4	0.647	0.568	0.0986	1950.00	1460.00
P_5	2.0	2.31	2.04	16.00	16.00
P_6	0.539	0.909	0.554	3030.00	3030.00
P_7	3.47	4.74	2.76	2.27	1.68
P_8	3.26	5.36	2.23	7.63	2.19
P_9	1.4	1.0	0.62	66.60	66.60
P_{10}	1.4	0.96	0.60	66.60	66.60
P_{11}	1.2	0.93	0.70	123.00	123.00
P_{12}	1.4	0.95	0.62	66.60	66.60
P_{13}	1.1	0.98	0.59	175.00	175.00

Table 11: Bounds on the minimal absolute interaction

The standard interpretation of a high Hill coefficient is “if one side is occupied, the affinity of other sites to the ligand is increased”. These types of relations are easy to infer when the molecule is composed of physically indistinguishable sites. For instance, given a binding polynomial, we can calculate all interaction energies easily when we assume that $w_{ij} = w_{kl}$, $w_{ijk} = w_{lmn}$, etc. A more difficult mathematical problem appears when we would like to characterise the binding behavior of a transporter without assuming it to be symmetrical that is to be composed of physically identical units. We addressed a criterion mapping a polynomial to the minimal interaction which is required to generate the observed equilibrium binding behavior. The corresponding mathematical algebraic optimisation problem can be worked out using the method explained in Subsection 3.2.2. However, the setup of looking for the minimal absolute interaction by this method becomes complicated rapidly with the increase in the number of binding sites. Ligand binding theory possess a lot of interesting question related to algebraic optimisation and algebraic geometry, in particular when different types of ligands and polynomials in several variables are considered [104].

4 Coordinate-wise Powers

The content in this chapter is a joint work with Papri Dey and Paul Görlach [41] and has been submitted for publication. Hadamard products of algebraic varieties are given by multiplying coordinate-by-coordinate any two points $x \in X, y \in Y$ in given subvarieties X, Y of \mathbb{P}^n . We focus on the r -th Hadamard power $X^{\star r} := X \star \dots \star X$ of an algebraic variety X and study the subvariety of $X^{\star r}$ given by coordinate-wise r -th powers of points in $X \subset \mathbb{P}^n$. Formally, for a projective variety $X \subset \mathbb{P}^n$ and an integer $r \in \mathbb{Z}$, we are interested in studying its image under the rational map

$$\varphi_r: \mathbb{P}^n \dashrightarrow \mathbb{P}^n, \quad [x_0 : \dots : x_n] \mapsto [x_0^r : \dots : x_n^r].$$

We denote the image of X under φ_r by $X^{\circ r}$ and call it the r -th *coordinate-wise power* of $X \subset \mathbb{P}^n$.

We investigate these coordinate-wise powers $X^{\circ r}$ with a main focus on the case $r > 0$. These varieties show up naturally in many applications. For the Grassmannian variety $\text{Gr}(k, \mathbb{P}^n)$ in its Plücker embedding, the intersection with its r -th coordinate-wise power $\text{Gr}(k, \mathbb{P}^n) \cap \text{Gr}(k, \mathbb{P}^n)^{\circ r}$ was described combinatorially in terms of matroids in [82] for even r . In [15], highly singular surfaces in \mathbb{P}^3 have been constructed as preimages of a specific singular surface under the morphism φ_r for $r > 0$. The case $r = -1$ is the study of *reciprocal varieties* which has received particular attention in the case of linear spaces, see [37], [78] and [50].

For $r > 0$, the coordinate-wise powers $X^{\circ r}$ of a variety $X \subset \mathbb{P}^n$ have the following natural interpretation: The quotient of \mathbb{P}^n by the finite subgroup \mathbb{Z}_r^{n+1} of the torus $(\mathbb{C}^*)^{n+1}$ is again a projective space. The image of a variety $X \subset \mathbb{P}^n$ in $\mathbb{P}^n / \mathbb{Z}_r^{n+1} \cong \mathbb{P}^n$ is the variety $X^{\circ r}$, since $\varphi_r: \mathbb{P}^n \rightarrow \mathbb{P}^n$ is the geometric quotient of \mathbb{P}^n by \mathbb{Z}_r^{n+1} . In other words, coordinate-wise powers of algebraic varieties are images of subvarieties of \mathbb{P}^n under the quotient by a certain finite group. The case $r = 2$ has the special geometric significance of quotienting by the group generated by reflections at the coordinate hyperplanes of \mathbb{P}^n . We are, therefore, especially interested in *coordinate-wise squares* of varieties.

In Subsection 4.1 we compute the degree of $X^{\circ r}$. We use this to derive the degree of the variety of orthostochastic matrices. In Subsection 4.2, we find explicitly the defining equations of the coordinate-wise powers of hypersurfaces. We also define *generalised power sum hypersurfaces* and give relations between their dual and reciprocal varieties.

We study in more detail coordinate-wise powers of linear spaces in the Subsection 4.3. For low-dimensional linear spaces we give a complete classification. We also describe the defining ideal for the coordinate-wise square of general linear spaces of arbitrary dimension in a high-dimensional ambient space, and we link this question to the study of symmetric matrices with a codimension one eigenspace.

4.1 Degree Formula

Throughout this chapter, we work over \mathbb{C} . We denote the homogeneous coordinate ring of \mathbb{P}^n by $\mathbb{C}[\mathbf{x}] := \mathbb{C}[x_0, \dots, x_n]$. For any integer $r \in \mathbb{Z}$, we consider the rational map

$$\varphi_r: \mathbb{P}^n \dashrightarrow \mathbb{P}^n, \quad [x_0 : \dots : x_n] \mapsto [x_0^r : \dots : x_n^r].$$

For $r \geq 0$, the rational map φ_r is a morphism. Throughout, let $X \subset \mathbb{P}^n$ be a projective variety, not necessarily irreducible. We denote by $X^{or} \subset \mathbb{P}^n$ the image of X under the rational map φ_r . More explicitly,

$$X^{or} := \begin{cases} \overline{\varphi_r(X \setminus V(x_0 x_1 \dots x_n))} & \text{if } r < 0, \\ \varphi_r(X) & \text{if } r \geq 0. \end{cases}$$

For $r < 0$, we will only consider the case that no irreducible component of X is contained in any coordinate hyperplane of \mathbb{P}^n . We call the image $X^{or} \subset \mathbb{P}^n$ the r -th coordinate-wise power of X . In the case $r = -1$, the variety $X^{o(-1)}$ is called the reciprocal variety of X . We primarily focus on positive coordinate-wise powers, and therefore we will from now on always assume $r > 0$ unless explicitly stated otherwise. Observe that $\varphi_r: \mathbb{P}^n \rightarrow \mathbb{P}^n$ is a finite morphism, and hence, the image X^{or} of X under φ_r has same dimension as X .

The cyclic group \mathbb{Z}_r of order r is identified with the group of r -th roots of unity $\{\xi \in \mathbb{C} \mid \xi^r = 1\}$. We consider the action of the $(n+1)$ -fold product $\mathbb{Z}_r^{n+1} := \mathbb{Z}_r \times \dots \times \mathbb{Z}_r$ on $\mathbb{C}[\mathbf{x}]$ given by rescaling the variables x_0, \dots, x_n with r -th roots of unity. We denote the quotient of \mathbb{Z}_r^{n+1} by the subgroup $\{(\xi, \xi, \dots, \xi) \in \mathbb{C}^r \mid \xi^r = 1\} \subset \mathbb{Z}_r^{n+1}$ as $\mathcal{G}_r := \mathbb{Z}_r^{n+1}/\mathbb{Z}_r$. The group action of \mathbb{Z}_r^{n+1} on $\mathbb{C}[\mathbf{x}]$ determines a linear action of \mathcal{G}_r on \mathbb{P}^n . In this way, we can also view \mathcal{G}_r as a subgroup of $\text{Aut}(\mathbb{P}^n)$. For $r = 2$, this has the geometric interpretation of being the linear group action generated by reflections at coordinate hyperplanes. Note that \mathcal{G}_r does not act on the vector space $\mathbb{C}[\mathbf{x}]_d$ of homogeneous polynomials of degree d , instead it acts on $\mathbb{P}(\mathbb{C}[\mathbf{x}]_d)$.

Given a projective variety, the following proposition describes the preimage under φ_r of its coordinate-wise r -th power.

Proposition 4.1.1 (Preimages of coordinate-wise powers). *Let $X \subset \mathbb{P}^n$ be a variety and let $X^{or} \subset \mathbb{P}^n$ be its coordinate-wise r -th power. The preimage $\varphi_r^{-1}(X^{or})$ is given by $\bigcup_{\tau \in \mathcal{G}_r} \tau \cdot X$.*

Proof. This follows from $X^{or} = \varphi_r(X)$ and the fact that $\varphi_r^{-1}(\varphi_r(p)) = \{\tau \cdot p \mid \tau \in \mathcal{G}_r\}$ for all $p \in X$. \square

In particular, for $r = 2$, we obtain the following geometric description.

Corollary 4.1.2. *The preimage of X^{o2} under $\varphi_2: \mathbb{P}^n \rightarrow \mathbb{P}^n$ is the union over the orbit of X under the subgroup of $\text{Aut}(\mathbb{P}^n)$ generated by the reflections in the coordinate hyperplanes.*

In the following theorem, we give a degree formula for the coordinate-wise powers of an irreducible variety.

Theorem 4.1.3 (Degree formula). *Let $X \subset \mathbb{P}^n$ be an irreducible projective variety. Let $\text{Stab}_r(X) := \{\tau \in \mathcal{G}_r \mid \tau \cdot X = X\}$ and $\text{Fix}_r(X) := \{\tau \in \mathcal{G}_r \mid \tau|_X = \text{id}_X\}$. Then the degree of the r -th coordinate-wise power of X is*

$$\deg X^{or} = \frac{|\text{Fix}_r(X)|}{|\text{Stab}_r(X)|} r^{\dim X} \deg X.$$

Proof. Let $H_1, \dots, H_k \subset \mathbb{P}^n$ for $k := \dim X^{or} = \dim X$ be general hyperplanes whose common intersection with X^{or} consists of finitely many reduced points. We want to determine $|X^{or} \cap \bigcap_{i=1}^k H_i|$. By Proposition 4.1.1, we have

$$\varphi_r^{-1} \left(X^{or} \cap \bigcap_{i=1}^k H_i \right) = \bigcup_{\tau \in \mathcal{G}_r} \tau \cdot \left(X \cap \bigcap_{i=1}^k \varphi_r^{-1} H_i \right).$$

Note that each $\varphi_r^{-1} H_i$ is a hypersurface of degree r and their common intersection with X consists of finitely many reduced points by a version of Bertini's theorem (as in [51, 3.4.8]). By Bézout's theorem, $\left| X \cap \bigcap_{i=1}^k \varphi_r^{-1} H_i \right| = r^k \deg X$.

We note that $Z := X \cap \left(\bigcup_{\tau \in \mathcal{G}_r \setminus \text{Stab}_r(X)} \tau \cdot X \right)$ is of dimension $< k$ by irreducibility of X . Therefore, the common intersection of k general hyperplanes H_i with $\varphi_r(Z)$ is empty, hence we can write the above as the following disjoint union:

$$\bigcup_{\tau \in \mathcal{G}_r} \tau \cdot \left(X \cap \bigcap_{i=1}^k \varphi_r^{-1} H_i \right) = \bigsqcup_{\tau \in \mathcal{G}_r / \text{Stab}_r(X)} \tau \cdot \left(X \cap \bigcap_{i=1}^k \varphi_r^{-1} H_i \right).$$

In particular,

$$\left| \varphi_r^{-1} \left(X^{or} \cap \bigcap_{i=1}^k H_i \right) \right| = \frac{|\mathcal{G}_r|}{|\text{Stab}_r(X)|} r^k \deg X.$$

For a general point $p \in X$, we have $\{\tau \in \mathcal{G}_r \mid \tau \cdot p = p\} = \text{Fix}_r(X)$. Then Proposition 4.1.1 shows that a general point of $X^{or} = \varphi_r(X)$ has $|\mathcal{G}_r|/|\text{Fix}_r(X)|$ preimages under φ_r , so for general hyperplanes H_i we conclude

$$\deg X^{or} = \left| X^{or} \cap \bigcap_{i=1}^k H_i \right| = \frac{|\text{Fix}_r(X)|}{|\mathcal{G}_r|} \left| \varphi_r^{-1} \left(X^{or} \cap \bigcap_{i=1}^k H_i \right) \right| = \frac{|\text{Fix}_r(X)|}{|\text{Stab}_r(X)|} r^k \deg X. \quad \square$$

4.1.1 Orthostochastic Matrices

We use Theorem 4.1.3 to compute the degree of the variety of orthostochastic matrices. By $\mathbb{O}(m) \subset \mathbb{P}^{m^2}$ (resp. $\mathbb{SO}(m) \subset \mathbb{P}^{m^2}$) we mean the projective closure of the affine variety of orthogonal (resp. special orthogonal) matrices in \mathbb{A}^{m^2} . It was shown in [39] that the problem of deciding whether a bivariate polynomial can be expressed as the determinant of a definite/monic symmetric linear matrix polynomial (a *determinantal representation*) is closely linked to the problem of finding the defining equations of the variety $\mathbb{O}(m)^{\circ 2}$. In the case $m = 3$, the defining equations of $\mathbb{O}(3)^{\circ 2}$ are known [28, Proposition 3.1] and based on this knowledge, it was shown in [40, Section 4.2] how to compute a determinantal representation for a cubic bivariate polynomial or decide that none exists. For arbitrary m , the ideal of defining equations may be very complicated, but we are still able to compute its degree:

Proposition 4.1.4 (Degree of $\mathbb{O}(m)^{\circ 2}$). *We have $\mathbb{O}(m)^{\circ 2} = \mathbb{SO}(m)^{\circ 2}$ and its degree is*

$$\deg \mathbb{O}(m)^{\circ 2} = 2^{(m-1)^2} \frac{\deg \mathbb{O}(m)}{2^{\binom{m+1}{2}}} \leq 2^{(m-1)^2}.$$

Proof. The variety $\mathbb{O}(m)$ consists of two connected components that are isomorphic to $\mathbb{SO}(m)$. The images of these components under $\varphi_2: \mathbb{P}^{m^2} \rightarrow \mathbb{P}^{m^2}$ coincide. In particular, $\mathbb{O}(m)^{\circ 2} = \mathbb{SO}(m)^{\circ 2}$ and $\deg \mathbb{O}(m) = 2 \deg \mathbb{SO}(m)$. We determine $\text{Fix}_2(\mathbb{SO}(m))$ and $\text{Stab}_2(\mathbb{SO}(m))$.

Identify elements of \mathcal{G}_2 with $m \times m$ -matrices whose entries are ± 1 . Then a group element $S \in \mathcal{G}_2 = \{\pm 1\}^{m \times m}$ acts on the affine open subset $\mathbb{A}^{m^2} \subset \mathbb{P}^{m^2}$ corresponding to $m \times m$ -matrices $M \in \mathbb{C}^{m \times m}$. The action $S \circ M$ is the Hadamard product (i.e. entry-wise product) of matrices. Clearly, $\text{Fix}_2(\mathbb{SO}(m))$ is trivial, or else every special orthogonal matrix would need to have a zero entry at a certain position.

We claim that $\text{Stab}_2(\mathbb{SO}(m)) \subset \{S \in \{\pm 1\}^{m \times m} \mid \text{rk } S = 1\}$. Indeed, assume that $S \in \{\pm 1\}^{m \times m}$ lies in $\text{Stab}_2(\mathbb{SO}(m))$, but is not of rank 1. Then $m \geq 2$ and we may assume that the first two columns of S are linearly independent. Consider the vectors $u, v \in \mathbb{C}^m$ given by

$$u_i := \begin{cases} 1 & \text{if } i < m, \\ -1 & \text{if } i = m \end{cases} \quad \text{and} \quad v_i := \begin{cases} 2^{i-1} & \text{if } i < m, \\ 2^{m-1} - 1 & \text{if } i = m \end{cases} \quad \text{for all } i \in \{1, \dots, m\}.$$

Since u and v are orthogonal, we can find a special orthogonal matrix $M \in \mathbb{C}^{m \times m}$ whose first two columns are $M_{\bullet 1} = u/\|u\|_2$ and $M_{\bullet 2} = v/\|v\|_2$. But $S \in \text{Stab}_2(\mathbb{SO}(m))$, so the matrix $S \circ M$ must be a special orthogonal matrix. In particular, the first two columns of $S \circ M$ must be orthogonal, i.e.

$$0 = \sum_{i=1}^m (S_{i1} u_i)(S_{i2} v_i) = -(S_{m1} S_{m2})(2^{m-1} - 1) + \sum_{i=1}^{m-1} (S_{i1} S_{i2}) 2^{i-1}. \quad (59)$$

Since $S_{i1} S_{i2} = \pm 1$ for all i , we have $|\sum_{i=1}^{m-1} (S_{i1} S_{i2}) 2^{i-1}| \leq 2^{m-1} - 1$, and equality in (59) holds if and only if $S_{i1} S_{i2} = S_{j1} S_{j2}$ for all $i, j \in \{1, \dots, m\}$. However, this contradicts the linear independence of the first two columns of S . Hence, the claim follows.

Any rank 1 matrix in $\{\pm 1\}^{m \times m}$ can be uniquely written as uv^T with $u, v \in \{\pm 1\}^m$ and $u_1 = 1$. Such a rank 1 matrix $S = uv^T$ lies in $\text{Stab}_2(\mathbb{SO}(m))$ if and only if for each special orthogonal matrix $M \in \mathbb{C}^{m \times m}$ the matrix

$$S \circ M = (uv^T) \circ M = \text{diag}(u_1, \dots, u_m) M \text{diag}(v_1, \dots, v_m)$$

is again a special orthogonal matrix. This is true if and only if $\prod_{i=1}^m u_i = \prod_{i=1}^m v_i$. Therefore,

$$\text{Stab}_2(\mathbb{SO}(m)) = \{uv^T \mid u, v \in \{\pm 1\}^m, u_1 = 1, \prod_i u_i = \prod_i v_i\},$$

and, thus, $|\text{Stab}_2(\mathbb{SO}(m))| = 2^{2m-2}$.

Since $\mathbb{S}\mathbb{O}(m) \subset \mathbb{P}^{m^2}$ is irreducible, applying Theorem 4.1.3 gives

$$\deg \mathbb{S}\mathbb{O}(m)^{\circ 2} = \frac{1}{2^{2m-2}} 2^{\binom{m}{2}} \deg \mathbb{S}\mathbb{O}(m) = 2^{\binom{m}{2}-2m+1} \deg \mathbb{O}(m) = 2^{(m-1)^2} \frac{\deg \mathbb{O}(m)}{2^{\binom{m+1}{2}}}.$$

Finally, we observe that the affine variety of orthogonal matrices in \mathbb{A}^{m^2} is an intersection of $\binom{m+1}{2}$ quadrics which correspond to the polynomials given by the equation $M^T M = \text{id}$ satisfied by orthogonal matrices $M \in \mathbb{C}^{m \times m}$. Therefore, its projective closure $\mathbb{O}(m) \subset \mathbb{P}^{m^2}$ must satisfy $\deg \mathbb{O}(m) \leq 2^{\binom{m+1}{2}}$. This shows $\deg \mathbb{O}(m)^{\circ 2} \leq 2^{(m-1)^2}$. \square

Remark 4.1.5. The degree of $\mathbb{O}(m)$ (resp. $\mathbb{S}\mathbb{O}(m)$) is known for all m by [17], namely

$$\deg \mathbb{O}(m) = 2^m \det \left(\begin{pmatrix} 2m - 2i - 2j \\ m - 2i \end{pmatrix} \right)_{1 \leq i, j \leq \lfloor m/2 \rfloor}.$$

Table 12 shows the resulting degrees of $\mathbb{O}(m)^{\circ 2} = \mathbb{S}\mathbb{O}(m)^{\circ 2}$ for some values of m .

m	1	2	3	4	5	6	7	8
$\deg \mathbb{S}\mathbb{O}(m)$	1	2	8	40	384	4768	111616	3433600
$\deg \mathbb{S}\mathbb{O}(m)^{\circ 2}$	1	1	4	40	1536	152576	57147392	56256102400

Table 12: The degrees of $\mathbb{S}\mathbb{O}(m)$ and $\mathbb{S}\mathbb{O}(m)^{\circ 2}$ in comparison.

4.1.2 Linear Spaces

We now determine the degree of coordinate-wise powers $L^{\circ r}$ for a linear space $L \subset \mathbb{P}^n$, based on Theorem 4.1.3. It can be expressed in terms of the combinatorics captured by the matroid of $L \subset \mathbb{P}^n$. We briefly recall some basic definitions for matroids associated to linear spaces in \mathbb{P}^n . We refer to [99] for a detailed introduction to matroid theory.

Let $L \subset \mathbb{P}^n$ be a linear space. The combinatorial information about the intersection of L with the linear coordinate spaces in \mathbb{P}^n is captured in the *linear matroid* \mathcal{M}_L . It is the collection of index sets $I \subset \{0, 1, \dots, n\}$ such that L does not intersect $V(\{x_i \mid i \notin I\})$. Formally,

$$\mathcal{M}_L := \{I \subset \{0, 1, \dots, n\} \mid L \cap V(\{x_i \mid i \notin I\}) = \emptyset\}.$$

Different conventions about linear matroids exist in the literature, and some authors take a dual definition for the linear matroid of L .

The set $\{0, 1, \dots, n\}$ is the *ground set* of the matroid. Index sets $I \in \mathcal{M}_L$ are called *independent*, while index sets $I \in \text{Pow}(\{0, 1, \dots, n\}) \setminus \mathcal{M}_L$ are called dependent. An index $i \in \{0, 1, \dots, n\}$ is called a *coloop* of \mathcal{M}_L if, for all $I \subset \{0, 1, \dots, n\}$, the condition $I \in \mathcal{M}_L$ holds if and only if $I \cup \{i\} \in \mathcal{M}_L$ holds. Geometrically, an index $i \in \{0, 1, \dots, n\}$ is a coloop of \mathcal{M}_L if and only if $L \subset V(x_i)$.

A subset $E \subset \{0, 1, \dots, n\}$ is called *irreducible* if there is no non-trivial partition $E = E_1 \sqcup E_2$ with

$$I \in \mathcal{M}_L \iff I \cap E_1 \in \mathcal{M}_L \text{ and } I \cap E_2 \in \mathcal{M}_L \quad \forall I \subset E.$$

The maximal irreducible subsets of $\{0, 1, \dots, n\}$ are called *components* of \mathcal{M}_L and they form a partition of $\{0, 1, \dots, n\}$. Geometrically, a component of \mathcal{M}_L is a minimal subset of $\{0, 1, \dots, n\}$ with the property that $L \cap V(x_i \mid i \in I)$ and $L \cap V(x_i \mid i \notin I)$ together span the linear space L .

In the following result, we determine the degree of $L^{\circ r} \subset \mathbb{P}^n$ as an invariant of the linear matroid \mathcal{M}_L .

Theorem 4.1.6. *Let $L \subset \mathbb{P}^n$ be a linear space of dimension k . Let s be the number of coloops and t the number of components of the associated linear matroid \mathcal{M}_L . Then*

$$\deg L^{\circ r} = r^{k+s-t+1}.$$

Proof. By Theorem 4.1.3, we need to determine the cardinality of the groups

$$\text{Stab}_r(L) = \{\tau \in \mathcal{G}_r \mid \tau \cdot L = L\} \quad \text{and} \quad \text{Fix}_r(L) = \{\tau \in \mathcal{G}_r \mid \tau|_L = \text{id}_L\}.$$

Consider the affine cone over L , which is a $(k+1)$ -dimensional subspace $W \subset \mathbb{C}^{n+1}$. We denote the canonical basis of \mathbb{C}^{n+1} by e_0, \dots, e_n .

We observe that $|\text{Fix}_r(L)| = |\{\tau \in \mathbb{Z}_r^{n+1} \mid \tau|_W = \text{id}\}|$. For $\tau \in \mathbb{Z}_r^{n+1}$, we have

$$\begin{aligned} \tau|_W = \text{id} &\Leftrightarrow W \subset \langle e_i \mid i \in \{0, 1, \dots, n\} \text{ s.t. } \tau_i = 1 \rangle \\ &\Leftrightarrow L \subset V(x_i) \quad \forall i \in \{0, 1, \dots, n\} \text{ s.t. } \tau_i \neq 1 \\ &\Leftrightarrow \tau_i = 1 \text{ for all } i \in \{0, 1, \dots, n\} \text{ which are not a coloop of } \mathcal{M}_L. \end{aligned}$$

From this, we see that $|\text{Fix}_r(L)| = r^s$.

For the stabiliser of L , we have $|\text{Stab}_r(L)| = \frac{1}{r} |\{\tau \in \mathbb{Z}_r^{n+1} \mid \tau \cdot W = W\}|$. If $\tau \in \mathbb{Z}_r^{n+1}$, then

$$\begin{aligned} \tau \cdot W = W &\Leftrightarrow W = \bigoplus_{\xi \in \mathbb{Z}_r} W \cap \langle e_i \mid i \in \{0, 1, \dots, n\} \text{ s.t. } \tau_i = \xi \rangle \\ &\Leftrightarrow \text{For each } \xi \in \mathbb{Z}_r, \text{ the set } \{i \in \{0, 1, \dots, n\} \mid \tau_i = \xi\} \text{ is a union of} \\ &\quad \text{components of } \mathcal{M}_L. \\ &\Leftrightarrow \forall C \subset \{0, 1, \dots, n\} \text{ component of } \mathcal{M}_L, \exists \xi \in \mathbb{Z}_r \text{ s.t. } \tau_i = \xi \text{ for all } i \in C. \end{aligned}$$

In particular, there are precisely r^t elements $\tau \in \mathbb{Z}_r^{n+1}$ with $\tau \cdot W = W$. We deduce that $|\text{Stab}_r(L)| = r^{t-1}$, which concludes the proof by Theorem 4.1.3. \square

Corollary 4.1.7. *The degree of the coordinate-wise r -th power of a linear space only depends on the associated linear matroid. If $L_1, L_2 \subset \mathbb{P}^n$ are linear spaces such that the linear matroids \mathcal{M}_{L_1} and \mathcal{M}_{L_2} are isomorphic (i.e. they only differ by a permutation of $\{0, 1, \dots, n\}$), then $L_1^{\circ r} \subset \mathbb{P}^n$ and $L_2^{\circ r} \subset \mathbb{P}^n$ have the same degree.*

Corollary 4.1.8. *Let $L \subset \mathbb{P}^n$ be a linear space of dimension k . Then $\deg L^{\circ r} \leq r^k$. For general k -dimensional linear spaces in \mathbb{P}^n , equality holds.*

Proof. Every coloop of \mathcal{M}_L forms a component of \mathcal{M}_L and the set $\{0, 1, \dots, n\} \setminus \{\text{coloops}\}$ is a union of components, hence $t \leq s + 1$. Therefore, by Proposition 4.1.6, $\deg L^{\circ r} \leq r^k$. For a *general* linear space $L \in \text{Gr}(k, \mathbb{P}^n)$, the linear matroid \mathcal{M}_L has no coloops and only one component. \square

Example 4.1.9. We illustrate Theorem 4.1.6 for hyperplanes. Up to permuting and rescaling the coordinates of \mathbb{P}^n , each hyperplane is given by $L = V(f)$ with $f = x_0 + \dots + x_m$ for some $m \in \{0, 1, \dots, n\}$. Its linear matroid is

$$\mathcal{M}_L = \{\emptyset, \{0\}, \{1\}, \dots, \{m\}\}.$$

The components of this matroid are the set $\{0, 1, \dots, m\}$ and the singletons $\{i\}$ for $i \geq m+1$. The matroid \mathcal{M}_L has no coloops for $m \geq 1$ and the unique coloop 0 if $m = 0$. Then Theorem 4.1.6 shows $\deg L^{\circ r} = r^{m-1}$ for $m \geq 1$, and $\deg L^{\circ r} = 1$ for $m = 0$. For $m = 3$, $n = 3$ and $r = 2$, we obtain a quartic surface which we illustrate in Figure 28.

4.2 Hypersurfaces

In this subsection, we study the coordinate-wise powers of hypersurfaces. Here, by a hypersurface, we mean a pure codimension 1 variety. In particular, hypersurfaces are assumed to be reduced, but are allowed to have multiple irreducible components. We describe a way to find the explicit equation describing the image of the given hypersurface under the morphism φ_r . We define generalised power sum symmetric polynomials and we give a relation between duality and reciprocity of hypersurfaces defined by them. Finally, we raise the question whether and how the explicit description of coordinate-wise powers of hypersurfaces may lead to results on the coordinate-wise powers for arbitrary varieties.

4.2.1 The Defining Equation

The defining equation of a degree d hypersurface is a square-free (i.e. reduced) polynomial unique up to scaling, corresponding to a unique $f \in \mathbb{P}(\mathbb{C}[\mathbf{x}]_d)$. We work with points in $\mathbb{P}(\mathbb{C}[\mathbf{x}]_d)$, i.e. polynomials up to scaling. We do not always make explicit which degree d we are talking about if it is irrelevant to the discussion. The product of $f \in \mathbb{P}(\mathbb{C}[\mathbf{x}]_d)$ and $g \in \mathbb{P}(\mathbb{C}[\mathbf{x}]_{d'})$ is well-defined up to scaling, i.e. as an element $fg \in \mathbb{P}(\mathbb{C}[\mathbf{x}]_{d+d'})$. Equally, we talk about irreducible factors etc. of elements of $\mathbb{P}(\mathbb{C}[\mathbf{x}]_d)$.

Since the finite morphism φ_r preserves dimensions, the coordinate-wise r -th power of a hypersurface is again a hypersurface, leading to the following definition.

Definition 4.2.1. *Let $f \in \mathbb{P}(\mathbb{C}[\mathbf{x}]_d)$ be square-free and $V(f) \subset \mathbb{P}^n$ be the corresponding hypersurface. We denote by $f^{\circ r} \in \mathbb{P}(\mathbb{C}[\mathbf{x}]_{d'})$ the defining equation of the hypersurface $V(f)^{\circ r}$, i.e.*

$$V(f^{\circ r}) = V(f)^{\circ r}.$$

For a given square-free polynomial f , we want to compute $f^{\circ r}$. To this end, we introduce the following auxiliary notion.

Definition 4.2.2. Let $f \in \mathbb{P}(\mathbb{C}[\mathbf{x}]_d)$ be square-free. We define $\mathfrak{s}_r(f) \in \mathbb{P}(\mathbb{C}[\mathbf{x}]_d)$ as follows:

(i) If f is irreducible and $f \neq x_i \forall i \in \{0, 1, \dots, n\}$, then we define $\mathfrak{s}_r(f) \in \mathbb{P}(\mathbb{C}[\mathbf{x}]_d)$ to be the product over the orbit $\mathcal{G}_r \cdot f \subset \mathbb{P}(\mathbb{C}[\mathbf{x}]_d)$. For $f = x_i$, we define $\mathfrak{s}_r(f) := x_i^r$.

(ii) If $f = f_1 f_2 \dots f_m$ where $f_i \in \mathbb{P}(\mathbb{C}[\mathbf{x}]_d)$ are irreducible, then we define

$$\mathfrak{s}_r(f) := \text{lcm}\{\mathfrak{s}_r(f_1), \mathfrak{s}_r(f_2), \dots, \mathfrak{s}_r(f_m)\}.$$

Observe that in case (ii), determining $\mathfrak{s}_r(f) = \text{lcm}\{\mathfrak{s}_r(f_1), \mathfrak{s}_r(f_2), \dots, \mathfrak{s}_r(f_m)\}$ is straightforward, assuming the decomposition of f into irreducible factors f_1, \dots, f_m is known. Indeed, the irreducible factors of each $\mathfrak{s}_r(f_i)$ are immediate from case (i) of the definition, so determining the least common multiple does not require any additional factorisation.

Lemma 4.2.3. Let $f \in \mathbb{P}(\mathbb{C}[\mathbf{x}]_d)$ be square-free. Then $\mathfrak{s}_r(f) \in \mathbb{P}(\mathbb{C}[x_0^r, \dots, x_n^r]_d)$, and the principal ideal generated by $\mathfrak{s}_r(f)$ in the subring $\mathbb{C}[x_0^r, \dots, x_n^r] \subset \mathbb{C}[\mathbf{x}]$ is $(f) \cap \mathbb{C}[x_0^r, \dots, x_n^r]$.

Proof. It is enough to show the claim for f irreducible because we can deduce the general case in the following manner. If f factors into irreducible factors as $f = f_1 f_2 \dots f_m$, then

$$\begin{aligned} (f) \cap \mathbb{C}[x_0^r, \dots, x_n^r] &= (f_1) \cap \dots \cap (f_m) \cap \mathbb{C}[x_0^r, \dots, x_n^r] = \bigcap_{i=1}^m ((f_i) \cap \mathbb{C}[x_0^r, \dots, x_n^r]) \\ &= \bigcap_{i=1}^m (\mathfrak{s}_r(f_i)) = (\text{lcm}\{\mathfrak{s}_r(f_1), \mathfrak{s}_r(f_2), \dots, \mathfrak{s}_r(f_m)\}) = (\mathfrak{s}_r(f)). \end{aligned}$$

We now assume that f is irreducible. If $f = x_i$ for some $i \in \{0, 1, \dots, n\}$, then the claim holds trivially by the definition of $\mathfrak{s}_r(f)$. Let $f \neq x_i$ for all i and g be a polynomial representing $\mathfrak{s}_r(f) \in \mathbb{P}(\mathbb{C}[\mathbf{x}]_{md})$. By definition, $\mathfrak{s}_r(f)$ is fixed under the action of \mathcal{G}_r , hence $\tau \cdot g$ is a multiple of g for all $\tau \in \mathbb{Z}_r^{n+1}$. Since g is not divisible by x_i , it must contain a monomial not divisible by x_i . This shows that g is fixed by $\tau^{(i)} = (1, \dots, 1, \zeta, 1, \dots, 1) \in \mathbb{Z}_r^{n+1}$, where the i -th position of $\tau^{(i)}$ is a primitive r -th root of unity. Since $\tau^{(0)}, \tau^{(1)}, \dots, \tau^{(n)}$ generate the group \mathbb{Z}_r^{n+1} , we have $\tau \cdot g = g$ for all $\tau \in \mathbb{Z}_r^{n+1}$. Hence, g lies in the invariant ring $\mathbb{C}[\mathbf{x}]^{\mathbb{Z}_r^{n+1}} = \mathbb{C}[x_0^r, \dots, x_n^r]$, i.e. $\mathfrak{s}_r(f) \in \mathbb{P}(\mathbb{C}[x_0^r, \dots, x_n^r]_d)$.

If $h \in (f)$ is a polynomial in $\mathbb{C}[x_0^r, \dots, x_n^r]$, then h is invariant under the action of \mathbb{Z}_r^{n+1} on $\mathbb{C}[\mathbf{x}]$, so $h \in (\tau \cdot f)$ for all $\tau \in \mathcal{G}_r$. By the definition of $\mathfrak{s}_r(f)$ and irreducibility of $\tau \cdot f$, this shows $h \in \mathfrak{s}_r(f)$. We conclude $(f) \cap \mathbb{C}[x_0^r, \dots, x_n^r] = (\mathfrak{s}_r(f))$. \square

Based on Definition 4.2.2 and Lemma 4.2.3, the following proposition gives a method to find the equation of the coordinate-wise power of a hypersurface.

Proposition 4.2.4 (Powers of hypersurfaces). Let $V(f) \subset \mathbb{P}^n$ be a hypersurface. The defining equation f^{or} of its coordinate-wise r -th power is given by replacing each occurrence of x_i^r in $\mathfrak{s}_r(f)$ by x_i for all $i \in \{0, 1, \dots, n\}$.

Proof. Since $V(f)^{or} \subset \mathbb{P}^n$ is the image of $V(f)$ under $\varphi_r: \mathbb{P}^n \rightarrow \mathbb{P}^n$, its ideal $(f^{or}) \subset \mathbb{C}[\mathbf{x}]$ is the preimage under the ring homomorphism $\psi: \mathbb{C}[\mathbf{x}] \rightarrow \mathbb{C}[\mathbf{x}]$, $x_i \mapsto x_i^r$ of the ideal $(f) \subset \mathbb{C}[\mathbf{x}]$. The claim is therefore an immediate consequence of Lemma 4.2.3. \square

For clarity, we illustrate the above results for a hyperplane in \mathbb{P}^3 .

Example 4.2.5. For $n = 3$ and $f := x_0 + x_1 + x_2 + x_3 \in \mathbb{P}(\mathbb{C}[\mathbf{x}]_1)$, we have

$$\mathfrak{s}_2(f) = (x_0 + x_1 + x_2 + x_3)(x_0 + x_1 + x_2 - x_3)(x_0 + x_1 - x_2 + x_3)(x_0 + x_1 - x_2 - x_3) \\ (x_0 - x_1 + x_2 + x_3)(x_0 - x_1 + x_2 - x_3)(x_0 - x_1 - x_2 + x_3)(x_0 - x_1 - x_2 - x_3).$$

Expanding this expression, we obtain a polynomial in $\mathbb{C}[x_0^2, x_1^2, x_2^2, x_3^2]$. Substituting x_i^2 by x_i , we obtain by Proposition 4.2.4 that the coordinate-wise square $V(f)^{\circ 2} \subset \mathbb{P}^3$ is cut out by

$$f^{\circ 2} = x_0^4 - 4x_0^3x_1 + 6x_0^2x_1^2 - 4x_0x_1^3 + x_1^4 - 4x_0^3x_2 + 4x_0^2x_1x_2 + 4x_0x_1^2x_2 - 4x_1^3x_2 + 6x_0^2x_2^2 + 4x_0x_1x_2^2 + 6x_1^2x_2^2 \\ - 4x_0x_2^3 - 4x_1x_2^3 + x_2^4 - 4x_0^3x_3 + 4x_0^2x_1x_3 + 4x_0x_1^2x_3 - 4x_1^3x_3 + 4x_0^2x_2x_3 - 4x_0x_1x_2x_3 + 4x_1^2x_2x_3 + 4x_0x_2^2x_3 \\ + 4x_1x_2^2x_3 - 4x_2^3x_3 + 6x_0^2x_3^2 + 4x_0x_1x_3^2 + 6x_1^2x_3^2 + 4x_0x_2x_3^2 + 4x_1x_2x_3^2 + 6x_2^2x_3^2 - 4x_0x_3^3 - 4x_1x_3^3 - 4x_2x_3^3 + x_3^4.$$

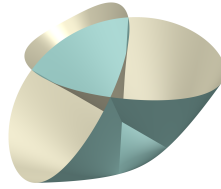


Figure 28: The coordinate-wise square of the plane $V(x_0 + x_1 + x_2 + x_3) \subset \mathbb{P}^3$.

This rational quartic surface is illustrated in Figure 28. It is a Steiner surface with three singular lines forming the ramification locus of $\varphi_2|_{V(f)}: V(f) \rightarrow V(f)^{\circ 2}$.

Example 4.2.6 (Squaring the circle). Consider the plane conic $C = V(f) \subset \mathbb{P}^2$ given by $f := (x_1 - ax_0)^2 + (x_2 - bx_0)^2 - (cx_0)^2$ for some $a, b, c \in \mathbb{R}$ with $c > 0$. In the affine chart $x_0 = 1$, this corresponds over the real numbers to the circle with center (a, b) and radius c . From Proposition 4.2.4, we show that the coordinate-wise square of the circle $C \subset \mathbb{P}^2$ can be a line, a parabola or a singular quartic curve. See Figure 29 for an illustration of the following three cases:

- (i) If the circle C is centered at the origin (i.e. $a = b = 0$), then $\mathfrak{s}_r(f) = f$ and $C^{\circ 2} \subset \mathbb{P}^2$ is the line defined by the equation $f^{\circ 2} = x_1 + x_2 - c^2x_0$.
- (ii) If the center of the circle lies on a coordinate-axis and is not the origin (i.e. $ab = 0$, but $(a, b) \neq (0, 0)$), then $C^{\circ 2} \subset \mathbb{P}^2$ is a conic. Say $a = 0$, then $C^{\circ 2}$ is defined by the equation $f^{\circ 2} = (x_1 + x_2)^2 + 2(b^2 - c^2)x_0x_1 - 2(b^2 + c^2)x_0x_2 + (b^2 - c^2)^2x_0^2$. In the affine chart $x_0 = 1$, C is a circle and $C^{\circ 2}$ is a parabola.
- (iii) If the center of the circle does not lie on a coordinate-axis, then $|\mathcal{G}_r \cdot f| = 4$. Therefore, $C^{\circ 2}$ is a quartic plane curve. Its equation can be computed explicitly using Proposition 4.2.4. Being the image of a conic, the quartic curve $C^{\circ 2}$ is rational, hence

it cannot be smooth. In fact, its singularities are the two points $[0 : 1 : -1]$ and $[a^2 + b^2 : b^2(c^2 - a^2 - b^2) : a^2(c^2 - a^2 - b^2)]$ in \mathbb{P}^2 . They form the branch locus of $\varphi_2|_C : C \rightarrow C^{\circ 2}$. The point $[0 : 1 : -1] \in \mathbb{P}^2$ is the image of the two complex points $[0 : 1 : \pm i]$ at infinity lying on all of the four conics $\tau \cdot C$ for $\tau \in \mathcal{G}_2$. The other singular point of $C^{\circ 2}$ is the image under φ_2 of the two intersection points of the two circles C and $\tau \cdot C$ for $\tau = [1 : -1 : -1] \in \mathcal{G}_2$ inside the affine chart $x_0 = 1$.

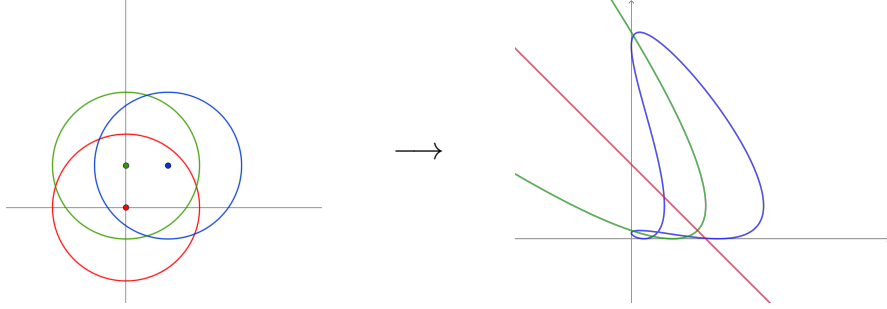


Figure 29: Circles and their coordinate-wise squares

Remark 4.2.7 (Newton polytope of $f^{\circ r}$). Let $f \in \mathbb{P}(\mathbb{C}[\mathbf{x}]_d)$ be irreducible and $f \neq x_i$. Then the Newton polytope of $f^{\circ r}$ arises from the Newton polytope of f by rescaling according to the cardinality of the orbit $\mathcal{G}_r \cdot f \subset \mathbb{P}(\mathbb{C}[\mathbf{x}]_d)$:

$$\text{Newt}(f^{\circ r}) = \frac{|\mathcal{G}_r \cdot f|}{r} \cdot \text{Newt}(f) \subset \mathbb{R}^{n+1}.$$

Indeed, we have $\text{Newt}(\tau \cdot f) = \text{Newt}(f)$ for all $\tau \in \mathcal{G}_r$, and since $\text{Newt}(gh) = \text{Newt}(g) + \text{Newt}(h)$ holds for all polynomials g, h , we have $\text{Newt}(\mathfrak{s}_r(f)) = |\mathcal{G}_r \cdot f| \cdot \text{Newt}(f)$ by Definition 4.2.2. Replacing x_i^r by x_i rescales the Newton polytope with the factor $\frac{1}{r}$, so the claim follows.

4.2.2 Duals and Reciprocals of Power Sum Hypersurfaces

We now highlight the interactions between coordinate-wise powers, dual and reciprocal varieties for the case of *power sum hypersurfaces* $V(x_0^p + \dots + x_n^p) \subset \mathbb{P}^n$. Specifically, we determine explicitly all hypersurfaces that arise from power sum hypersurfaces by repeatedly taking duals and reciprocals as the coordinate-wise r -th power of some hypersurface. In this subsection, we also allow r to take negative integer values.

Recall that the *reciprocal variety* $V(f)^{\circ(-1)}$ of a hypersurface $V(f) \subset \mathbb{P}^n$ not containing any coordinate hyperplane of \mathbb{P}^n is defined as the closure of $\varphi_{-1}(V(f) \setminus V(x_0 x_1 \dots x_n))$ in \mathbb{P}^n . We denote it also by $\mathcal{R}V(f)$. For linear spaces the reciprocal variety and its Chow form has been studied in detail in [78].

We also recall the definition of the *dual variety* of $V(f) \subset \mathbb{P}^n$. Consider the set of hyperplanes in \mathbb{P}^n that arise as the projective tangent space at a smooth point of $V(f)$. This is a subset of the dual projective space and its Zariski closure is the *dual variety* of $V(f)$. Similar to the notation in Subsection 3.1.5 the dual projective space is denoted by $(\mathbb{P}^n)^\vee$ and the dual variety is written as $V(f)^\vee$ or $\mathcal{D}V(f)$. We identify $(\mathbb{C}^{n+1})^\vee$ with \mathbb{C}^{n+1} via the standard bilinear form and therefore identify $(\mathbb{P}^n)^\vee$ with \mathbb{P}^n .

Consider the *power sum polynomial* $\mathbf{f}_p := x_0^p + \dots + x_n^p \in \mathbb{P}(\mathbb{C}[\mathbf{x}]_p)$ for $p \in \mathbb{N}$. As before, we regard polynomials only up to scaling. For power sums with negative exponents we consider the numerator of the rational function as

$$\mathbf{f}_{-p} := (x_1 x_2 x_3 \dots x_n)^p + (x_0 x_2 x_3 \dots x_n)^p + \dots + (x_0 x_1 x_2 \dots x_{n-1})^p \in \mathbb{P}(\mathbb{C}[\mathbf{x}]_{np}) \quad \text{for } p \in \mathbb{N}.$$

In particular, $\mathbf{f}_{-1} \in \mathbb{P}(\mathbb{C}[\mathbf{x}]_n)$ is the elementary symmetric polynomial of degree n .

Recall that the morphism $\varphi_r: \mathbb{P}^n \rightarrow \mathbb{P}^n$ for $r > 0$ is finite, hence preserves dimension. Since $\varphi_{-1}: \mathbb{P}^n \dashrightarrow \mathbb{P}^n$ is a birational map, the rational map $\varphi_{-r} = \varphi_{-1} \circ \varphi_r$ also preserves dimensions: $\dim V(\mathbf{f}_p)^{\circ(-r)} = \dim V(\mathbf{f}_p)$. We therefore extend Definition 4.2.1 to include the defining equation of $V(\mathbf{f}_p)^{\circ r}$ by $\mathbf{f}_p^{\circ r}$ for all $p, r \in \mathbb{Z} \setminus \{0\}$. For the constant polynomial $\mathbf{f}_0 = 1 \in \mathbb{P}(\mathbb{C}[\mathbf{x}]_0)$, we define $\mathbf{f}_0^{\circ r} := 1$ for all $r \in \mathbb{Z} \setminus \{0\}$.

Lemma 4.2.8. *For all $s \in \mathbb{Z}$ and $r, \lambda \in \mathbb{Z} \setminus \{0\}$, we have $\mathbf{f}_{\lambda s}^{\circ(\lambda r)} = \mathbf{f}_s^{\circ r}$.*

Proof. For $\lambda > 0$, we have $\varphi_\lambda^{-1}(V(\mathbf{f}_s)) = V(\mathbf{f}_{\lambda s})$, hence

$$V(\mathbf{f}_{\lambda s}^{\circ(\lambda r)}) = \varphi_r(\varphi_\lambda(V(\mathbf{f}_{\lambda s}))) = \varphi_r(V(\mathbf{f}_s)) = V(\mathbf{f}_s^{\circ r}),$$

where we have used the surjectivity of $\varphi_\lambda: \mathbb{P}^n \rightarrow \mathbb{P}^n$. For $\lambda < 0$, we use the above to see

$$V(\mathbf{f}_{\lambda s}^{\circ(\lambda r)}) = (V(\mathbf{f}_{\lambda s})^{\circ(-\lambda)})^{\circ(-r)} = V(\mathbf{f}_{-s})^{\circ(-r)} = (\mathcal{R}V(\mathbf{f}_{-s}))^{\circ r}.$$

The reciprocal variety of $V(\mathbf{f}_{-s})$ is $V(\mathbf{f}_s)$ for all $s \in \mathbb{Z}$. Hence, $V(\mathbf{f}_{\lambda s}^{\circ(\lambda r)}) = V(\mathbf{f}_s)^{\circ r}$. \square

This naturally leads us to the our next definition.

Definition 4.2.9 (Generalised power sum polynomial). *For any rational number $p = \frac{s}{r} \in \mathbb{Q}$ ($r, s \in \mathbb{Z}, r \neq 0$), we define the generalised power sum polynomial $\mathbf{f}_p := \mathbf{f}_s^{\circ r} \in \mathbb{P}(\mathbb{C}[\mathbf{x}]_d)$.*

By Lemma 4.2.8, the generalised power sum polynomial \mathbf{f}_p is well-defined. With this definition, we get the following duality result for hypersurfaces generalising Example 4.16 in [55].

Proposition 4.2.10 (Duality of generalised power sum hypersurfaces). *Let $p, q \in \mathbb{Q} \setminus \{0\}$ be such that $\frac{1}{p} + \frac{1}{q} = 1$. Then $V(\mathbf{f}_p)^\vee = V(\mathbf{f}_q)$.*

Proof. Write $p = \frac{s}{r}$ with $r \in \mathbb{Z} \setminus \{0\}$, $s \in \mathbb{Z}_{>0}$. Let $b \in V(\mathbf{f}_p) = \varphi_r(V(\mathbf{f}_s))$ be a smooth point of $V(\mathbf{f}_p) \setminus V(x_0 x_1 \dots x_n)$, and let $a \in V(\mathbf{f}_s) \setminus V(x_0 x_1 \dots x_n)$ be such that $b = \varphi_r(a)$. The morphism $\varphi_r: \mathbb{P}^n \setminus V(x_0 x_1 \dots x_n) \rightarrow \mathbb{P}^n \setminus V(x_0 x_1 \dots x_n)$ induces a linear isomorphism on

projective tangent spaces $\mathbb{T}_a\mathbb{P}^n = \mathbb{P}^n \rightarrow \mathbb{P}^n = \mathbb{T}_b\mathbb{P}^n$ given by $\text{diag}(ra_0^{r-1}, ra_1^{r-1}, \dots, ra_n^{r-1})$. This maps

$$\mathbb{T}_a V(\mathbf{f}_s) = V\left(\sum_{i=0}^n (\partial_i \mathbf{f}_s)(a) x_i\right) \subset \mathbb{P}^n \quad \text{onto} \quad \mathbb{T}_b V(\mathbf{f}_p) = V\left(\sum_{i=0}^n \frac{(\partial_i \mathbf{f}_s)(a)}{ra_i^{r-1}} x_i\right) \subset \mathbb{P}^n.$$

In particular, $V(\mathbf{f}_p)^\vee \subset \mathbb{P}^n$ is the image of the rational map

$$V(\mathbf{f}_s) \dashrightarrow \mathbb{P}^n, \quad x \mapsto \left[\frac{\partial_0 \mathbf{f}_s}{rx_0^{r-1}} : \frac{\partial_1 \mathbf{f}_s}{rx_1^{r-1}} : \dots : \frac{\partial_n \mathbf{f}_s}{rx_n^{r-1}} \right].$$

From $\partial_i \mathbf{f}_s = sx_i^{s-1}$ we conclude that $V(\mathbf{f}_p)^\vee = \varphi_{s-r}(V(\mathbf{f}_s)) = V(\mathbf{f}_{s/(s-r)}) = V(\mathbf{f}_p)$. \square

Remark 4.2.11. This statement can be understood as an algebraic analogue of the duality theory for ℓ^p -spaces $(\mathbb{R}^n, |\cdot|_p)$. Indeed, let $p, q \geq 1$ be rational with $\frac{1}{p} + \frac{1}{q} = 1$. The unit ball in $(\mathbb{R}^n, |\cdot|_p)$ is $U_p := \{v \in \mathbb{R}^n \mid \sum_i v_i^p = 1\}$ and by ℓ_p -duality, hyperplanes tangent to U_p correspond to the points on the unit ball U_q of the dual normed vector space $(\mathbb{R}^n, |\cdot|_q)$. The complex projective analogues of the unit balls $U_p \subseteq \mathbb{R}^n$ are the generalised power sum hypersurfaces $V(\mathbf{f}_p) \subseteq \mathbb{P}^n$ and Proposition 4.2.10 shows the previous statement in this setting.

Using Proposition 4.2.4 we can compute \mathbf{f}_p for any $p \in \mathbb{Q}$ explicitly. In particular, we make the following observation:

Lemma 4.2.12. *Let $s \in \mathbb{N}$ and $r \in \mathbb{Z}$ be relatively prime. Then $\mathbf{f}_{s/r}$ arises from $\mathbf{f}_{1/r}$ by substituting $x_i \mapsto x_i^s$ for all $i \in \{0, 1, \dots, n\}$.*

Proof. This follows from the explicit description of the polynomials $\mathbf{f}_{s/r} = \mathbf{f}_s^{\circ r}$ and $\mathbf{f}_{1/r} = \mathbf{f}_1^{\circ r}$ given by Proposition 4.2.4. \square

By Lemma 4.2.12, in order to determine the generalised power sum polynomials \mathbf{f}_p , we may restrict our attention to $\mathbf{f}_{1/r}$. These have a particular geometric interpretation as repeated dual-reciprocals of the linear space $V(x_0 + x_1 + \dots + x_n) \subset \mathbb{P}^n$ as in Corollary 4.2.14.

Theorem 4.2.13. *The repeated dual-reciprocals of generalised power sum hypersurfaces $V(\mathbf{f}_p)$ are given by*

$$\begin{aligned} (\mathcal{D}\mathcal{R})^k V(\mathbf{f}_p) &= V(\mathbf{f}_{p/(1+kp)}) \quad \forall k \in \mathbb{N}, p \in \mathbb{Q} \setminus \{0, -\frac{1}{k}, -\frac{1}{k-1}, \dots, -1\} \quad \text{and} \\ (\mathcal{R}\mathcal{D})^k V(\mathbf{f}_p) &= V(\mathbf{f}_{p/(1-kp)}) \quad \forall k \in \mathbb{N}, p \in \mathbb{Q} \setminus \{0, \frac{1}{k}, \frac{1}{k-1}, \dots, 1\}. \end{aligned}$$

Proof. We show the claim for $V(\mathbf{f}_p)$ by induction on k . For $k = 0$, the claim is trivial. For $k > 0$, we get by induction hypothesis:

$$\begin{aligned} (\mathcal{D}\mathcal{R})^k V(\mathbf{f}_p) &= \mathcal{D}\mathcal{R} V(\mathbf{f}_{p/(1+(k-1)p)}) = (V(\mathbf{f}_{p/(1+(k-1)p)})^{\circ(-1)})^\vee \\ &\stackrel{(*)}{=} V(\mathbf{f}_{-p/(1+(k-1)p)})^\vee \stackrel{(**)}{=} V(\mathbf{f}_{p/(1+kp)}), \end{aligned}$$

where (*) holds by Lemma 4.2.8 and (**) by Proposition 4.2.10. From this, we also see

$$(\mathcal{R}\mathcal{D})^k V(\mathfrak{f}_p) = \mathcal{R}(\mathcal{D}\mathcal{R})^k \mathcal{R}V(\mathfrak{f}_p) = \mathcal{R}(\mathcal{D}\mathcal{R})^k V(\mathfrak{f}_{-p}) = \mathcal{R}V(\mathfrak{f}_{-p/(1-kp)}) = V(\mathfrak{f}_{p/(1-kp)}),$$

concluding the proof. \square

Corollary 4.2.14. *For $r > 0$, the repeated alternating reciprocals and duals of the linear space $V(\mathfrak{f}_1) \subset \mathbb{P}^n$ are the coordinate-wise powers of $V(\mathfrak{f}_1)$ given as*

$$\underbrace{\mathcal{D}\mathcal{R}\mathcal{D}\mathcal{R}\dots\mathcal{D}\mathcal{R}}_{2r-2} V(\mathfrak{f}_1) = V(\mathfrak{f}_1)^{\circ r} \quad \text{and} \quad \underbrace{\mathcal{R}\mathcal{D}\mathcal{R}\dots\mathcal{D}\mathcal{R}}_{2r-1} V(\mathfrak{f}_1) = V(\mathfrak{f}_1)^{\circ(-r)}.$$

Example 4.2.15. Let $n = 3$ and $f := x_0 + x_1 + x_2 + x_3$. The reciprocal variety of the plane $V(f) \subset \mathbb{P}^3$ is given by $\mathfrak{f}_{-1} = x_1x_2x_3 + x_0x_2x_3 + x_0x_1x_3 + x_0x_1x_2$. Its dual is $V(\mathfrak{f}_{1/2}) = V(\mathfrak{f}_1)^{\circ 2} \subset \mathbb{P}^3$ by Proposition 4.2.10. This is the quartic surface from Example 4.2.5. Higher iterated dual-reciprocal varieties of $V(f)$ can be explicitly computed analogous to Example 4.2.5 via Theorem 4.2.13. For instance, the surface $\mathcal{D}\mathcal{R}\mathcal{D}\mathcal{R}V(f) \subset \mathbb{P}^3$ is the coordinate-wise cube of $V(f)$ which is the degree 9 surface illustrated in Figure 30.

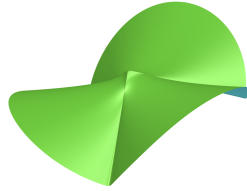


Figure 30: The iterated dual-reciprocal $\mathcal{D}\mathcal{R}\mathcal{D}\mathcal{R}V(f) \subset \mathbb{P}^3$

4.2.3 From Hypersurfaces to Arbitrary Varieties?

We briefly discuss to what extent Proposition 4.2.4 can be used to determine coordinate-wise powers of arbitrary varieties, and mention the difficulties involved in this approach.

If f_1, \dots, f_m are homogeneous polynomials vanishing on a variety $X \subset \mathbb{P}^n$, then their coordinate-wise powers give rise to the inclusion $X^{\circ r} \subset V(f_1^{\circ r}, \dots, f_m^{\circ r})$. To address the question when does the equality hold, we will now define *power basis*. The notion of power basis is reminiscent of the notion of *tropical bases* in Tropical Geometry [87, Section 2.6].

Definition 4.2.16 (Power bases). *A set of homogeneous polynomials $f_1, \dots, f_m \in \mathbb{C}[\mathbf{x}]$ is an r -th power basis of the ideal $I = (f_1, \dots, f_m)$ if the following equality of sets holds:*

$$V(f_1, \dots, f_m)^{\circ r} = V(f_1^{\circ r}, \dots, f_m^{\circ r}).$$

We show the existence of such power bases for a given ideal in the following proposition.

Proposition 4.2.17 (Existence of power bases). *Let $I \subset \mathbb{C}[\mathbf{x}]$ be a homogeneous ideal. Then for each r , there exists an r -th power basis of I .*

Proof. Let J denote the defining ideal of $V(I)^{or} \subset \mathbb{P}^n$. If J is generated by homogeneous polynomials $g_1, \dots, g_m \in \mathbb{C}[\mathbf{x}]$, we define $f_1, \dots, f_m \in \mathbb{C}[\mathbf{x}]$ to be their images under the ring homomorphism $\mathbb{C}[\mathbf{x}] \rightarrow \mathbb{C}[\mathbf{x}]$, $x_i \mapsto x_i^r$. Then $f_i \in I$, since

$$V(f_i) = \varphi_r^{-1}(V(g_i)) \supset \varphi_r^{-1}(V(I)^{or}) \supset V(I).$$

On the other hand, we have $f_i^{or} = g_i$, since $V(f_i)^{or} = \varphi_r(\varphi_r^{-1}(V(g_i))) = V(g_i)$ by surjectivity of φ_r . Therefore, $f_1^{or}, \dots, f_m^{or}$ generate J . Enlarging f_1, \dots, f_m to a generating set of I gives an r -th power basis of I . \square

Proposition 4.2.17 shows the existence of r -th power bases, but explicitly determining one a priori is nontrivial. In the following two examples, we will see that even in the case of squaring codimension 2 linear spaces, obvious candidates for f_1, \dots, f_m do not form a power basis.

Example 4.2.18. Let $I := (f_1, f_2) \subset \mathbb{C}[\mathbf{x}]$ be the ideal defining the line in \mathbb{P}^3 that is given by $f_1 := x_0 + x_1 + x_2 + x_3$ and $f_2 := x_1 + 2x_2 + 3x_3$. The polynomials $f_1^{\circ 2}$ and $f_2^{\circ 2}$ have degrees 4 and 2, respectively, by Proposition 4.2.4. Note that the polynomial $f_3 := 3x_0^2 - x_1^2 + x_2^2 - 3x_3^2 = 3(x_0 - x_1 - x_2 - x_3)f_1 + 2(x_1 + x_2)f_2$ also lies in I , so the ideal of $V(I)^{\circ 2}$ contains the linear form $f_3^{\circ 2} = 3x_0 - x_1 + x_2 - 3x_3$. The polynomials f_1, f_2 do not form a power basis of I . In fact, one can check that $V(f_1^{\circ 2}, f_2^{\circ 2}) \subset \mathbb{P}^3$ is the union of four rational quadratic curves, one of which is $V(I)^{\circ 2}$, see Figure 31 for an illustration. A power basis of I is given by f_1, f_2, f_3 .

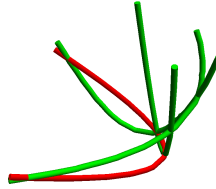


Figure 31: Distinction between $V(f_1^{\circ 2}, f_2^{\circ 2})$ and $V(f_1, f_2)^{\circ 2}$

Example 4.2.19. Another natural choice for polynomials f_1, \dots, f_m in the ideal of a linear space $X \subset \mathbb{P}^n$ consists of the *circuit forms*, i.e. linear forms vanishing on X that are minimal with respect to the set of occurring variables. However, for

$$X := V(x_0 + x_1 + x_2 + x_3 + x_4, x_1 + 2x_2 + 3x_3 + 4x_4) \subset \mathbb{P}^4,$$

these circuit forms are

$$\begin{aligned} f_1 &= x_1 + 2x_2 + 3x_3 + 4x_4, & f_2 &= x_0 - x_2 - 2x_3 - 3x_4, & f_3 &= 2x_0 + x_1 - x_3 - 2x_4, \\ f_4 &= 3x_0 + 2x_1 + x_2 - x_4, & f_5 &= 4x_0 + 3x_1 + 2x_2 + x_3, \end{aligned}$$

and one can check that the point $[16 : 16 : 1 : 36 : 9] \in \mathbb{P}^4$ lies in $V(f_1^{\circ 2}, \dots, f_5^{\circ 2})$, but not in $X^{\circ 2}$. In particular, f_1, \dots, f_5 is not an r -th power basis for $r = 2$.

We have seen in Example 4.2.18 and Example 4.2.19 that even for the case of linear spaces of codimension 2 it is not an easy task to a priori identify an r -th power basis.

The following proposition shows how one can straightforwardly find a very large r -th power basis of an ideal I , without first computing the ideal of $V(I)^{\circ r}$.

Proposition 4.2.20. *If $g_1, \dots, g_k \in \mathbb{C}[\mathbf{x}]_d$ are forms of degree d , then taking $(k - 1)r^n + 1$ general linear combinations of g_1, \dots, g_k produces an r -th power basis of (g_1, \dots, g_k) .*

Proof. We assume that g_1, \dots, g_k are linearly independent, or else we can replace them with a linearly independent subset. For $m := (k - 1)r^n + 1$, let $f_1, \dots, f_m \in \langle g_1, \dots, g_k \rangle$ be such that no k of them are linearly dependent. For $X := V(g_1, \dots, g_k)$, we will show that $V(f_1^{\circ r}, \dots, f_m^{\circ r}) = X^{\circ r}$ by comparing the preimages of both sides under $\varphi_r: \mathbb{P}^n \rightarrow \mathbb{P}^n$.

By Proposition 4.1.1, we have $\varphi_r^{-1}(X^{\circ r}) = \bigcup_{\tau \in \mathcal{G}_r} \tau \cdot X$ and

$$\varphi_r^{-1}(V(f_1^{\circ r}, \dots, f_m^{\circ r})) = \bigcap_{i=1}^m \varphi_r^{-1}(\varphi_r(V(f_i))) = \bigcap_{i=1}^m \bigcup_{\tau \in \mathcal{G}_r} \tau \cdot V(f_i).$$

Let $p \in \varphi_r^{-1}(V(f_1^{\circ r}, \dots, f_m^{\circ r})) \subset \mathbb{P}^n$. Then for each $i \in \{1, \dots, m\}$ there exists some $\tau \in \mathcal{G}_r$ with $p \in \tau \cdot V(f_i)$ using the last equality above. Since $m > (k - 1)|\mathcal{G}_r|$, by pigeonhole principle there must exist $\tau \in \mathcal{G}_r$ and $i_1, i_2, \dots, i_k \in \{1, \dots, m\}$ distinct with $p \in \bigcap_{j=1}^k \tau \cdot V(f_{i_j}) = \tau \cdot V(f_{i_1}, \dots, f_{i_k})$. Since, by assumption, no k of them are linearly dependent f_{i_1}, \dots, f_{i_k} span $\langle g_1, \dots, g_k \rangle$. Therefore, $V(f_{i_1}, \dots, f_{i_k}) = X$, and hence, $p \in \tau \cdot V(f_{i_1}, \dots, f_{i_k})$ implies that $p \in \tau \cdot X \subset \varphi_r^{-1}(X^{\circ r})$. This shows $\varphi_r^{-1}(V(f_1^{\circ r}, \dots, f_m^{\circ r})) \subset \varphi_r^{-1}(X^{\circ r})$. The reverse inclusion is trivial. \square

In particular, Proposition 4.2.20 shows that for a subvariety of \mathbb{P}^n defined by k forms of degree d , its coordinate-wise r -th power can be described set-theoretically by the vanishing of $(k - 1)r^n + 1$ forms of degree $\leq dr^{n-1}$. However, we will see in Section 4.3 that for linear spaces this bound is rather weak in many cases and should be expected to allow dramatic refinement in general. We raise the following as a broad open question:

Question 4.2.21. *When does a set of homogeneous polynomials form an r -th power basis? For a given ideal I , do there exist polynomials $f_1, \dots, f_m \in I$ that simultaneously form an r -th power basis for all r ?*

4.3 Linear Spaces

In this subsection, we specialise to linear spaces $L \subset \mathbb{P}^n$ and study their coordinate-wise powers $L^{\circ r}$. First, we highlight the dependence of $L^{\circ r}$ on the geometry of a finite point configuration associated to $L \subset \mathbb{P}^n$. For $r = 2$, we point out its relation to symmetric matrices with degenerate eigenvalues. Based on this, we classify the coordinate-wise squares of lines and planes. Finally, we turn to the case of squaring linear spaces in high-dimensional ambient space.

4.3.1 Point Configurations

We investigate the defining ideal of L^{or} for a linear space $L \subset \mathbb{P}^n$. The degrees of its minimal generators do not change under rescaling and permuting coordinates of \mathbb{P}^n , i.e. under the actions of the algebraic torus $\mathbb{G}_m^{n+1} = (\mathbb{C}^*)^{n+1}$ and the symmetric group \mathfrak{S}_{n+1} . Fixing a $(k+1)$ -dimensional vector space W , we have the identification

$$\begin{aligned} \{\text{orbits of } \text{Gr}(k, \mathbb{P}^n) \text{ under } \mathbb{G}_m^{n+1} \rtimes \mathfrak{S}_{n+1}\} &\leftrightarrow \left\{ \begin{array}{l} \text{finite multi-sets } Z \subset \mathbb{P}W^\vee \text{ with } \langle Z \rangle = \mathbb{P}W^\vee \\ \text{of cardinality } \leq n+1 \text{ up to } \text{Aut}(\mathbb{P}W^\vee) \end{array} \right\} \\ L = \text{im}(\mathbb{P}W \xrightarrow{[\ell_0:\ell_1:\dots:\ell_s:0:\dots:0]} \mathbb{P}^n) &\leftrightarrow Z = \{[\ell_0], [\ell_1], \dots, [\ell_s]\} \subset \mathbb{P}W^\vee, s \leq n. \end{aligned}$$

Hence, we may express coordinate-wise powers of a linear space L in terms of the corresponding finite multi-set $Z \subset \mathbb{P}W^\vee$. In fact, it is easy to check that the degrees of the minimal generators of the defining ideal only depend on the underlying set Z , forgetting repetitions in the multi-set. We study coordinate-wise powers of a linear space in terms of the corresponding non-degenerate finite point configuration.

For the entirety of Section 4.3, we establish the following notation: Let $L \subset \mathbb{P}^n$ be a linear space of dimension k . We understand L as the image of a chosen linear embedding $\iota: \mathbb{P}W \xrightarrow{[\ell_0:\dots:\ell_n]} \mathbb{P}^n$, where W is a $(k+1)$ -dimensional vector space and $\ell_0, \dots, \ell_n \in W^\vee$ are linear forms defining ι . Consider the finite set of points $Z \subset \mathbb{P}W^\vee$ given by

$$Z := \{[\ell_i] \in \mathbb{P}W^\vee \mid 0 \leq i \leq n \text{ such that } \ell_i \neq 0\}.$$

Since $\ell_0, \ell_1, \dots, \ell_n \in W^\vee$ define the linear embedding ι , they cannot have a common zero in W . Hence, the linear span of Z is the whole space $\mathbb{P}W^\vee$. We denote by $I(Z) \subset \text{Sym}^\bullet W$ the defining ideal of $Z \subset \mathbb{P}W^\vee$. The subspace of degree r forms vanishing on Z is written as $I(Z)_r \subset \text{Sym}^r W$.

The main technical tool is the following observation that $L^{or} \subset \mathbb{P}^n$ equals (up to a linear re-embedding) the image of the r -th Veronese variety $\nu_r(\mathbb{P}W) \subset \mathbb{P}\text{Sym}^r W$ under the projection from the linear space $\mathbb{P}(I(Z)_r) \subset \mathbb{P}\text{Sym}^r W$.

Lemma 4.3.1. *The diagram*

$$\begin{array}{ccccc} & & \mathbb{P}W & \xrightarrow{\nu_r} & \mathbb{P}\text{Sym}^r W \\ & \swarrow \iota & \downarrow \varphi_r \circ \iota & \searrow \psi & \downarrow \pi \\ \mathbb{P}^n & \xrightarrow{\varphi_r} & \mathbb{P}^n & \xleftarrow{\vartheta} & \mathbb{P}(\text{Sym}^r W / I(Z)_r) \end{array}$$

commutes, where ν_r is the r -th Veronese embedding, π is the linear projection of $\mathbb{P}\text{Sym}^r W$ from the linear space $\mathbb{P}(I(Z)_r)$, ψ is a morphism and ϑ is a linear embedding.

Proof. We observe that the morphism $\varphi_r \circ \iota$ is given by

$$\varphi_r \circ \iota: \mathbb{P}W \rightarrow \mathbb{P}^n, \quad [v] \mapsto [\ell_0^r(v) : \ell_1^r(v) : \dots : \ell_n^r(v)].$$

The $n + 1$ elements $\ell_i^r \in \text{Sym}^r W^\vee$ correspond to a linear map $\chi: \text{Sym}^r W \rightarrow \mathbb{C}^{n+1}$ via the natural identification $(\text{Sym}^r W^\vee)^{n+1} = \text{Hom}_{\mathbb{C}}(\text{Sym}^r W, \mathbb{C}^{n+1})$.

The rational map $\bar{\chi}$ between projective spaces corresponding to the linear map χ gives the following commuting diagram:

$$\begin{array}{ccc} \mathbb{P}W & \xleftarrow{\nu_r} & \mathbb{P}\text{Sym}^r W \\ \downarrow \varphi_r \circ \iota & \bar{\chi} & \downarrow \pi \\ \mathbb{P}^n & \xleftarrow{\vartheta} & \mathbb{P}(\text{Sym}^r W / \ker \chi), \end{array}$$

where ϑ is the linear embedding of projective spaces induced by factoring χ over $\text{Sym}^r W / \ker \chi$. In particular, $\nu_r(\mathbb{P}W) \cap \mathbb{P}(\ker \chi) = \emptyset$, since $\varphi_r \circ \iota$ is defined everywhere on $\mathbb{P}W$. Hence, $\pi|_{\nu_r(\mathbb{P}W)}: \nu_r(\mathbb{P}W) \rightarrow \mathbb{P}(\text{Sym}^r W / \ker \chi)$ is a morphism.

Finally, we claim that $\ker \chi = I(Z)_r$. Once we know this, defining $\psi := \pi|_{\nu_r(\mathbb{P}W)} \circ \nu_r$ completes the claimed diagram.

Let $f \in \text{Sym}^r W$ such that $f \in I(Z)_r$. Naturally identifying W and $W^{\vee\vee}$, we may view f as a form of degree r on W^\vee . Then, the condition that $f \in I(Z)_r$ translates to $f(\ell_i) = 0 \forall i$. Viewing f as a symmetric r -linear form $W^\vee \times \dots \times W^\vee \rightarrow \mathbb{C}$, we have $f(\ell_i, \dots, \ell_i) = 0 \forall i$. Also, when f is considered as a linear form on $\text{Sym}^r W^\vee$, $f(\ell_i^r) = 0 \forall i$. The latter expression is equivalent to $f \in \ker \chi$, via the identification of W and $W^{\vee\vee}$. We conclude $I(Z)_r = \ker \chi$. \square

In particular, we deduce the following:

Proposition 4.3.2. *Let L be a linear space such that the finite set of points Z does not lie on a degree r hypersurface. Then the ideal of L^{or} is generated by linear and quadratic forms.*

Proof. Since $I(Z)_r = 0$, we deduce from Lemma 4.3.1 that $L^{or} = \varphi_r(L)$ is a linear re-embedding of the k -dimensional r -th Veronese variety $\nu_r(\mathbb{P}W) \subset \mathbb{P}\text{Sym}^r W$. The ideal of this Veronese variety is generated by quadrics. Since $\dim \text{Sym}^r W = \binom{k+r}{r}$, the linear re-embedding $\vartheta: \mathbb{P}\text{Sym}^r W \hookrightarrow \mathbb{P}^n$ adds $n - \binom{k+r}{r} + 1$ linear forms to the ideal. \square

4.3.2 Degenerate Eigenvalues and Squaring

We now specialise to the case of coordinate-wise squaring, i.e. $r = 2$. This case has special geometric importance, since it corresponds to computing the image of a linear space under the quotient of \mathbb{P}^n by the reflection group generated by the coordinate hyperplanes. In this subsection through Proposition 4.3.3 we point out that the case of coordinate-wise square of a linear space is closely related to studying symmetric matrices with a degenerate spectrum of eigenvalues. Here, we interpret $\mathbb{P}\text{Sym}^2 \mathbb{F}^{k+1}$ (for $\mathbb{F} = \mathbb{R}$ or \mathbb{C}) as the projective space consisting of symmetric $(k + 1) \times (k + 1)$ -matrices up to scaling with entries in \mathbb{F} .

Proposition 4.3.3. *Let $X \subset \mathbb{P}\mathrm{Sym}^2 \mathbb{R}^{k+1}$ be the set of real symmetric $(k+1) \times (k+1)$ -matrices with an eigenvalue of multiplicity $\geq k$. Then the Zariski closure of X in $\mathbb{P}\mathrm{Sym}^2 \mathbb{C}^{k+1}$ is projectively equivalent to the projective cone over the coordinate-wise square $L^{\circ 2}$ of any k -dimensional linear space L whose point configuration $Z \subseteq \mathbb{P}W^\vee$ lies on a unique and smooth quadric.*

Proof. Let $L \subset \mathbb{P}^n$ be a k -dimensional linear space such that $I(Z)_2$ is spanned by a smooth quadric $q \in \mathbb{P}\mathrm{Sym}^2 W$. Choosing coordinates of $W \cong \mathbb{C}^{k+1}$, we identify points in $\mathbb{P}\mathrm{Sym}^2 W$ with complex symmetric $(k+1) \times (k+1)$ -matrices up to scaling and we can assume $q = \mathrm{id} \in \mathbb{P}\mathrm{Sym}^2 W$. The second Veronese variety $\nu_2(\mathbb{P}W) \subset \mathbb{P}\mathrm{Sym}^2 W$ consists of rank 1 matrices. Let $X_0 \subset \mathbb{P}(\mathrm{Sym}^2 W / \langle q \rangle)$ be the image of $\nu_2(\mathbb{P}W)$ under the natural projection. By Lemma 4.3.1, X_0 is the coordinate-wise square $L^{\circ 2}$ up to a linear re-embedding.

The projective cone over $X_0 \cong L^{\circ 2}$ is the subvariety $X_1 \subset \mathbb{P}\mathrm{Sym}^2 W$ consisting of complex symmetric matrices M such that the set $M + \langle \mathrm{id} \rangle$ contains a matrix of rank ≤ 1 . We observe that the rank of $M - \lambda \mathrm{id}$ is the codimension of the eigenspace of M with respect to $\lambda \in \mathbb{C}$. Hence,

$$X_1 = \{M \in \mathbb{P}\mathrm{Sym}^2 \mathbb{C}^{k+1} \mid M \text{ has an eigenspace of codimension } \leq 1\}.$$

We are left to show that X_1 is the Zariski closure in $\mathbb{P}\mathrm{Sym}^2 \mathbb{C}^{k+1}$ of $X \subset \mathbb{P}\mathrm{Sym}^2 \mathbb{R}^{k+1}$. Since real symmetric matrices are diagonalisable, the multiplicity of an eigenvalue is the dimension of the corresponding eigenspace. Hence, $X_1 \cap \mathbb{P}\mathrm{Sym}^2 \mathbb{R}^{k+1} = X$. The set X is the orbit of the line $V := \{\mathrm{diag}(\lambda, \dots, \lambda, \mu) \mid [\lambda : \mu] \in \mathbb{P}_\mathbb{R}^1\}$ under the action of $O(k+1)$. The action is given by conjugation with orthogonal matrices and the stabiliser is $O(k) \times \{\pm 1\}$. Therefore, X has real dimension $\dim V + \dim O(k+1) - \dim O(k) = k+1$. Also, X_1 is the projective cone over $X_0 \cong L^{\circ 2}$, so it is a $(k+1)$ -dimensional irreducible complex variety. We conclude that X_1 is the Zariski closure of X in $\mathbb{P}\mathrm{Sym}^2 \mathbb{C}^{k+1}$. \square

We illustrate Proposition 4.3.3 in the case of 3×3 -matrices:

Example 4.3.4. Consider the set of real symmetric 3×3 -matrices with a repeated eigenvalue. We denote its Zariski closure in $\mathbb{P}\mathrm{Sym}^3 \mathbb{C}^2$ by Y . By Proposition 4.3.3, it can be understood in terms of the coordinate-wise square $L^{\circ 2}$ for some plane L . We make this explicit as follows: Consider the planar point configuration

$$Z = \{[1 : i : 0], [1 : -i : 0], [1 : 0 : i], [1 : 0 : -i], [0 : 1 : i]\} \subseteq \mathbb{P}^2,$$

lying only on the conic $V(x^2 + y^2 + z^2)$. Let L be the corresponding plane in \mathbb{P}^4 , given as the image of

$$\iota: \mathbb{P}^2 \hookrightarrow \mathbb{P}^4, \quad [x : y : z] \mapsto [x + iy : x - iy : x + iz : x - iz : y + iz].$$

Under the linear embedding

$$\begin{aligned} \psi: \mathbb{P}^4 &\hookrightarrow \mathbb{P}\mathrm{Sym}^2 \mathbb{C}^3, \\ [a : b : c : d : e] &\mapsto \begin{bmatrix} 2(a+b+c+d) & 3i(-a+b) & 3i(-c+d) \\ 3i(-a+b) & 6(-2a-2b+c+d) & 3i(-a-b+c+d-2e) \\ 3i(-c+d) & 3i(-a-b+c+d-2e) & 6(a+b-2c-2d) \end{bmatrix}, \end{aligned}$$

the plane L gets mapped into Y . Indeed, it is easily checked that a point $[x : y : z]$ gets mapped to the matrix $-4(x^2 + y^2 + z^2) \text{id} + 12(x, y, z)^T(x, y, z)$ under the composition $\psi \circ \iota: \mathbb{P}^2 \rightarrow \mathbb{P} \text{Sym}^2 \mathbb{C}^3$. Note that this matrix has a repeated eigenvalue. More precisely, Proposition 4.3.3 shows that Y is the projective cone over $\psi(L^{\circ 2})$ with the vertex id .

In Subsection 4.3.4 we give an explicit set-theoretic description of the coordinate-wise square of a linear space in high-dimensional ambient space. We will show the following result as a special case of Theorem 4.3.11. Given a matrix $A \in \mathbb{C}^{s \times s}$, we denote a 2×2 minor of A by $A_{ij|k\ell}$ where $i \neq j$ are the rows and $k \neq \ell$ are the columns of the minor.

Corollary 4.3.5. *Let $s \geq 4$. A symmetric matrix $A \in \mathbb{C}^{s \times s}$ has an eigenspace of codimension ≤ 1 if and only if its 2×2 -minors satisfy the following for $i, j, k, \ell \leq s$ distinct:*

$$A_{ij|k\ell} = 0, \quad A_{ik|i\ell} = A_{jk|j\ell} \quad \text{and} \quad A_{ik|ik} - A_{i\ell|i\ell} = A_{jk|jk} - A_{j\ell|j\ell}.$$

These equations describe the Zariski closure in the complex vector space $\text{Sym}^2 \mathbb{C}^s$ of the set of real symmetric matrices with an eigenvalue of multiplicity $\geq s - 1$.

4.3.3 Squaring Lines and Planes

In this subsection we consider the low-dimensional cases and classify the coordinate-wise squares of lines and planes in arbitrary ambient spaces.

Theorem 4.3.6 (Squaring lines). *Let L be a line in \mathbb{P}^n .*

(i) *If $|Z| = 2$, then $L^{\circ 2}$ is a line in \mathbb{P}^n .*

(ii) *If $|Z| > 2$, then $L^{\circ 2}$ is a smooth conic contained in a plane inside \mathbb{P}^n .*

Proof. Since $Z \subset \mathbb{P}W^\vee$ spans the projective line $\mathbb{P}W^\vee$, we must have $|Z| \geq 2$.

If $|Z| > 2$, then $I(Z)_2 = 0$, since no non-zero quadratic form on the projective line $\mathbb{P}W^\vee$ vanishes on all points of Z . Then Lemma 4.3.1 implies that $L^{\circ 2} = (\varphi_2 \circ \iota)(\mathbb{P}W)$ is a linear re-embedding of $\nu_2(\mathbb{P}W)$, which is a smooth conic in the plane $\mathbb{P} \text{Sym}^2 W \cong \mathbb{P}^2$.

If $|Z| = 2$, then $\dim I(Z)_2 = 1$, since up to scaling there is a unique quadric vanishing on the points Z . By Lemma 4.3.1, the image $\varphi_2(L)$ lies in a projective line $\mathbb{P}^1 \cong \vartheta(\mathbb{P}(\text{Sym}^2 W / I(Z)_2)) \subset \mathbb{P}^n$. On the other hand $\dim L^{\circ 2} = \dim L = 1$. Hence, $L^{\circ 2} = \varphi_2(L)$ is a line in \mathbb{P}^n . \square

Remark 4.3.7. We observe that the two possibilities in Theorem 4.3.6 for the coordinate-wise square of a line L differ in degree. In particular, Corollary 4.1.7 shows that it only depends on the linear matroid \mathcal{M}_L whether $L^{\circ 2}$ is a line or a (re-embedded) plane conic.

Remark 4.3.8. In the Grassmannian of lines $\text{Gr}(1, \mathbb{P}^n)$, consider the locus $\Gamma \subset \text{Gr}(1, \mathbb{P}^n)$ of those lines L whose coordinate-wise square $L^{\circ 2}$ is a line. Considering Plücker coordinates

p_{ij} on the Grassmannian $\text{Gr}(1, \mathbb{P}^n)$, we observe that Γ is the subvariety of $\text{Gr}(1, \mathbb{P}^n)$ given by the vanishing of $p_{ij}p_{jk}p_{ki}$ for all $i, j, k \in \{0, 1, \dots, n\}$ distinct:

$$\Gamma = V(p_{ij}p_{jk}p_{ki} \mid i, j, k \in \{0, 1, \dots, n\} \text{ distinct}) \subset \text{Gr}(1, \mathbb{P}^n).$$

Indeed, if L is the image of an embedding $\mathbb{P}^1 \xrightarrow{B} \mathbb{P}^n$ given by a chosen rank 2 matrix $B \in \mathbb{C}^{(n+1) \times 2}$, then $Z \subset (\mathbb{P}^1)^\vee$ is the set of points corresponding to the non-zero rows of B . Then $|Z| = 2$ if and only if among any three distinct rows of B there always exist two linearly dependent rows. In terms of the Plücker coordinates, which are given by the 2×2 -minors of B , this translates into the vanishing condition above.

Theorem 4.3.9 (Squaring planes). *Let L be a plane in \mathbb{P}^n . The defining ideal $I \subset \mathbb{C}[\mathbf{x}]$ of $L^{\circ 2}$ depends on the geometry of the planar configuration of $Z \subset \mathbb{P}W^\vee$ as follows (see Figure 32):*

- (i) *If Z is not contained in any conic, then I is minimally generated by $n - 5$ linear forms and 6 quadratic forms.*
- (ii) *If Z is contained in a unique conic $Q \subset \mathbb{P}W^\vee$, we distinguish two cases:*
 - (a) *If Q is irreducible, then I is minimally generated by $n - 4$ linear forms and 7 cubic forms.*
 - (b) *If Q is reducible, then $L^{\circ 2}$ is the complete intersection of $n - 4$ hyperplanes and 2 quadrics.*
- (iii) *If Z is contained in several conics, we distinguish three cases:*
 - (a) *If $|Z| = 3$, then I is minimally generated by $n - 2$ linear forms.*
 - (b) *If $|Z| = 4$ and no three points of Z are collinear, then I is minimally generated by $n - 3$ linear forms and one quartic form.*
 - (c) *If Z contains at least three collinear points, then I is minimally generated by $n - 3$ linear forms and one quadratic form.*

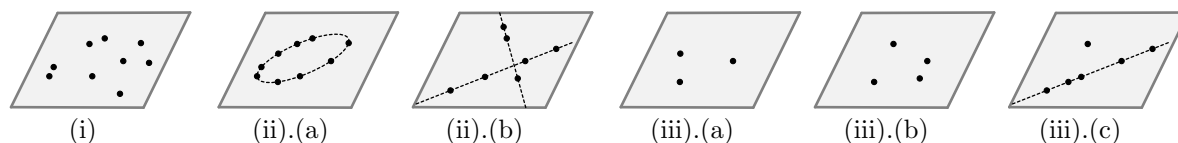


Figure 32: Dependence of $L^{\circ 2}$ on the planar point configuration Z

Proof. Notice that $k = 2$, so $\dim W = 3$.

(i) If $I(Z)_2 = 0$, then by Lemma 4.3.1 $L^{\circ 2} \subset \mathbb{P}^n$ is a linear re-embedding of the Veronese surface $\nu_2(\mathbb{P}W) \subset \mathbb{P}\text{Sym}^2 W$. The ideal of the $\nu_2(\mathbb{P}W)$ is minimally generated by six quadrics. Indeed, choosing a basis for W , we may understand points in $\mathbb{P}\text{Sym}^2 W$ as symmetric 3×3 -matrices up to scaling. Then $\nu_2(\mathbb{P}W)$ is the subvariety corresponding to symmetric rank 1 matrices, which is cut out by the six quadratic polynomials imposing vanishing 2×2 -minors. Since $\dim \mathbb{P}\text{Sym}^2 W = 5$, the linear re-embedding $\mathbb{P}\text{Sym}^2 W \hookrightarrow \mathbb{P}^n$ adds $n - 5$ linear forms to I .

(ii) We can choose a basis $\{z_0, z_1, z_2\}$ of W such that the unique reduced plane conic through $Z \subset \mathbb{P}W^\vee$ is with respect to these coordinates given by the vanishing of either $q_1 := z_0^2 - 2z_1z_2 \in \text{Sym}^2 W$ or $q_2 := z_1z_2 \in \text{Sym}^2 W$.

We consider the basis $\{z_1^2, z_2^2, 2z_0z_1, 2z_0z_2, 2z_1z_2\}$ of $\text{Sym}^2 W/\langle q_1 \rangle$ and the basis $\{z_0^2, z_1^2, z_2^2, 2z_0z_1, 2z_0z_2\}$ of $\text{Sym}^2 W/\langle q_2 \rangle$. With respect to these choices of bases, the morphism $\psi: \mathbb{P}W \rightarrow \mathbb{P}(\text{Sym}^2 W/I(Z)_2)$ is given as

$$\begin{aligned} \psi: \mathbb{P}^2 &\rightarrow \mathbb{P}^4, & [a_0 : a_1 : a_2] &\mapsto [a_1^2 : a_2^2 : a_0a_1 : a_0a_2 : a_0^2 + a_1a_2] \\ \text{or } \psi: \mathbb{P}^2 &\rightarrow \mathbb{P}^4, & [a_0 : a_1 : a_2] &\mapsto [a_0^2 : a_1^2 : a_2^2 : a_0a_1 : a_0a_2]. \end{aligned}$$

In the first case, we checked computationally with `Macaulay2` [58] that the ideal is minimally generated by seven cubics. A structural description of these quadrics and cubics will be given in the proof of Theorem 4.3.11. The image of the second morphism is a complete intersection of two binomial quadrics. By Lemma 4.3.1, the coordinate-wise square $L^{\circ 2}$ arises from the image of ψ via a linear re-embedding $\mathbb{P}^4 \hookrightarrow \mathbb{P}^n$, producing additional $n - 4$ linear forms in I .

(iii) In case (a), the set Z consists of three points spanning the projective plane $\mathbb{P}W^\vee$, so $\dim \text{Sym}^2 W/I(Z)_2 = 3$. Then by Lemma 4.3.1, the coordinate-wise square $L^{\circ 2}$ is contained in a plane $\mathbb{P}^2 \cong \vartheta(\mathbb{P}(\text{Sym}^2 W/I(Z)_2)) \subset \mathbb{P}^n$. On the other hand, $\dim L^{\circ 2} = \dim L = 2$, so $L^{\circ 2} \subset \mathbb{P}^n$ must be a plane in \mathbb{P}^n .

For case (b), we may assume that

$$Z = \{[1 : 0 : 0], [0 : 1 : 0], [0 : 0 : 1], [-1 : -1 : -1]\}$$

for a suitably chosen basis $\{\ell_0, \ell_1, \ell_2\}$ of W^\vee . By Lemma 4.3.1, $L^{\circ 2} \subset \mathbb{P}^n$ is a linear re-embedding of the image of $\psi: \mathbb{P}W \rightarrow \mathbb{P}(\text{Sym}^2 W/I(Z)_2)$. On the other hand, the plane $L' := V(x_0 + x_1 + x_2 + x_3) \subset \mathbb{P}^3$ is the image of $\mathbb{P}W \xrightarrow{[\ell_0:\ell_1:\ell_2:-\ell_0-\ell_1-\ell_2]} \mathbb{P}^3$, so Z can also be viewed as the finite set of points associated to L' . Applying Lemma 4.3.1 to $L' \subset \mathbb{P}^3$ shows that the image of $\psi: \mathbb{P}W \rightarrow \mathbb{P}(\text{Sym}^2 W/I(Z)_2)$ is the coordinate-wise square $L'^{\circ 2} \subset \mathbb{P}^3$. Hence, $L^{\circ 2} \subset \mathbb{P}^n$ is a linear re-embedding of the quartic surface from Example 4.2.5 into higher dimension.

Finally, we consider the case (c). Consider three points $p_1, p_2, p_3 \in Z$ lying on a line $T \subset \mathbb{P}W^\vee$. Then T must be an irreducible component of each conic through Z . Since Z spans the projective plane $\mathbb{P}W^\vee$, there must also be a point $p_0 \in Z$ outside of T .

All points in $Z \setminus \{p_0\}$ must lie on the line T , as otherwise there could be at most one conic passing through Z . If $Z' := \{p_0, p_1, p_2, p_3\} \subset Z$, then each conic passing through Z' also passes through Z , i.e. $I(Z)_2 = I(Z')_2$.

We may choose a basis z_0, z_1, z_2 of W such that $Z' \subset \mathbb{P}W^\vee$ with respect to these coordinates is given by

$$Z' = \{[1 : 0 : 0], [0 : 1 : 0], [0 : 0 : 1], [0 : 1 : 1]\}.$$

The plane $L' := V(x_1 + x_2 - x_3) \subset \mathbb{P}^3$ is the image of $\mathbb{P}^2 \xrightarrow{[z_0:z_1:z_2:z_1+z_2]} \mathbb{P}^3$, so Z' can be viewed as the finite set of points associated to L' . Lemma 4.3.1 shows that $L'^{\circ 2} \subset \mathbb{P}^3$ coincides with the image of the morphism $\psi: \mathbb{P}W \rightarrow \mathbb{P}(\text{Sym}^2 W/I(Z')_2)$. On the other hand, Lemma 4.3.1 shows that $L^{\circ 2} \subset \mathbb{P}^n$ is a linear re-embedding of $\mathbb{P}W \rightarrow \mathbb{P}(\text{Sym}^2 W/I(Z)_2)$. From $I(Z)_2 = I(Z')_2$, we deduce that $L^{\circ 2} \subset \mathbb{P}^n$ is a linear re-embedding of the quadratic surface

$$L'^{\circ 2} = V(x_1 + x_2 - x_3)^{\circ 2} = V(x_1^2 + x_2^2 + x_3^2 - 2x_1x_2 - 2x_2x_3 - 2x_3x_1) \subset \mathbb{P}^3,$$

as we compute from Proposition 4.2.4. □

Remark 4.3.10. Opposed to Remark 4.3.7, the structure of the coordinate-wise square of a plane $L \subset \mathbb{P}^n$ does *not* only depend on the linear matroid of L : For $n = 5$, it can happen both in case (i) and case (ii).(a) of Theorem 4.3.9 that $\mathcal{M}_L = \{I \subset \{0, 1, \dots, 5\} \mid |I| \leq 3\}$.

4.3.4 Squaring in High Ambient Dimensions

Consider the case of k -dimensional linear spaces in \mathbb{P}^n for $n \gg k$. For a *general* linear space $L \in \text{Gr}(k, \mathbb{P}^n)$, the finite set of points Z does not lie on a quadric. We know from Proposition 4.3.2 that the coordinate-wise square $L^{\circ 2}$ is a linear re-embedding of the k -dimensional second Veronese variety. In this subsection, we investigate the first degenerate case where the point configuration Z is a unique quadric.

The following theorem gives the structure of coordinate-wise squares as the one appearing in Proposition 4.3.3. We will also prove Corollary 4.3.5 by deriving the polynomials vanishing on the set of symmetric matrices with a comultiplicity 1 eigenvalue. Proposition 4.3.3 shows that Corollary 4.3.5 is a special case of the theorem stated below.

Theorem 4.3.11. *Let $L \subset \mathbb{P}^n$ be linear space of dimension k . If the point configuration Z lies on a unique quadric of rank s , then $L^{\circ 2}$ can be cut out set-theoretically by $n - \binom{k+2}{2} + 2$ linear forms and*

$$\begin{cases} (k+3)(k+2)(k+1)(k-2)/12 \text{ quadratic forms,} & \text{if } s \geq 4, \\ (k+3)(k+2)(k+1)(k-2)/12 \text{ quadratic and 7 cubic forms,} & \text{if } s = 3, \\ (k+3)(k+2)(k+1)(k-2)/12 + 2 \text{ quadratic forms,} & \text{if } s = 2. \end{cases}$$

In fact, for $s \geq 3$, we show that the claim holds *scheme-theoretically*, see Remark 4.3.17. We believe that in fact for arbitrary s the claim is even true *ideal-theoretically*.

The remainder of this subsection is dedicated to the proof of Theorem 4.3.11. It reduces to the following elimination problem. Let $k \geq 1$ and $s \geq 2$. Consider a symmetric $(k + 1) \times (k + 1)$ -matrix of variables $Y := (y_{ij})_{1 \leq i, j \leq k+1}$ and the corresponding polynomial ring $\mathbb{C}[\mathbf{y}] := \mathbb{C}[y_{ij}]/(y_{ij} - y_{ji})$. Over the polynomial ring $\mathbb{C}[\mathbf{y}, t]$, we consider the matrix $M := Y + tI_s$, where we define the matrix

$$I_s := \text{diag}(\underbrace{1, \dots, 1}_s, \underbrace{0, \dots, 0}_{k+1-s}) \in \mathbb{C}^{(k+1) \times (k+1)}.$$

Henceforth, we denote the 2×2 -minors of Y with rows $i \neq j$ and columns $\ell \neq m$ by $Y_{ij|\ell m} := y_{i\ell}y_{jm} - y_{im}y_{j\ell} \in \mathbb{C}[\mathbf{y}]$, and correspondingly $M_{ij|\ell m} \in \mathbb{C}[\mathbf{y}, t]$ for the 2×2 -minors of M . Let $J_0 \subset \mathbb{C}[\mathbf{y}, t]$ denote the ideal generated by the 2×2 -minors of M . By $J := J_0 \cap \mathbb{C}[\mathbf{y}]$ we denote the ideal in $\mathbb{C}[\mathbf{y}]$ obtained by eliminating t from J_0 . We explicitly describe the elimination ideal J for all values of k and s .

Proposition 4.3.12. *The vanishing set $V(J) \subset \mathbb{P}^{\binom{k+2}{2}-1}$ is set-theoretically cut out by*

$$\begin{cases} (k+3)(k+2)(k+1)(k-2)/12 \text{ quadratic forms,} & \text{if } s \geq 4, \\ (k+3)(k+2)(k+1)(k-2)/12 \text{ quadratic and 7 cubic forms,} & \text{if } s = 3, \\ (k+3)(k+2)(k+1)(k-2)/12 + 2 \text{ quadratic forms,} & \text{if } s = 2. \end{cases}$$

First, we observe that Theorem 4.3.11 follows directly from Proposition 4.3.12.

Proof of Theorem 4.3.11. Analogous to the proof of Proposition 4.3.3, we identify $\mathbb{P}\text{Sym}^2 W$ with $\mathbb{P}\text{Sym}^2 \mathbb{C}^{k+1}$ such that $q = I_s$. By Lemma 4.3.1, the coordinate-wise square $L^{\circ 2}$ is a linear re-embedding of the variety obtained by the projection of $\nu_2(\mathbb{P}W)$ from the point $q = I_s \in \mathbb{P}\text{Sym}^2 W$. Note that $V(J)$ describes the set of points $Y \in \mathbb{P}\text{Sym}^2 W$ lying on the line joining q with some point in $\nu_2(\mathbb{P}W)$. Hence, the projection from q is given by intersecting $V(J)$ with a hyperplane $H \subset \mathbb{P}\text{Sym}^2 W$ not containing $q = I_s$.

From Proposition 4.3.12, we know that $V(J) \cap H$ is set-theoretically cut out inside $H \cong \mathbb{P}^{\binom{k+2}{2}-2}$ by the indicated number of quadrics and cubics. The coordinate-wise square $L^{\circ 2}$ is, by Lemma 4.3.1, obtained as the image of $V(J) \cap H$ under a linear embedding $\vartheta: H \hookrightarrow \mathbb{P}^n$, leading to additional $n - \binom{k+2}{2} + 2$ linear forms vanishing on $L^{\circ 2}$. \square

We prove Proposition 4.3.12 in several steps. First, we describe a set \mathcal{X} of certain low-degree polynomials in the ideal J . Secondly, we show that $V(\mathcal{X}) = V(J)$. Finally, we identify a subset of \mathcal{X} providing minimal generators of the ideal $(\mathcal{X}) \subset \mathbb{C}[\mathbf{y}]$, consisting of the claimed number of quadratic and cubic forms.

Lemma 4.3.13. *The following sets of polynomials in $\mathbb{C}[\mathbf{y}]$ are contained in the ideal J :*

$$\begin{aligned}\mathcal{E} &:= \{Y_{ij|\ell m} \mid \{i, j\} \cap \{\ell, m\} \subset \{s+1, \dots, k+1\}\}, \\ \mathcal{F} &:= \{Y_{i\ell|im} - Y_{j\ell|jm} \mid i, j \leq s, \{\ell\} \cap \{m\} \subset \{s+1, \dots, k+1\}\}, \\ \mathcal{G} &:= \{Y_{ij|ij} - Y_{j\ell|j\ell} + Y_{\ell m|\ell m} - Y_{mi|mi} \mid i, j, \ell, m \leq s \text{ distinct}\}, \\ \mathcal{H}_1 &:= \{y_{i\ell}(Y_{ij|ij} - Y_{i\ell|i\ell}) - (y_{\ell\ell} - y_{jj})Y_{ij|j\ell} \mid i, j, \ell \leq s\}, \\ \mathcal{H}_2 &:= \{(y_{ii} - y_{jj})Y_{ij|ij} + (y_{jj} - y_{\ell\ell})Y_{j\ell|j\ell} + (y_{\ell\ell} - y_{ii})Y_{\ell i|\ell i} \mid i, j, \ell \leq s\}.\end{aligned}$$

Proof. Using that

$$\begin{aligned}Y_{ij|ij} &= M_{ij|ij} - (y_{ii} + y_{jj})t - t^2 && \text{for all } i, j \leq s \text{ distinct and} \\ Y_{i\ell|j\ell} &= M_{i\ell|j\ell} - ty_{ij} && \text{for all } \ell \leq s, \{i\} \cap \{j\} \subset \{s+1, \dots, k+1\},\end{aligned}\tag{60}$$

we can check that

$$\begin{aligned}Y_{ij|\ell m} &= M_{ij|\ell m}, \\ Y_{i\ell|im} - Y_{j\ell|jm} &= M_{i\ell|im} - M_{j\ell|jm}, \\ Y_{ij|ij} - Y_{j\ell|j\ell} + Y_{\ell m|\ell m} - Y_{mi|mi} &= M_{ij|ij} - M_{j\ell|j\ell} + M_{\ell m|\ell m} - M_{mi|mi}, \\ y_{i\ell}(Y_{ij|ij} - Y_{i\ell|i\ell}) - (y_{\ell\ell} - y_{jj})Y_{ij|j\ell} &= y_{i\ell}(M_{ij|ij} - M_{i\ell|i\ell}) - (y_{\ell\ell} - y_{jj})M_{ij|j\ell}, \\ (y_{ii} - y_{jj})Y_{ij|ij} + (y_{jj} - y_{\ell\ell})Y_{j\ell|j\ell} + (y_{\ell\ell} - y_{ii})Y_{\ell i|\ell i} &= (y_{ii} - y_{jj})M_{ij|ij} + (y_{jj} - y_{\ell\ell})M_{j\ell|j\ell} + (y_{\ell\ell} - y_{ii})M_{\ell i|\ell i}\end{aligned}$$

holds for respective indices i, j, ℓ, m . From this, we conclude that these polynomials are contained in $J_0 \cap \mathbb{C}[\mathbf{y}] = J$. \square

From now on, we denote $\mathcal{X} := \mathcal{E} \cup \mathcal{F} \cup \mathcal{G} \cup \mathcal{H}_1 \cup \mathcal{H}_2$. These polynomials cut out $V(J)$:

Lemma 4.3.14. *Inside $\mathbb{P}\text{Sym}^2 \mathbb{C}^{k+1} = \mathbb{P}^{\binom{k+2}{2}-1}$, we consider the open sets*

$$U_1 := \mathbb{P}\text{Sym}^2 \mathbb{C}^{k+1} \setminus \{I_s\} \quad \text{and} \quad U_2 := \mathbb{P}\text{Sym}^2 \mathbb{C}^{k+1} \setminus \left\{ \begin{pmatrix} * & * & 0 \\ * & * & 0 \\ 0 & * & 0 \end{pmatrix} \right\}.$$

(i) *If $s \geq 3$, then $V(\mathcal{X})$ and $V(J)$ agree scheme-theoretically on U_1 .*

(ii) *If $s = 2$, then $V(\mathcal{X})$ and $V(J)$ agree scheme-theoretically on U_2 .*

(iii) *For s arbitrary, $V(\mathcal{X})$ and $V(J)$ agree set-theoretically.*

Proof. For $k \leq 5$, we have checked computationally with a straightforward implementation in `Macaulay2` [58] that even the ideal-theoretic equality $(\mathcal{X}) = J$ holds. We now argue that from this we can conclude the claim for arbitrary k .

(i) Let $s \geq 3$. We need to show that the ideal generated by $\mathcal{X} \subset \mathbb{C}[\mathbf{y}]$ coincides with $J \subset \mathbb{C}[\mathbf{y}]$ after localisation at any element in the set

$$\{y_{ij} \mid \{i\} \cap \{j\} \subset \{s+1, \dots, k+1\}\} \cup \{y_{ii} - y_{jj} \mid i, j \leq s\},$$

since the union of the corresponding non-vanishing sets $D(y_{ij}), D(y_{ii} - y_{jj})$ is U_1 .

In order to show that (\mathcal{X}) and J agree after localisation at $y_{i_0 j_0}$ for $\{i_0\} \cap \{j_0\} \subset \{s+1, \dots, k+1\}$, we may substitute $y_{i_0 j_0} = 1$ in both ideals. For a fixed $\ell_0 \leq s$ distinct from i_0 and j_0 , we note that $t + Y_{i_0 \ell_0 | j_0 \ell_0} = M_{i_0 \ell_0 | j_0 \ell_0} \in J_0|_{y_{i_0 j_0}=1}$. Hence, eliminating t from $J_0|_{y_{i_0 j_0}=1}$ just amounts to replacing $t = -Y_{i_0 \ell_0 | j_0 \ell_0}$ in each occurrence of t in the minors $M_{ij|\ell m}$ (for $i \neq j, \ell \neq m$) generating the ideal J_0 .

According to (60), this leads to the following generators of $J|_{y_{i_0 j_0}=1}$:

- $Y_{i_0 \ell_0 | j_0 \ell_0}^2 - (y_{ii} + y_{jj})Y_{i_0 \ell_0 | j_0 \ell_0} + Y_{ij|ij}$ for $i \neq j \leq s$,
- $-y_{ij}Y_{i_0 \ell_0 | j_0 \ell_0} + Y_{i\ell|j\ell}$ for $\ell \leq s, \{i\} \cap \{j\} \subset \{s+1, \dots, k+1\}$,
- $Y_{ij|\ell m}$ for $\{i, j\} \cap \{\ell, m\} \subset \{s+1, \dots, k+1\}$.

To check that $J|_{y_{i_0 j_0}=1} = (\mathcal{X})|_{y_{i_0 j_0}=1}$, we need to check that each of these polynomials belong to $(\mathcal{X})|_{y_{i_0 j_0}=1}$. For this, it is enough to see that they can be expressed in terms of those polynomials in \mathcal{X} that only involve variables with indices among $\{i_0, j_0, \ell_0, i, j, \ell\}$. This corresponds to showing the claim for a corresponding symmetric submatrix of M of size at most 6×6 . We conclude that it is enough to check $J|_{y_{i_0 j_0}=1} = (\mathcal{X})|_{y_{i_0 j_0}=1}$ for $k \leq 5$.

Similarly, in order to show that $J|_{y_{i_0 i_0} - y_{j_0 j_0} = 1} = (\mathcal{X})|_{y_{i_0 i_0} - y_{j_0 j_0} = 1}$ holds for $i_0, j_0 \leq s$ distinct, we realise that $t + Y_{i_0 \ell_0 | i_0 \ell_0} - Y_{j_0 \ell_0 | j_0 \ell_0} = M_{i_0 \ell_0 | i_0 \ell_0} - M_{j_0 \ell_0 | j_0 \ell_0} \in J_0|_{y_{i_0 j_0}=1}$ holds for fixed $\ell_0 \leq s$ distinct from i_0 and j_0 . Therefore, replacing $t = Y_{j_0 \ell_0 | j_0 \ell_0} - Y_{i_0 \ell_0 | i_0 \ell_0}$ in the expressions for the 2×2 -minors of M describes generators of $J|_{y_{i_0 i_0} - y_{j_0 j_0} = 1}$. As before, these polynomials involve variables with at most six distinct indices, so it is enough to verify the claim for $k \leq 5$ by the same argument as above.

(ii) For $s = 2$, the argument from (i) still shows $J_0|_{y_{i_0 j_0}=1} = (\mathcal{X})|_{y_{i_0 j_0}=1}$ for $\{i_0, j_0\} \cap \{3, \dots, k+1\} \neq \emptyset$. For the localisation at y_{12} and at $y_{11} - y_{22}$, the argument does not apply since we cannot choose ℓ_0 distinct from $\{i_0, j_0\} = \{1, 2\}$ as before. Hence, we have shown the equality of $V(\mathcal{X})$ and $V(J)$ only on U_2 .

(iii) We observe that the polynomials in \mathcal{X} vanish on the point $I_s \in \mathbb{P}\text{Sym}^2 \mathbb{C}^{k+1}$, and that $I_s \in V(J)$ by definition of J . Together with (i), this proves the claim for $s \geq 3$.

For $s = 2$, the polynomials in \mathcal{X} vanish on all symmetric matrices of the form $A = \begin{pmatrix} a & c & 0 \\ c & b & 0 \\ 0 & 0 & 0 \end{pmatrix} \in \text{Sym}^2 \mathbb{C}^{k+1}$. On the other hand, each such matrix is a point in $V(J)$, since $A + t_0 I_2$ is a matrix of rank ≤ 1 for $t_0 \in \mathbb{C}$ such that $t_0^2 + (a+b)t_0 + (ab - c^2) = 0$. Together with (ii), we conclude that $V(\mathcal{X}) = V(J)$ holds set-theoretically. \square

Lemma 4.3.15. *The vector spaces spanned by the polynomials in \mathcal{X} satisfy:*

- (i) $\langle \mathcal{E} \cup \mathcal{F} \cup \mathcal{G} \rangle = \langle \mathcal{E} \rangle \oplus \langle \mathcal{F} \rangle \oplus \langle \mathcal{G} \rangle$,
- (ii) $\langle \mathcal{H}_1 \cup \mathcal{H}_2 \rangle \cap \langle \mathcal{E}, \mathcal{F}, \mathcal{G} \rangle = \emptyset$ for $s = 3$,

(iii) $\mathcal{H}_1 \cup \mathcal{H}_2 \subset (\mathcal{E}, \mathcal{F}, \mathcal{G})$ for $s \neq 3$.

Proof. Let $\mathcal{M}_{\mathcal{E}} \subset \mathbb{C}[\mathbf{y}]$ denote the set of monomials occurring in one of the polynomials of \mathcal{E} , and analogously for \mathcal{F} , \mathcal{G} , \mathcal{H}_1 and \mathcal{H}_2 .

- (i) This follows from the observation that $\mathcal{M}_{\mathcal{E}}$, $\mathcal{M}_{\mathcal{F}}$ and $\mathcal{M}_{\mathcal{G}}$ are disjoint sets.
- (ii) For $s = 3$, note that $\mathcal{G} = \emptyset$ and none of the monomials in $\mathcal{M}_{\mathcal{E}} \cup \mathcal{M}_{\mathcal{F}}$ is of the form $y_{ij}y_{\ell m}$ with $i, j, \ell, m \leq 3$. On the other hand, the monomials in $\mathcal{M}_{\mathcal{H}_1} \cup \mathcal{M}_{\mathcal{H}_2}$ are of the form $y_{i_1 j_1} y_{i_2 j_2} y_{i_3 j_3}$ with $i_1, i_2, i_3, j_1, j_2, j_3 \leq 3$. Hence, no monomial in $\mathcal{M}_{\mathcal{H}_1} \cup \mathcal{M}_{\mathcal{H}_2}$ is a multiple of any of the monomials in $\mathcal{M}_{\mathcal{E}} \cup \mathcal{M}_{\mathcal{F}}$, so $\langle \mathcal{H}_1 \cup \mathcal{H}_2 \rangle \cap (\mathcal{E}, \mathcal{F}, \mathcal{G}) = \emptyset$.
- (iii) If $s = 2$ we have $\mathcal{H}_1 \cup \mathcal{H}_2 = \emptyset$, so the claim is trivial. Let $s \geq 4$. Then for all $i, j, \ell, m \leq s$ distinct, we have

$$\begin{aligned}
& y_{i\ell}(Y_{ij|ij} - Y_{i\ell|i\ell}) - (y_{\ell\ell} - y_{jj})Y_{ij|j\ell} \\
&= -2y_{jm}Y_{ij|\ell m} - y_{jm}Y_{im|j\ell} - y_{i\ell}(Y_{i\ell|i\ell} - Y_{\ell j|\ell j} + Y_{jm|jm} - Y_{mi|mi}) + y_{im}(Y_{j\ell|jm} - Y_{i\ell|im}) \\
&\quad + y_{ij}(Y_{ij|i\ell} - Y_{mj|m\ell}) + (y_{ii} - y_{jj})(Y_{ij|\ell j} - Y_{im|\ell m}) - y_{j\ell}(Y_{i\ell|j\ell} - Y_{im|jm}) \in (\mathcal{E}, \mathcal{F}, \mathcal{G}), \\
& (y_{ii} - y_{jj})Y_{ij|ij} + (y_{jj} - y_{\ell\ell})Y_{j\ell|j\ell} + (y_{\ell\ell} - y_{ii})Y_{\ell i|\ell i} \\
&= (y_{ii} - y_{jj})(Y_{ij|ij} - Y_{j\ell|j\ell} + Y_{\ell m|\ell m} - Y_{mi|mi}) + (y_{\ell\ell} - y_{ii})(Y_{i\ell|i\ell} - Y_{\ell j|\ell j} + Y_{jm|jm} - Y_{mi|mi}) \\
&\quad + y_{\ell m}(Y_{i\ell|im} - Y_{j\ell|jm}) - y_{jm}(Y_{ij|im} - Y_{\ell j|\ell m}) + y_{im}(Y_{j\ell|jm} - Y_{\ell i|\ell m}) \in (\mathcal{E}, \mathcal{F}, \mathcal{G}).
\end{aligned}$$

The equation above show that \mathcal{H}_1 and \mathcal{H}_2 lie in the ideal generated by \mathcal{E} , \mathcal{F} and \mathcal{G} . \square

Next, we identify maximal linearly independent subsets of \mathcal{E} , \mathcal{F} , \mathcal{G} .

Lemma 4.3.16. *The following sets form bases for the vector spaces $\langle \mathcal{E} \rangle$, $\langle \mathcal{F} \rangle$ and $\langle \mathcal{G} \rangle$:*

$$\begin{aligned}
\mathcal{B}_{\mathcal{E}} &:= \{Y_{ij|\ell m} \mid i < j, \ell < m, i \leq \ell \leq j \text{ s.t. } \{i, j\} \cap \{\ell, m\} \subset \{s+1, \dots, k+1\} \text{ and } j \leq m \text{ if } i = \ell\}, \\
\mathcal{B}_{\mathcal{F}} &:= \{Y_{i\ell|im} - Y_{1\ell|1m} \mid 2 \leq i \leq s, 2 \leq \ell \leq m \text{ s.t. } i \notin \{\ell, m\}, \{\ell\} \cap \{m\} \subset \{s+1, \dots, k+1\}\} \\
&\quad \cup \{Y_{i1|im} - Y_{21|2m} \mid 3 \leq i \leq s, 3 \leq m \leq k+1, i \neq m\} \cup \{Y_{i1|i2} - Y_{31|32} \mid i \in \{4, \dots, s\}\}, \\
\mathcal{B}_{\mathcal{G}} &:= \{Y_{12|12} - Y_{2\ell|2\ell} + Y_{\ell m|\ell m} - Y_{m1|m1} \mid 3 \leq m \leq s-1, \ell \in \{3, 4, \dots, m-1\} \cup \{s\}\} \\
&\quad \cup \{Y_{1s|1s} - Y_{s2|s2} + Y_{2m|2m} - Y_{m1|m1} \mid 3 \leq m \leq s-1\}.
\end{aligned}$$

Proof. The polynomials in \mathcal{E} not contained in $\mathcal{B}_{\mathcal{E}} \cup (-\mathcal{B}_{\mathcal{E}})$ are the polynomials $Y_{ij|\ell m}$ for $i < j < \ell < m$. However, these can be expressed as $Y_{ij|\ell m} = Y_{i\ell|jm} - Y_{im|j\ell} \in \langle \mathcal{B}_{\mathcal{E}} \rangle$. Hence $\mathcal{B}_{\mathcal{E}}$ spans $\langle \mathcal{E} \rangle$. For $i < j, \ell < m$ with $i \leq \ell \leq j$ such that $\{i, j\} \cap \{\ell, m\} \subset \{s+1, \dots, k+1\}$, we note that $Y_{ij|\ell m} \in \mathbb{C}[\mathbf{y}]$ is the unique polynomial in $\mathcal{B}_{\mathcal{E}}$ containing the monomial $y_{im}y_{\ell j}$. In particular, the polynomials in $\mathcal{B}_{\mathcal{E}}$ are linearly independent, so $\mathcal{B}_{\mathcal{E}}$ forms a basis of $\langle \mathcal{E} \rangle$.

If $i, j, \ell, m \in \{1, \dots, k+1\}$ with $\ell < m$ are such that $Y_{i\ell|im} - Y_{j\ell|jm} \in \mathcal{F} \setminus (\mathcal{B}_{\mathcal{F}} \cup -\mathcal{B}_{\mathcal{F}})$, then

$$Y_{i\ell|im} - Y_{j\ell|jm} = \begin{cases} (Y_{i\ell|im} - Y_{1\ell|1m}) - (Y_{j\ell|jm} - Y_{1\ell|1m}) & \text{if } \ell, m \neq 1, \\ (Y_{i1|im} - Y_{21|2m}) - (Y_{j1|jm} - Y_{21|2m}) & \text{if } \ell = 1, m \neq 2, \\ (Y_{i1|i2} - Y_{31|32}) - (Y_{j1|j2} - Y_{31|32}) & \text{if } \ell = 1, m = 2, \end{cases}$$

and hence, $\mathcal{B}_{\mathcal{F}}$ spans $\langle \mathcal{F} \rangle$. Each of the polynomials $Y_{i\ell|im} - Y_{j\ell|jm}$ in $\mathcal{B}_{\mathcal{F}}$ contains a monomial not occurring in any of the other polynomials of $\mathcal{B}_{\mathcal{F}}$, namely $y_{ii}y_{\ell m}$. Therefore, the polynomials in $\mathcal{B}_{\mathcal{F}}$ are linearly independent.

For $3 \leq m \leq s-1$ and $\ell \in \{3, \dots, m-1\} \cup \{s\}$, the polynomial $Y_{12|12} - Y_{2\ell|2\ell} + Y_{\ell m|\ell m} - Y_{m1|m1}$ is the unique polynomial in $\mathcal{B}_{\mathcal{G}}$ containing the monomial $y_{\ell\ell}y_{mm}$. In particular, if a linear combination of polynomials in $\mathcal{B}_{\mathcal{G}}$ is zero, then none of the above polynomials can occur in this linear combination. The remaining polynomials in $\mathcal{B}_{\mathcal{G}}$ are of the form $Y_{1s|1s} - Y_{s2|s2} + Y_{2m|2m} - Y_{m1|m1}$ for $3 \leq m \leq s-1$. Among these, the polynomial containing the monomial $y_{22}y_{mm}$ is unique. We conclude that the polynomials in $\mathcal{B}_{\mathcal{G}}$ are linearly independent.

We observe that

$$\mathcal{G} \subset \left\{ \sum_{i,j=1}^s a_{ij} Y_{ij|ij} \mid A = (a_{ij}) \in \mathbb{C}^{s \times s} \text{ symmetric with } a_{ii} = 0 \text{ and } (1, \dots, 1)A = 0 \right\}.$$

The vector space of symmetric $s \times s$ -matrices with zero diagonal and whose columns all sum to zero is of dimension $\binom{s}{2} - s$, so $\dim_{\mathbb{C}} \langle \mathcal{G} \rangle \leq \binom{s}{2} - s$. On the other hand, we can count that $|\mathcal{B}_{\mathcal{G}}| = \binom{s-3}{2} + 2(s-3) = \binom{s}{2} - s$, so $\mathcal{B}_{\mathcal{G}}$ is a basis of $\langle \mathcal{G} \rangle$. \square

Proof of Proposition 4.3.12. By Lemma 4.3.14, $V(J) = V(\mathcal{X})$ holds set-theoretically. For $s = 3$, we observe that $\mathcal{H}_1 \cup \mathcal{H}_2$ consists up to sign of seven linearly independent cubics, so by Lemma 4.3.15, the ideal (\mathcal{X}) is in this case minimally generated by those seven cubics and the polynomials in $\mathcal{B}_{\mathcal{E}}$, $\mathcal{B}_{\mathcal{F}}$ and $\mathcal{B}_{\mathcal{G}}$ from Lemma 4.3.16.

For $s \neq 3$, Lemma 4.3.15 and Lemma 4.3.16 show that (\mathcal{X}) is minimally generated just by the polynomials $\mathcal{B}_{\mathcal{E}} \cup \mathcal{B}_{\mathcal{F}} \cup \mathcal{B}_{\mathcal{G}}$. Straightforward counting gives:

$$\begin{aligned} |\mathcal{B}_{\mathcal{E}}| &= 2\binom{k+1}{4} + (k-s+1)\binom{k}{2} + \binom{k-s+1}{2} \\ &= (k^4 - 6sk^2 + 4k^3 + 6s^2 - 6sk + 5k^2 - 6s + 2k)/12, \\ |\mathcal{B}_{\mathcal{F}}| &= (s-1)\left(\binom{k-1}{2} + (k-s+1)\right) + (s-2)(k-2) + \binom{s-3}{1} \\ &= \begin{cases} (sk^2 - k^2 + sk - 2s^2 - 3k + 4s - 2)/2 & \text{if } s \geq 3, \\ (sk^2 - k^2 + sk - 2s^2 - 3k + 4s)/2 & \text{if } s = 2, \end{cases} \\ |\mathcal{B}_{\mathcal{G}}| &= \begin{cases} \binom{s}{2} - s = (s^2 - 3s)/2 & \text{if } s \geq 3, \\ 0 & \text{if } s = 2. \end{cases} \end{aligned}$$

Adding up these cardinalities gives the claimed number of quadratic forms. \square

Remark 4.3.17. In fact, for $s \geq 3$, our proof shows that $V(\mathcal{X})$ is the same scheme as $V(J)$ away from the point $I_s \in \mathbb{P}\text{Sym}^2 \mathbb{C}^{k+1}$. In the proof of Theorem 4.3.11, we considered $V(J) \cap H$, where H is a hyperplane not containing I_s . Since $V(J) \cap H = V(\mathcal{X}) \cap H$ scheme-theoretically, we conclude that our equations for $L^{\circ 2}$ in Theorem 4.3.11 cut out not only the correct set, but even the correct scheme. In fact, we believe that we have ideal-theoretic equality for the specified set of polynomials, but our proof stops short of verifying this.

We now prove the result about eigenspaces of symmetric matrices stated as Corollary 4.3.5. It follows directly from the proof of Proposition 4.3.12.

Proof of Corollary 4.3.5. A complex symmetric matrix $A \in \mathbb{C}^{s \times s}$ has an eigenspace of codimension 1 with respect to an eigenvalue $\lambda \in \mathbb{C}$ if and only if the matrix $A - \lambda \text{id}$ is of rank 1, which means that $A \in V(J)$ for the case $s = k + 1$. By Lemma 4.3.14 and Lemma 4.3.15, this is equivalent to the vanishing of the equations $\mathcal{E} \cup \mathcal{F} \cup \mathcal{G}$, which are the above relations among 2×2 -minors for $s = k + 1 \geq 4$. The second claim was proved in Proposition 4.3.3. \square

The proof of Theorem 4.3.11 was based on relating the coordinate-wise square $L^{\circ 2}$ in the case $\dim_{\mathbb{C}} I(Z)_2 = 1$ to the question when a symmetric matrix can be completed to a rank 1 matrix by adding a multiple of I_s . In the same spirit, for *arbitrary* linear spaces L (no restrictions on the set of quadrics containing Z), determining the ideal of the coordinate-wise square $L^{\circ 2}$ boils down to the following problem in symmetric rank 1 matrix completion:

Problem 4.3.18. *For a fixed matrix $B \in \mathbb{C}^{(n+1) \times (k+1)}$ of rank $k + 1$, find the defining equations of the set*

$$\left\{ M \in \mathbb{C}^{(k+1) \times (k+1)} \text{ symmetric} \mid \exists P \in \mathbb{C}^{(k+1) \times (k+1)} \text{ symmetric such that } BPB^T \text{ has a zero diagonal and } \text{rk}(M + P) = 1 \right\}.$$

Indeed, let L be an arbitrary linear space of dimension k and let $B \in \mathbb{C}^{(n+1) \times (k+1)}$ be a chosen matrix of full rank describing L as the image of the linear embedding $\mathbb{P}^k \hookrightarrow \mathbb{P}^n$ given by B . Then the rows of B form the finite set of points $Z \subset (\mathbb{P}^k)^\vee$. Identifying quadratic forms on \mathbb{P}^k with symmetric $(k + 1) \times (k + 1)$ -matrices, the subspace $I(Z)_2 \subset \text{Sym}^2(\mathbb{C}^{k+1})^\vee$ corresponds to

$$I(Z)_2 = \{P \in \mathbb{C}^{(k+1) \times (k+1)} \text{ symmetric such that } BPB^T \text{ has a zero diagonal}\}.$$

By Lemma 4.3.1, the coordinate-wise square $L^{\circ 2}$ is a linear re-embedding of projection of the second Veronese variety

$$\nu_2(\mathbb{P}^k) = \{\text{rank 1 symmetric } (k + 1) \times (k + 1)\text{-matrices up to scaling}\}$$

from $\mathbb{P}(I(Z)_2)$. Therefore, describing the ideal of $L^{\circ 2}$ corresponds to solving Problem 4.3.18 for the given matrix B . Similarly, describing the coordinate-wise r -th power of a linear space corresponds to the analogous problem in symmetric rank 1 tensor completion.

By Lemma 4.3.1, determining the coordinate-wise r -th power of a linear space corresponds to describing the projection of the r -th Veronese variety from a linear space of the form $\mathbb{P}(I(Z)_r)$ for a non-degenerate finite set of points Z . We may ask how general this problem is, and pose the question which linear subspaces of $\mathbb{P}\text{Sym}^r W$ are of the form $\mathbb{P}(I(Z)_r)$:

Question 4.3.19. *Which linear subspaces of $\mathbb{C}[z_0, \dots, z_k]_r$ can be realised as the set of degree r polynomials vanishing on some non-degenerate finite set of points in \mathbb{P}^k of cardinality $\leq n + 1$?*

We envision that an answer to this question may lead to insights into describing which varieties can occur as the coordinate-wise r -th power of some linear space in \mathbb{P}^n .

5 References

- [1] H. Abeliovich: *An empirical extremum principle for the hill coefficient in ligand-protein interactions showing negative cooperativity*, Biophysical journal, **89** (1), 76–79, (2005).
- [2] H. Abeliovich: *On Hill coefficients and subunit interaction energies*, Journal of Mathematical Biology, **73**, 1399–1411, (2016).
- [3] H. Abo, A. Seigal and B. Sturmfels: *Eigenconfigurations of tensors*, in Algebraic and Geometric Methods in Discrete Mathematics, (eds. H. Harrington, M. Omar and M. Wright), Contemporary Mathematics, **685**, American Mathematical Society, 1–25, (2017).
- [4] F. Acquistapace, F. Broglia and J.F. Fernando: *On globally defined semianalytic sets*, Mathematische Annalen, **366**, 613–654, (2016).
- [5] G. S. Adair, A. V. Bock, and H. Field Jr.: *The hemoglobin system VI. The oxygen dissociation curve of hemoglobin*, Journal of Biological Chemistry, **63**, 529–545, (1925).
- [6] V. I. Arnol'd: *The situation of ovals of real plane algebraic curves, the involutions of four-dimensional smooth manifolds, and the arithmetic of integral quadratic forms*, Akademiya Nauk SSSR. Funkcional'nyi Analiz i ego Priloženija, **5** (3), 1–9 (1971).
- [7] J. Barcroft: *The combinations of haemoglobin with oxygen and with carbon monoxide. II*, Biochemical Journal, **7**, (1913).
- [8] N. Beerenwinkel, L. Pachter and B. Sturmfels: *Epistasis and shapes of fitness landscapes*, Statistica Sinica **17**, 1317–1342, (2007).
- [9] A. Ben-Naim: *Cooperativity and regulation in biochemical processes*, Springer Science & Business Media, 2013.
- [10] G. Blekherman, P. Parrilo and R. Thomas: *Semidefinite Optimization and Convex Algebraic Geometry*, MOS-SIAM Series on Optimization **13**, 2012.
- [11] C. Bocci, E. Carlini, and J. Kileel: *Hadamard products of linear spaces*. Journal of Algebra, **448**, 595–617, (2016).
- [12] J. Bochnak, M. Coste and M.-F. Roy: *Real Algebraic Geometry*, Ergebnisse der Mathematik und ihrer Grenzgebiete (3), vol. 36, Springer-Verlag, Berlin, 1998.
- [13] C. Bohr, K. Hasselbalch, and A. Krogh: *Ueber einen in biologischer Beziehung wichtigen Einfluss, den die Kohlensäurespannung des Blutes auf dessen Sauerstoffbindung übt 1*, Skandinavisches Archiv für Physiologie, **16**, 402–412, (1904).
- [14] J. A. Bondy and U. S. R. Murty: *Graph theory with applications*, American Elsevier Publishing Co., Inc., New York, (1976).
- [15] C. Bonnafé: *A surface of degree 24 with 1440 singularities of type D_4* , arXiv: 1804.08388.
- [16] B. Boros: *Existence of positive steady states for weakly reversible mass-action systems*, SIAM Journal on Mathematical Analysis, **51** (1), 435–449, (2019).
- [17] M. Brandt, J. Bruce, T. Brysiewicz, R. Krone, and E. Robeva: *The degree of $SO(n, \mathbb{C})$* , Combinatorial Algebraic Geometry: Selected Papers From the 2016 Apprenticeship Program, Ed. by G. G. Smith and B. Sturmfels. Springer New York, New York, NY, 229–246, (2017).
- [18] H. Bräuner-Osborne, J. Egebjerg, E. O. Nielsen, U. Madsen, and P. Krogsgaard-Larsen: *Ligands for Glutamate Receptors: Design and Therapeutic Prospects*, Journal of Medicinal Chemistry, **43**, 2609–2645, (2000).

- [19] K. Brejc, W. J. van Dijk, R. V. Klaassen, M. Schuurmans, J. van der Oost, A. B. Smit, and T. K. Sixma: *Crystal structure of an ACh-binding protein reveals the ligand-binding domain of nicotinic receptors*, *Nature*, **411**, 269–276, (2001).
- [20] W. E. Briggs: *A new measure of cooperativity in protein-ligand binding*, *Biophysical Chemistry*, **18**, 67–71, (1983).
- [21] W. E. Briggs: *Cooperativity and extrema of the Hill slope for symmetric protein-ligand binding polynomials*, *Journal of Theoretical Biology*, **108**, 77–83, (1984).
- [22] W. E. Briggs: *The relationship between zeros and factors of binding polynomials and cooperativity in protein-ligand binding*, *Journal of Theoretical Biology*, **114**, 605–614, (1985).
- [23] C. Brown: *Constructing cylindrical algebraic decomposition of the plane quickly*, Manuscript, 2002.
- [24] E. Brugallé and L. López de Medrano: *Inflection points of real and tropical plane curves*, *Journal of Singularities* **4**, 74–103, (2012).
- [25] L. Brusotti: *Sulla “piccola variazione” di una curva piana algebrica reale. (Italian)* *Accademia dei Lincei, Rendiconti* **30**, 375–379, (1921).
- [26] P. Bürgisser and F. Cucker: *Condition. The Geometry of Numerical Algorithms*, *Grundlehren der Mathematischen Wissenschaften*, vol. 349, Springer, Heidelberg, 2013.
- [27] G. Calussi, E. Carlini, G. Fatabbi, and A. Lorenzini: *The Hilbert function of some Hadamard products*, *Collectanea Mathematica*, **69**, 205–220, (2018).
- [28] O. Chterental and D. Ž. Đoković: *On orthostochastic, unistochastic and gustochastic matrices*, *Linear Algebra and its Applications*, **428**(4), 1178–1201, (2008).
- [29] J. Cheng, S. Lazard, L. Peñaranda, M. Pouget, F. Rouillier and E. Tsigaridas: *On the topology of planar curves*, *Mathematics in Computer Science* **4**, 113–137, (2010).
- [30] D. Ciripoi, N. Kaihnsa, A. Löhne, and B. Sturmfels: *Computing convex hulls of trajectories*, *arXiv:1810.03547*.
- [31] D. Ciripoi, A. Löhne, and B. Weißing: *Bensolve tools - Calculus of convex polyhedra, calculus of polyhedral convex functions, global optimization, vector linear programming for Octave and Matlab*, Version 1.1, <http://tools.bensolve.org>.
- [32] S. Colley and G. Kennedy: *A higher-order contact formula for plane curves*, *Communications in Algebra*, **19**, 479–508, (1991).
- [33] F. Colonius and W. Kliemann: *Dynamical Systems and Linear Algebra*, *Graduate Studies in Mathematics*, American Mathematical Society, 2014.
- [34] P. R. Connelly, C. H. Robert, W. E. Briggs, and S. J. Gill: *Analysis of zeros of binding polynomials for tetrameric hemoglobins*, *Biophysical chemistry*, **24**, 295–309, (1986).
- [35] G. Craciun, A. Dickenstein, A. Shiu, and B. Sturmfels: *Toric dynamical systems*, *Journal of Symbolic Computation* **44**, 1551–1565, (2009) .
- [36] M. A. Cueto, J. Morton, and B. Sturmfels: *Geometry of the restricted Boltzmann machine*, *Algebraic methods in statistics and probability II*, **516** of *Contemp. Math. Amer. Math. Soc.*, Providence, RI, 135–153, (2010).
- [37] J. A. De Loera, B. Sturmfels, and C. Vinzant: *The central curve in linear programming*, *Foundations of Computational Mathematics*, **12**(4), 509–540, (2012).

- [38] J. Deng, C. Jones, M. Feinberg, and A. Nachman: *On the steady states of weakly reversible chemical reaction networks*, [arXiv:1111.2386](#).
- [39] P. Dey: *Characterization of determinantal bivariate polynomials*, [arXiv: 1708.09559](#).
- [40] P. Dey: *Monic symmetric/hermitian determinantal representations of multi-variate polynomials*. PhD thesis. Department of Electrical Engineering, Indian Institute of Technology Bombay, (2017).
- [41] P. Dey, P. Görlach, and N. Kaihsa: *Coordinate-wise powers of algebraic varieties*, [arXiv:1807.03295](#).
- [42] A. Dickenstein and E. Feliu: *Algebraic Methods for Biochemical Reaction Networks*, textbook in preparation.
- [43] W. L. Edge: *Determinantal representations of $x^4 + y^4 + z^4$* , *Math. Proc. Cambridge Phil. Society* **34**, 6–21, (1938).
- [44] M. Ehrgott, A. Löhne, and L. Shao: *A dual variant of Benson’s “outer approximation algorithm” for multiple objective linear programming*, *Journal of Global Optimization*, **52**, 757–778, (2012).
- [45] A. Eigenwillig, M. Kerber, and N. Wolpert: *Fast and exact geometric analysis of real algebraic plane curves*, *Proc. Int. Symp. Symbolic and Algebraic Computation*, (2007)
- [46] M. Feinberg: *Lectures on Chemical Reaction Networks*. Notes of lectures given at the Mathematics Research Center of the University of Wisconsin in 1979, <http://www.che.eng.ohio-state.edu/FEINBERG/LecturesOnReactionNetworks>.
- [47] M. Feinberg: *Toward a theory of process synthesis*, *Industrial and Engineering Chemistry Research*, **41** (16), 3751–3761, (2002).
- [48] M. Feinberg and D. Hildebrandt: *Optimal reactor design from a geometric viewpoint–I. Universal properties of the attainable region*, *Chemical Engineering Science*, **52**, 1637–1665, (1997).
- [49] T. Fiedler: *Eine Beschränkung für die Lage von reellen ebenen algebraischen Kurven*, *Beiträge zur Algebra und Geometrie* **11**, 7–19, (1981).
- [50] A. Fink, D. E. Speyer, and A. Woo: *A Grbner basis for the graph of the reciprocal plane*, *Journal of Commutative Algebra*, Advance publication, (2018).
- [51] H. Flenner, L. O’Carroll, and W. Vogel: *Joins and intersections*, Springer Monographs in Mathematics, (1999).
- [52] N. Friedenber, A. Oneto, and R. L. Williams: *Minkowski sums and Hadamard products of algebraic varieties*, *Combinatorial Algebraic Geometry: Selected Papers From the 2016 Apprenticeship Program*, Ed. by G. G. Smith and B. Sturmfels, Springer New York, New York, NY, 133–157, (2017).
- [53] J. Fu: *Algebraic integral geometry*, *Integral Geometry and Valuations*, 47–112, *Adv. Courses Math. CRM Barcelona*, Birkhäuser/Springer, Basel, 2014.
- [54] A. Gabard: *Ahlfors circle maps and total reality: from Riemann to Rohlin*, [arXiv:1211.3680](#).
- [55] I. M. Gelfand, M. M. Kapranov, and A. V. Zelevinsky: *Discriminants, resultants, and multidimensional determinants*, *Mathematics: Theory & Applications*. Birkhäuser Boston, Inc., Boston, MA, (1994).

- [56] A. Gleixner et al: *The SCIP Optimization Suite 6.0*, Technical Report, Optimization Online, July 2018, http://www.optimization-online.org/DB_HTML/2018/07/6692.html.
- [57] L. González-Vega and I. Necula: *Efficient topology determination of implicitly defined algebraic plane curves*, Computer Aided Geometric Design **19**, 719–743, (2002).
- [58] D. R. Grayson and M. E. Stillman: Macaulay2, a software system for research in algebraic geometry. Available at <http://www.math.uiuc.edu/Macaulay2/>.
- [59] D.A. Gudkov: *Ovals of sixth order curves*, Gor’kov. Gos.Univ.Uën.Zap.Vyp. **87**, 14–20, (1969).
- [60] V. Hárs and J. Tóth: *On the inverse problem of reaction kinetics*, Colloquia Math. Societatis János Bolyai **30**, *Qualitative Theory of Differential Equations*, 363–379, Szeged, (1979).
- [61] D. Hilbert: *Über die reellen Züge algebraischer Curven*, Math. Annalen, **38**, 115–138, (1891).
- [62] A. V. Hill: *The combinations of haemoglobin with oxygen and with carbon monoxide. I*, Biochemical Journal, **7**, (1913).
- [63] T. L. Hill: *Cooperativity theory in biochemistry: steady-state and equilibrium systems*, Springer Science & Business Media, (2013).
- [64] A. Horn: *Doubly stochastic matrices and the diagonal of a rotation matrix*, American Journal of Mathematics, **76**, 620–630, (1954).
- [65] F. Horn: *Attainable and non-attainable regions in chemical reaction technique*, Proceedings of the Third European Symposium on Chemical Reaction Engineering, Amsterdam, The Netherlands, Pergamon Press, Oxford, UK, 293–303, (1964).
- [66] F. Horn and R. Jackson: *General mass action kinetics*, Archive for Rational Mechanics and Analysis, **47** (2),81-116, (1972).
- [67] M. Ikeda-Saito, T. Yonetani, E. Chiancone, F. Ascoli, D. Verzili, and E. Antonini: *Thermodynamic properties of oxygen equilibria of dimeric and tetrameric hemoglobins from Scapharca inaequalvis*, Journal of Molecular Biology, **170** (4), 1009–1018,(1983).
- [68] K. Imai: *Analyses of oxygen equilibriums of native and chemically modified human adult hemoglobins on the basis of Adir’s stepwise oxygenation theory and the allosteric model of Monod, Wyman, and Changeux*, Biochemistry, **12**, 798–808, (1973).
- [69] I.V. Itenberg: *Rigid isotopy classification of curves of degree 6 with one nondegenerate double point*, Topology of Manifolds and Varieties, Advances in Soviet Math. **18**, AMS, 193–208, (1994).
- [70] B. Joshi and A. Shiu: *Which small reaction networks are multistationary?* SIAM Journal on Applied Dynamical Systems, **16**, 802–833, (2017).
- [71] N. Kainhsa: *Attainable regions of dynamical systems*, arXiv:1802.07298.
- [72] N. Kaihsa, M. Kummer, D. Plaumann, M.N. Sayyary, and B. Sturmfels: *Sixty-four curves of degree six*, Experimental Mathematics, published online, 2017.
- [73] N. Kaihsa, Y. Ren, M. Safey El Din, and J. W. Maritini: *Cooperativity, Minimal Interaction Energy and Algebraic Optimization*, In Preparation.
- [74] C. Kalla and C. Klein: *Computation of the topological type of a real Riemann surface*, Mathematics of Computation, **83**, 1823–1844, (2014).
- [75] V. M. Kharlamov: *Isotopic types of nonsingular surfaces of degree 4 in \mathbb{RP}^3* , Functional Analysis and Its Applications **12**, 86–87, (1978).

- [76] V. M. Kharlamov: *Rigid classification up to isotopy of real plane curves of degree 5*, Functional Analysis and Its Applications **15**, 73–74, (1981).
- [77] V. M. Kharlamov: *Classification of nonsingular surfaces of degree 4 in \mathbb{RP}^3 with respect to rigid isotopies*, Functional Analysis and Its Applications **18**, 39–45, (1984).
- [78] M. Kummer and C. Vinzant: *The Chow form of a reciprocal linear space*, arXiv: 1610.04584.
- [79] A. Kunert and C. Scheiderer: *Extreme positive ternary sextics*, Transactions of the American Mathematical Society, **370**, 3997–4013, (2018).
- [80] J. M. Landsberg: *Tensors: geometry and applications*, Graduate Studies in Mathematics, **128**, American Mathematical Society, Providence, RI, (2012).
- [81] H. Lee and B. Sturmfels: *Duality of multiple root loci*, Journal of Algebra **446**, 499–526, (2016).
- [82] M. Lenz: *On powers of Plücker coordinates and representability of arithmetic matroids*, arXiv:1703.10520.
- [83] A. Lerario and E. Lundberg: *Statistics on Hilbert’s 16th problem*, International Mathematics Research Notices, **12**, 4293–4321, (2015).
- [84] A. Löhne and B. Weißing: *Equivalence between polyhedral projection, multiple objective linear programming and vector linear programming*, Mathematical Methods of Operations Research, **84**, 411–426, (2016).
- [85] A. Löhne and B. Weißing: *The vector linear program solver Bensolve – notes on theoretical background*, European Journal of Operational Research, **260**, 807–813, (2017).
- [86] M. Maccioni: *The number of real eigenvectors of a real polynomial*, Bollettino dell’Unione Matematica Italiana, **11**, 125–145, (2018).
- [87] D. Maclagan and B. Sturmfels: *Introduction to tropical geometry*, Graduate Studies in Mathematics, American Mathematical Society, Providence, RI, (2015).
- [88] A. W. Marshall, I. Olkin, and B. C. Arnold: *Inequalities: theory of majorization and its applications*, Springer Series in Statistics, Springer, New York, second edition, (2011).
- [89] J. W. Martini: *On the relation of different definitions of cooperative binding for systems with two binding sites*, Match-Communications in Mathematical and in Computer Chemistry, **78**, 739–752, (2017).
- [90] J. W. R. Martini: *A measure to quantify the degree of cooperativity in overall titration curves*, Journal of Theoretical Biology, **432**, 33–37, (2017).
- [91] J. W. Martini, L. Diambra, and M. Habeck: *Cooperative binding: a multiple personality*, Journal of Mathematical Biology, **72**, 1747–1774, (2016).
- [92] Mathematica, Wolfram Research, Inc., Version 11.1.1.0, Champaign, IL, 2017
- [93] MATLAB R2017a, version 9.2.0. Natick, Massachusetts: The MathWorks Inc., 2017.
- [94] M. Michalek, H. Moon, B. Sturmfels and E. Ventura: *Real rank geometry of ternary forms*, Annali di Matematica Pura ed Applicata, (2017).
- [95] D. Ming, D. Glasser, D. Hildebrandt, B. Glasser and M. Metzger: *Attainable Region Theory: An Introduction to Choosing an Optimal Reactor*, John Wiley and Sons, 2016.
- [96] L. Mirsky: *Results and problems in the theory of doubly-stochastic matrices*, Z. Wahrscheinlichkeitstheorie und Verw. Gebiete, **1**, 319–334, (1963).

- [97] V.V. Nikulin: *Integer symmetric bilinear forms and some of their geometric applications*, USSR-Izv. **14**, 103–167, (1980).
- [98] A. Onufriev and G. M. Ullmann: *Decomposing complex cooperative ligand binding into simple components: connections between microscopic and macroscopic models*, The Journal of Physical Chemistry B, **108**, 11157–11169, (2004).
- [99] James Oxley: *Matroid theory*, Oxford Graduate Texts in Mathematics, Oxford University Press, Oxford, second edition, (2011).
- [100] I. Petrovsky: *On the topology of real plane algebraic curves*, Annals of Mathematics, **39**, 189–209, (1938).
- [101] D. Plaumann, B. Sturmfels and C. Vinzant: *Quartic curves and their bitangents*, Journal of Symbolic Computation, **46**, 712–733, (2011).
- [102] K. Ranestad and B. Sturmfels: *On the convex hull of a space curve*, Advances in Geometry, **12**, 157–178, (2012).
- [103] M. W. Reichelt and L. F. Shampine: *The MATLAB ODE Suite*, SIAM Journal on Scientific Computing, **18** (1), (1997).
- [104] Y. Ren, J. W. R. Martini, and J. Torres: *Decoupled molecules with binding polynomials of bidegree $(n,2)$* , Journal of Mathematical Biology, **78** (4), 879–898, (2019).
- [105] V.A. Rokhlin: *Complex topological characteristics of real algebraic curves*, Russian Math. Surveys, **33:5**, 85–98, (1978).
- [106] K. Rohn: *Die Maximalzahl und Anordnung der Ovale bei der ebenen Kurve 6. Ordnung und bei der Fläche 4. Ordnung*, Mathematische Annalen, **73**, 177–229, (1913).
- [107] C. Rong, D. Zhao, D. Yu, and S. Liu: *Quantification and origin of cooperativity: Insights from density functional reactivity theory*, Physical Chemistry Chemical Physics, **20**, 17990–17998 (2018).
- [108] SageMath, the Sage Mathematics Software System (Version 7.6.0), The Sage Developers, 2017, <http://www.sagemath.org>.
- [109] C. Scheiderer: *Semidefinite representation for convex hulls of real algebraic curves*, SIAM Journal on Applied Algebra and Geometry, **2**(1), 1-25, (2018).
- [110] C. Scheiderer: *Spectrahedral Shadows*, SIAM Journal on Applied Algebra and Geometry, **2**(1), 26-44, (2018).
- [111] R. Seidel and N. Wolpert: *On the exact computation of the topology of real algebraic curves.*, Proc 21st ACM Symposium on Computational Geometry, 107–115, (2005).
- [112] A. Shiu: *Algebraic methods for biochemical reaction network theory*, Ph.D. thesis, 2010.
- [113] R. Silhol: *Real Algebraic Surfaces*, Lecture Notes in Mathematics **1392**, Springer, Berlin, 1989.
- [114] Z. Smilansky: *Convex hulls of generalized moment curves*, Israel Journal of Mathematics, **52**, 115–128, (1985).
- [115] M. I. Stefan and N. Le Novère: *Cooperative binding*, PLoS computational biology, **9**, e1003106, (2013).
- [116] G. A. Utkin: *Construction of certain types of nonsingular fourth order surfaces*, Gor’kov. Gos. Univ. Uën. Zap. Vyp., **87**, 196–211, (1969).

- [117] N. Vervliet, O. Debals, L. Sorber, M. Van Barel and L. De Lathauwer: *Tensorlab 3.0*, Available online, March 2016, <http://www.tensorlab.net>.
- [118] C. Vinzant: *Real Algebraic Geometry in Convex Optimization*, PhD Thesis, University of California, Berkeley, Spring 2011.
- [119] O. Viro: *Gluing of plane real algebraic curves and constructions of curves of degrees 6 and 7*, In *Topology (Leningrad, 1982)*, *Lecture Notes in Math.*, **1060**, Springer, Berlin, 187–200, (1984).
- [120] O. Viro: *Progress in the topology of real algebraic varieties over the last six years*, *Russian Math. Surveys*, **41**, 55-82, (1986).
- [121] O. Viro: *From the sixteenth Hilbert problem to tropical geometry*, *Japanese Journal of Mathematics*, **3**, 185–214, (2008).
- [122] J. Wyman and S. J. Gill: *Binding and linkage: functional chemistry of biological macromolecules*, University Science Books, 1990.
- [123] H.G. Zeuthen: *Sur les différentes formes des courbes planes du quatrième ordre*, *Mathematische Annalen*, **7**, 408–432, (1873).
- [124] G. Ziegler: *Lectures on Polytopes*, *Graduate Texts in Mathematics*, **152**, Springer-Verlag, New York, 1995.

Bibliographische Daten

Algebraic Methods for Dynamical Systems and Optimisation
(Algebraische Methoden für Dynamische Systeme und Optimierung)
Kaihnsa, Nidhi
Universität Leipzig, Dissertation, 2019
117 Seiten,
32 Abbildungen,
124 Referenzen.

Selbstständigkeitserklärung

Hiermit erkläre ich, die vorliegende Dissertation selbständig und ohne unzulässige fremde Hilfe angefertigt zu haben. Ich habe keine anderen als die angeführten Quellen und Hilfsmittel benutzt und sämtliche Textstellen, die wörtlich oder sinngemäß aus veröffentlichten oder unveröffentlichten Schriften entnommen wurden, und alle Angaben, die auf mündlichen Auskünften beruhen, als solche kenntlich gemacht. Ebenfalls sind alle von anderen Personen bereitgestellten Materialien oder erbrachten Dienstleistungen als solche gekennzeichnet.

Leipzig, den 26 July, 2019



(Nidhi Kaihnsa)

Daten zum Autor

Name: Nidhi Kaihnsa
Geburtsdatum: 10.12.1992 in Kaithal, Haryana, India

08/2010 - 05/2015 Dual degree Bachelors and Masters in Mathematics
Indian Institute of Science Education and Research,
Mohali, India

seit 04/2016 Doktorand
Max Planck Institute, Mathematics in the Sciences,
Leipzig